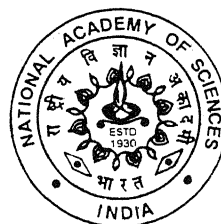


Vol. 74, Part III, 2004

ISSN 0369-8211

Proceedings of the National Academy of Sciences India

SECTION A — PHYSICAL SCIENCES



The National Academy of Sciences, India, Allahabad

राष्ट्रीय विज्ञान अकादमी, भारत, इलाहाबाद

The National Academy of Sciences, India

(Registered under Act XXI of 1860)

Founded 1930

COUNCIL FOR 2004

President

- 1 Prof Jay Pal Mittal, Ph D (Notre Dame), FNA, FA Sc, FN A Sc, FTWAS, Mumbai
Two Past Presidents (including the Immediate Past President)
- 2 Prof S K Joshi, D Phil, D Sc (h c), FNA, FA Sc, FN A Sc, FTWAS, New Delhi
- 3 Dr V P Sharma, D Phil, D Sc, FAMS, FESI, FISCD, FNA, FA Sc, FN A Sc, FRAS, New Delhi

Vice-Presidents

- 4 Dr P K Seth, Ph D, FNA, FN A Sc, Lucknow
- 5 Prof M Vijayan, Ph D, FNA, FA Sc, FN A Sc, FTWAS, Bangalore

Treasurer

- 6 Prof S L Srivastava, D Phil, FIETE, FNA Sc, Allahabad

Foreign Secretary

- 7 Dr S E Hasnain, Ph D, FNA, FA Sc, FN A Sc, FTWAS, Hyderabad

General Secretaries

- 8 Dr V P Kamboj, Ph D, D Sc, FNA, FN A Sc, Allahabad

- 9 Prof Pramod Tandon, Ph D, FN A Sc, Shillong

Members

- 10 Dr Samir Bhattacharya, Ph D, FNA, FA Sc, FN A Sc, Kolkata

- 11 Prof Suresh Chandra, D Phil, Grad Brit IRE, FN A Sc, Varanasi

- 12 Prof Virander Singh Chauhan, Ph D, D Phil (Oxford), FNA, FN A Sc, New Delhi

- 13 Prof Asis Datta, Ph D, D Sc, FNA, FA Sc, FN A Sc, FTWAS, New Delhi

- 14 Prof Kasturi Datta, Ph D, FNA, FA Sc, FN A Sc, FTWAS, New Delhi

- 15 Prof Sushanta Dattagupta, Ph D, FNA, FA Sc, FN A Sc, FTWAS, Kolkata

- 16 Dr Amit Ghosh, Ph D, FNA, FA Sc, FN A Sc, Chandigarh

- 17 Prof H S Mani, Ph D (Columbia), FA Sc, FN A Sc, Chennai

- 18 Prof G K Mehta, Ph D, FN A Sc, Allahabad

- 19 Dr G C Mishra, Ph D, FN A Sc, Pune

- 20 Dr Ashok Misra, M S (Chem Engg), M S (Polymer Sc), Ph D, FN A Sc, Mumbai

- 21 Prof Kambadur Muralidhar, Ph D, FNA, FA Sc, FN A Sc, Delhi

- 22 Dr Vijayalakshmi Ravindranath, Ph D, FNA Sc, FTWAS, Manesar

- 23 Prof Ajay Kumar Sood, Ph D, FNA, FA Sc, FN A Sc, FTWAS, Bangalore

Special Invitees

- 1 Prof M G K Menon, Ph D (Bristol), D Sc (h c), FNA, FA Sc, Hon FN A Sc, FTWAS, FRS, Mem Pontifical Acad Sc, New Delhi

- 2 Dr (Mrs) Manju Sharma, Ph D, FNA Sc, FAMI, FISAB, FN A Sc, FTWAS, New Delhi

- 3 Prof PN Tandon, M S, D Sc (h c), FRCS, FAMS, FNA, FA Sc, FN A Sc, FTWAS, Delhi

- 4 Prof Girjesh Govil, Ph D, FNA, FA Sc, FTWAS, Mumbai

The *Proceedings of the National Academy of Sciences, India*, is published in two Sections Section A (Physical Sciences) and Section B (Biological Sciences) Four parts of each section are published annually (since 1960).

The Editorial Board in its work of examining papers received for publication is assisted, in an honorary capacity by a large number of distinguished scientists. The Academy assumes no responsibility for the statements and opinions advanced by the authors. The papers must conform strictly to the rules for publication of papers in the *Proceedings*. A total 25 reprints is supplied free of cost to the author or authors. The authors may ask for a reasonable number of additional reprints at cost price, provided they give prior intimation while returning the proof.

Communication regarding contributions for publications in the *Proceedings*, books for review, subscriptions etc. should be sent to the Managing Editor, The National Academy of Sciences, India, 5, Lajpatrai Road, Allahabad - 211002 (India)

Annual Subscription for both Sections : Rs. 500.00; for each Section Rs. 250.00; Single Copy : Rs. 100.00. Foreign Subscription : (a) for one Section : US \$100, (b) for both Sections US \$200.
(Air-Mail charges included in foreign subscription)

PROCEEDINGS
OF THE
NATIONAL ACADEMY OF SCIENCES, INDIA
2004

VOL LXXIV

SECTION-A

PART III

Ternary complexes of bivalent metals with kojic acid or maltol and selected amino acids

MOHD. ZAKEE and DEVA DAS MANWAL*

Department of Chemistry, Nizam College, Osmania University, Hyderabad – 500 001, India

Received April 30, 2002, Revised April 6, 2003, Accepted September 18, 2003

Abstract

Stability constants associated with formation of ternary complexes of the type MLA [where M = Co(II), Ni(II), Cu(II) and Zn(II), L = 3-Hydroxy-2-methyl-4(H)-pyran-4-one (maltol) or 5-Hydroxy-2-(hydroxy methyl)-4(H)pyran-4-one (kojic acid), A = lysine, arginine, histidine, aspartic acid and glutamic acid] are determined potentiometrically at 30°C and $I = 0.1\text{M}$ KNO_3 , in aqueous medium. Ternary complexes of Cu(II) with histidine or aspartic acid suffer loss of stability because of less number of sites available on square planar copper compared to distorted octahedral copper.

(Keywords: potentiometry / stability constants / maltol / kojic acid / amino acids)

Introduction

Specificity leading to selective and preferred interactions is obviously important in biological systems. As far as species containing metal ions of $3d$ series are concerned, it is now well established that among mixed ligand complexes those composed of the π accepting imidazole group of histidine residue and an O donor are

preferably formed¹⁻³. Certainly another possibility favouring specificity and selectivity are stacking interactions between aromatic residues^{4,5}. As one may expect that specific interactions, for example between nucleotides and amino acids, play a role during the first step of biochemical evolution, we felt that it would be of interest to study the stability of single ternary system consisting of metal ion / amino acid / oxygen donor in order to see if certain ligand combinations are favoured and if any selectivity is achieved.

Owing to the biological importance of histidine, we have undertaken the study of selected amino acids with transition metals. In continuation of our earlier studies^{6,7}, we now report the stabilities associated with the metal complexes of selected amino acids with bivalent metals in the presence of oxygen donors such as kojic acid or maltol.

Materials and Method

The ligands kojic acid and maltol were obtained from Lancaster (UK). Other ligands, lysine, arginine, histidine, aspartic and glutamic acid were obtained from Sigma Chemical Company. The metal salts of Co(II), Ni(II), Cu(II) and Zn(II) were of AnalaR grade, and their solutions were standardized volumetrically by titration with the sodium salt of EDTA.⁸ Potentiometric measurements were carried out at 30°C with 0.1 M KNO₃ as background electrolyte in aqueous medium using a control dynamics pH meter. The pH meter readings were plotted against *a* (moles of base added per mole of ligand) or *m* (moles of base added per mole of metal ion). Calculations were made with the help of BEST computer programme⁹.

Results and Discussion

Binary Complexes : The structures of the ligands and metal complexes are shown in Fig. 1. In the binary complexes it is well established that histidine acts as the tridentate ligand binding through the carboxylate oxygen, amino nitrogen and imidazole nitrogen. But the other tridentate amino acids of the same groups (i.e. arg. or lys.) would necessarily be bidentate with a proton intact (whose pK_a is 11.98 and 10.20 for arg. and lys. respectively) on the side chain resulting in the protonated complexes (MHA). Hence, the binary constants refer to values for protonated complexes of lys. or arg. The stability constants for normal complexes could not be calculated owing to precipitation in the higher pH region. The values obtained are in good agreement with the values found in literature^{6,7}.

Ternary Complexes: The potentiometric titration curves of ternary complexes, MLA where M = Co(II), Ni(II) and Zn(II), L = maltol or kojic acid, A = lys or arg in 1:1:1 ratio show inflection at $m = 1$ and $m = 2$. Hence, the formation of ternary complexes are considered in a stepwise manner in which the ligand maltol or kojic acid binds first to the metal ion followed by the stepwise addition of amino acids. In case of histidine, two inflections obtained one at $m = 1$ and another at $m = 3$. The ternary complexes of Cu(II) show single inflection at $m = 2$ (in case of lys. or arg.) or $m = 3$ (in case of histidine).

The titration curves for glutamic acid or aspartic acid with bivalent metals in presence of maltol or kojic acid show inflection at $m = 3$. The calculations were made with BEST computer program⁹ and the values thus obtained are given in Table 1.

The stability of the various ternary complexes and the corresponding binary complexes have been compared in terms of the parameter $\Delta \log K$. Perusal of $\Delta \log K$ values (Table 1) reveals that the $\Delta \log K$ values for ternary complex [maltol-Cu-histidine] are more negative (-0.72) when compared to the value for [maltol-Cu-lys] or [maltol-Cu-arg]. The reason for this observation is due to the fact that in ternary complex of maltol or kojic acid and amino acid, the Cu(II) is essentially square planar because of the strong ligand field exerted by maltol or kojic acid. In such cases histidine would be forced to be bidentate and this would lead to decreased stability (i.e. $\Delta \log K = -0.72$). This sort of problem is not encountered by lys. or arg. as they behave bidentate in ternary as well as binary complexes. Hence the observed $\Delta \log K$ values (-0.43 or 0.44) have the origin of statistical reasons. Further these values are comparable with the values observed for the alanine complex (-0.40).

Perusal of the $\Delta \log K$ values also show that aspartic acid is destabilized considerably in [asp. + Cu + Maltol] or [asp. + Cu + Kojic acid] ternary complexes (i.e. -0.79 or -0.71) when compared to the ternary complexes of alanine ($\Delta \log K \approx -0.40$ or -0.45). The reason for destabilization is that asp. in binary complexes binds in a tridentate fashion to aquocupric ion, but when it comes to the ternary complexes containing strong field ligand like maltol or kojic acid, it becomes bidentate because the distorted octahedral Cu(II) ion would be converted to square planar making less number of coordinating sites available for asp.

Comparison of $\Delta \log K$ values for other metals (Co(II), Ni(II) and Zn(II)) show that the ternary complexes of glu. are more stable than the ternary complexes of asp.

whether the primary ligand is kojic acid or maltol. The $\Delta\log K$ values obtained for all these metals are consistent with the values obtained on the statistical grounds alone.

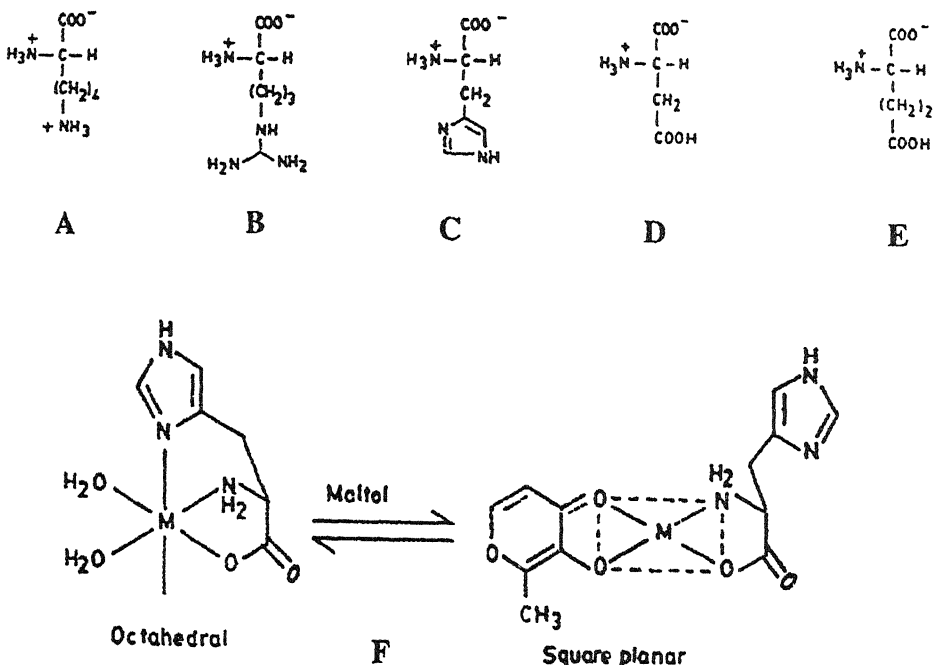


Fig. 1—Ternary complexes of bivalent metals with kojic acid or maltol and selected amino acids
A = lysine, B = arginine, C = histidine, D = aspartic acid, E = glutamic acid, F = tentative structure
showing histidine binding as tridentate in binary and bidentate in ternary complexes

The $\Delta\log K$ values obtained for ternary complexes of [asp. + M(II) + KA/MA] are less negative than values for [asp. + Cu(II) + KA/MA]. This shows that all the metal ions except Cu(II) have octahedral geometry in which asp. binds to the metal ion through three sites as it binds in binary complexes. Hence, in all these metal ions except Cu(II), the destabilisation due to loss of denticity is not observed.

Table 1— logarithms of stability constants of ternary complexes and their corresponding $\Delta \log K$ values
[$T = 30^{\circ}\text{C}$, $\mu = 0.1\text{ mol dm}^{-3}$ (KNO_3), aqueous medium]

Ligands	Co(II)	Ni(II)	Cu(II)	Zn(II)
<i>Kojic acid as Primary Ligand (L)</i>				
Alanine	8.65 (± 0.05) -0.38	10.06 (± 0.06) -0.37	14.05 (± 0.07) -0.45	9.56 (± 0.02) -0.39
Lysine HCl	ppt	9.78 (± 0.06) -0.40	13.73 (± 0.08) -0.44	ppt
Arginine HCl	ppt	9.82 (± 0.05) -0.39	13.68 (± 0.03) -0.41	ppt
Histidine HCl	12.13 (± 0.05) -0.42	12.73 (± 0.03) -0.41	15.34 (± 0.04) -0.68	11.03 (± 0.05) -0.43
Aspartic acid	9.98 (± 0.05) -0.49	11.77 (± 0.06) -0.48	14.19 (± 0.03) -0.71	10.17 (± 0.05) -0.49
Glutamic acid	8.86 (± 0.08) -0.40	10.33 (± 0.07) -0.42	13.80 (± 0.04) -0.45	9.94 (± 0.06) -0.45
<i>Maltol as Primary Ligand (L)</i>				
Alanine	9.28 (± 0.08) -0.35	10.77 (± 0.07) -0.30	15.14 (± 0.05) -0.40	10.26 (± 0.06) -0.32
Lysine HCl	ppt	10.45 (± 0.08) -0.37	14.78 (± 0.07) -0.43	ppt -
Arginine HCl	ppt	10.46 (± 0.07) -0.39	14.69 (± 0.06) -0.44	ppt
Histidine HCl	12.72 (± 0.07) -0.43	13.41 (± 0.08) -0.37	16.34 (± 0.08) -0.72	11.67 (± 0.07) -0.42
Aspartic acid	10.60 (± 0.06) -0.47	12.48 (± 0.08) -0.41	15.15 (± 0.03) -0.79	10.84 (± 0.06) -0.45
Glutamic acid	9.46 (± 0.08) -0.40	11.00 (± 0.06) -0.39	14.82 (± 0.04) -0.47	10.61 (± 0.05) -0.41

Sigma fit values are given in the parentheses.

$$\Delta \log K = \log K_{\text{MLA}}^M - [\log K_{\text{MA}}^M + \log K_{\text{ML}}^M]$$

Acknowledgements

One of the author (M.Z.) thanks the U.G.C. and the Principal, Mumtaz College for awarding teacher fellowship under FIP.

References

- 1 Enei, H , Nakazawa, H , Matsui, H , Okumura, S & Yamada, H (1973) *Japan Patent Kokai* 73 80,785 (Chemical Abstract No 80 58411C)
- 2 Pieben, M , Romero, C , Tirapegni, C , & Toha, J C (1969) *Z Naturforsch* **24b** 508
- 3 Pieber, M , Romero, C & Toha, J C (1969) *Arch Biol, Med Expz* **6** 58
- 4 Mitchell, P R & Sigel, H (1978) *J Am Chem Soc* **100** 1564
- 5 Mitchell, P R , Prijs , B & Sigel, H (1979) *Helv Chim Acta* **62** 1723
- 6 Rani, Usha, G & Manwal, Deva Das (2000) *J Electrochem Soc India* **49(1)** 13
- 7 Rani, Usha, G & Manwal, Deva Das (1999) *J Electrocchem Soc India* **48(4)** 335
- 8 Schwarzenbach, G (1957) *Complexeometric Titrations*, Interscience, New York, p 27
- 9 Motekaitis, R J & Marten, A E (1982) *Can J Chem* **60** 168 & 2403

Intramolecular hydrophobic ligand-ligand interaction in mixed ligand complexes containing kojic acid or maltol and aliphatic amino acids

MOHD. ZAKEE and DEVA DAS MANWAL*

Department of Chemistry, Nizam College, Osmania University, Hyderabad - 500 001, India

Received April 30, 2002, Revised March 31, 2003, Accepted September 18, 2003

Abstract

Mixed ligand complexes of the type $[ML(Aa)]$, where $M = \text{Co(II)}, \text{Ni(II)}, \text{Cu(II)} \text{ and } \text{Zn(II)}$, $L = \text{kojic acid or maltol}$, $Aa = \text{amino acids, viz glycinate, alaninate, } \alpha\text{-aminobutyrate, norvaline, norleucine, valinate, leucinate or isoleucinate}$ have been studied by potentiometric pH titrations. The potentiometric measurements reveal a slightly higher formation tendency for the system with leucinate as compared to those with alaninate. This increase in stabilization is attributed to an intramolecular hydrophobic ligand-ligand interaction between π electron cloud of kojic acid or maltol and the isopropyl group of leucine.

(Keywords : potentiometry / ternary complexes / formation constants / maltol / kojic acid / amino acids)

Introduction

Hydrophobic interactions are known to occur among other noncovalent interactions in biomolecules,¹ they contribute to the formation of distinct structural features.² Such hydrophobic interactions occur between two aliphatic groups or between aliphatic and aromatic moieties; the ring stacking between two aromatic systems is also often listed within this category.^{3,4}

In continuation of our earlier studies^{5,6} on the hydrophobic studies, we now report the stability constants associated with ternary complexes containing kojic acid or maltol as primary ligand and bivalent metals in presence of amino acids with aliphatic side chains such as glycine, alanine, α -aminobutyric acid, norvaline, norleucine, valine, leucine or isoleucine. These amino acids were selected such that the side chain varied in length and volume from a methyl group as in alanine to n-butyl group as in norleucine or an isopropyl group as in leucine.

It is obvious that the methyl side chain in alanine is too short to allow any interaction with the aromatic rings within the square planar Cu(II) complexes and for the octahedral metal complexes, it is expected to be insignificant if it does occur at all. The reason why alanine and not glycine was selected as the basis for the comparison is that Martin⁷ has shown that the stability of the glycine complexes is often somewhat exceptional. The alanine complexes are therefore a better basis for comparison.

Materials and Method

The ligands, maltol, kojic acid were obtained from Lancaster (U.K). The amino acids were obtained from Sigma Chemical Company. The metal salts of Co(II), Ni(II), Cu(II), and Zn(II) were of AnalaR grade and their solutions were standardized volumetrically by titration with the sodium salt of EDTA.⁸ Potentiometric measurements were carried out at 30°C in aqueous medium (with 0.1 M KNO₃ as background electrolyte) using control dynamics pH meter. The pH meter readings were plotted against a (moles of base added per mole of ligand) or m (moles of base added per mole of metal ion). Calculations were carried out with the help of computer program - BEST.⁹

Results and Discussion

Binary stability constants pertaining to the interaction of amino acids, kojic acid and maltol with bivalent metals were redetermined to have a better comparison between binary and ternary complexes under the same conditions and the values thus obtained are in good agreement with the literature values^{5,6}.

The potentiometric titration curves of [ML(Aa)] in 1:1:1 ratio where L = maltol or kojic acid; Aa = amino acids under study; M = Co(II), Ni(II), and Zn(II), show a inflection at $m = 1$ followed by another at $m = 2$. The ternary curve coincides with binary curve upto $m = 1$ where 1:1 [ML] complexes are formed. This indicates that only 1:1[M-L] complexes are formed in the region $m = 0$ to $m = 1$ and amino acid does not coordinate with M(II) in this region. The divergence of mixed ligand curve for the binary [M-L] curve beyond $m = 1$ suggests the coordination of amino acid as a secondary ligand. Hence, the formation of ternary complexes can be considered to occur in stepwise equilibria. The ternary constants thus obtained are presented in Table 1. In case of Cu(II) complexes in 1:1:1 ratio, the titration curve shows an inflection at $m = 2$ indicating the simultaneous complexation.

Table 1— logarithms of stability constants of ternary complexes

[$T = 30^{\circ}\text{C}$, $\mu = 0.1 \text{ mol dm}^{-3}$ (KNO_3), aqueous medium]

Ligands	Co(II)	Ni(II)	Cu(II)	Zn(II)
<i>Kojic acid as primary ligand (L)</i>				
Glycine	8.94	10.37	14.12	9.64
α -aminobutyric acid	8.60	9.79	14.20	9.32
Norvaline	8.63	10.39	14.42	9.53
Norleucine	8.70	10.17	14.58	9.42
Valine	8.68	10.36	14.36	9.50
Leucine	8.70	10.23	14.33	9.60
Isoleucine	8.65	10.19	14.29	9.50
<i>Maltol as primary ligand (L)</i>				
Glycine	9.57	11.13	15.18	10.32
α -aminobutyric acid	9.24	10.51	15.31	10.04
Norvaline	9.27	11.11	15.51	10.27
Norleucine	9.35	10.89	15.68	10.15
Valine	9.35	11.10	15.49	10.28
Leucine	9.35	10.97	15.46	10.33
Isoleucine	9.31	10.93	15.40	10.24

Sigma fit value are in the range ± 0.05 to 0.08 log units

Table 2 lists the $\Delta\log K$ values along with $\Delta\Delta\log K$ values. The parameters $\Delta\log K$ and $\Delta\Delta\log K$ are used to characterise the stability of ternary complexes formed.

Negative $\Delta\log K$ values suggest that the binary complexes are more stable than the ternary complexes, whereas a positive $\Delta\log K$ suggests greater stability of the ternary complexes. The magnitude of $\Delta\log K$ values depends on the denticities of both the ligands and coordination number of metal ion. In the present study kojic acid or maltol and all amino acids are listed as bidentate ligands. If both ligands in ternary complexes are bidentate and geometry is octahedral, then the statistical factor would be 5/12 and its corresponding log value shall be -0.4. Thus if the obtained $\Delta\log K$ values are positive or less negative than the statistical value (i.e. -0.4) then ternary complexes are more stable. However, it should be noted here that negative values of $\Delta\log K$ do not preclude the formation of ternary complexes in solution.

Table 2- Comparison of $\Delta\log K$ and $\Delta\Delta\log K$ values for ternary complexes

[$T = 30^\circ\text{C}$, $\mu = 0.1 \text{ mol dm}^{-3}$ (KNO_3), aqueous medium]

Secondary Ligands (A)	Co(II)	Ni(II)	Cu(II)	Zn(II)
<i>Kojic acid as primary ligand (L)</i>				
Glycine	-0.43	-0.48	-0.46	-0.43
α -aminobutyric acid	-0.36 (+0.02)	-0.33 (+0.04)	-0.39 (+0.06)	-0.35 (+0.04)
Norvaline	-0.32 (+0.05)	-0.29 (+0.08)	-0.33 (+0.12)	-0.33 (+0.06)
Norleucine	-0.28 (+0.10)	-0.24 (+0.13)	-0.30 (+0.15)	-0.30 (+0.09)
Valine	-0.32 (+0.06)	-0.28 (+0.09)	-0.33 (+0.12)	-0.29 (+0.10)
Leucine	-0.26 (+0.12)	-0.22 (+0.15)	-0.28 (+0.17)	-0.26 (+0.13)
Isoleucine	-0.35 (+0.03)	-0.32 (+0.05)	-0.37 (+0.08)	-0.34 (+0.05)

Table 2 Contd...

Table 2 Contd. .

	<i>Maltol as primary ligand (L)</i>			
Glycine	-0.40	-0.36	-0.44	-0.38
α -aminobutyric acid	-0.32	-0.25	-0.32	-0.26
	(+0.03)	(+0.05)	(+0.08)	(+0.06)
Norvaline	-0.28	-0.21	-0.28	-0.22
	(+0.07)	(+0.09)	(+0.12)	(+0.10)
Norleucine	-0.23	-0.16	-0.24	-0.20
	(+0.12)	(+0.14)	(+0.16)	(+0.12)
Valine	-0.25	-0.18	-0.24	-0.14
	(+0.10)	(+0.12)	(+0.16)	(+0.18)
Leucine	-0.21	-0.12	-0.19	-0.16
	(+0.14)	(+0.18)	(+0.21)	(+0.16)
Isoleucine	-0.29	-0.22	-0.30	-0.23
	(+0.06)	(+0.08)	(+0.10)	(+0.09)

$\Delta \log K = \log K_{MLA}^M - [\log K_{MA}^M + \log K_{ML}^M]$ The $\Delta\Delta\log K$ values are presented in parenthesis.

$\Delta\Delta\log K = [\Delta\log K_1 - \Delta\log K_2]$, where $\Delta\log K_1$ is for the reaction ($M + L + \text{amino acids except alanine}$) and $\Delta\log K_2$ is for the reaction ($M + L + \text{alanine}$).

Alanine is taken as a reference for zero based hydrophobic interactions

The determined stability constants of the ternary complexes i.e., especially the values of $\Delta\Delta\log K$, give hints into the direction of an intramolecular hydrophobic ligand-ligand interaction in $M(L)(Aa)$ complexes. A tentative structure of such a ternary complex is shown in Fig. 1. In this structure the isopropyl group of the amino acid is located above the π electron cloud of kojic acid / maltol, and the two ligands are linked together by the metal ion; in other words, the metal ion promotes the hydrophobic interactions.

Extent of the intramolecular ligand-ligand interactions

Based on the results, it can readily be understood why the M(L)(Aa) complexes show enhanced stability: the isopropyl group of amino acid is ideally suited for hydrophobic ligand-ligand interactions. The occurrence of complexes with a structure similar to other shown in Fig. 1, which is responsible for the slight increase in stability does not imply that all the M(L)(Aa) ternary species exist in this closed form.

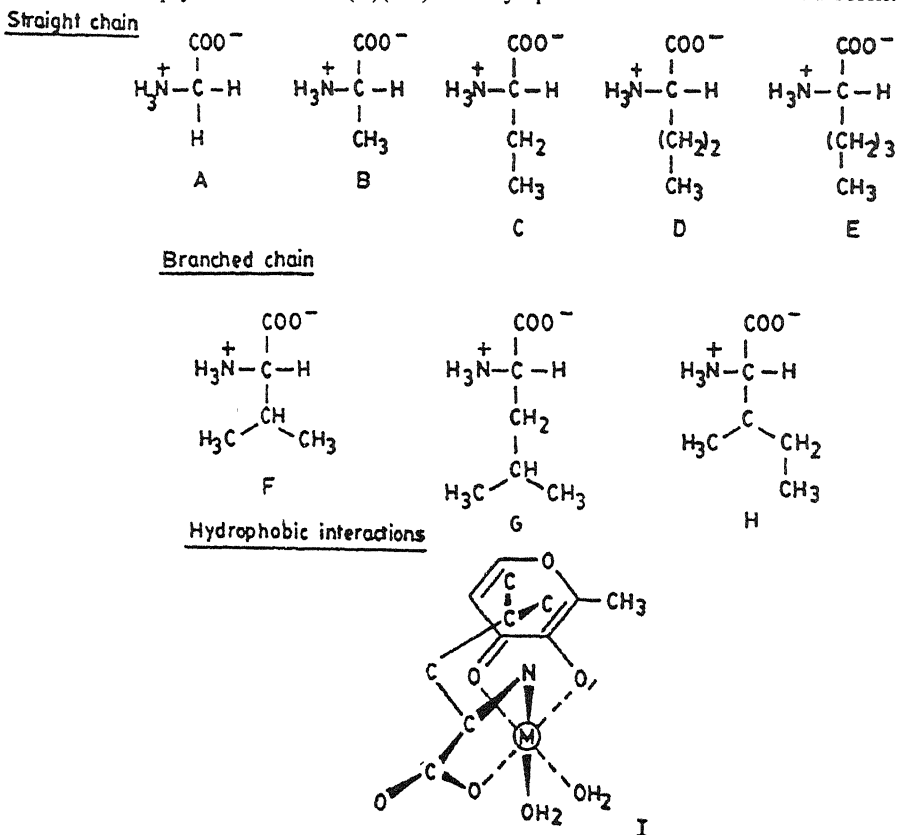
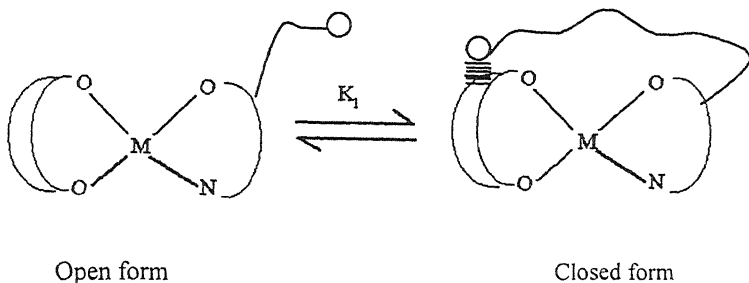


Fig 1—Structures of the amino acids under study

A = glycine, B = alanine, C = α -aminobutyric acid, D = norvaline, E = norleucine, F = valine, G = leucine, H = isoleucine, I = tentative structure showing the intramolecular hydrophobic interactions in the ternary complex of [maltool-M-leucine]

In solution there is certainly an intramolecular, and therefore concentration independent, equilibrium between an 'open' and a closed form as shown below.



The dimensionless constant K_1 of this intramolecular equilibrium is defined by the equation 1.

$$K_1 = 10^{\Delta\Delta\log K_{-1}} \quad (1)$$

The other parameter $\Delta\Delta\log K$ is given by relationship

$$\Delta\Delta\log K = (\Delta\log K_1 - \Delta\log K_2) \quad (2)$$

where $\Delta\log K_1$ is for the reaction $[M + L + Aa]$ and $\Delta\log K_2$ relates to the reaction $[M + L + \text{alanine}]$.

The percentage of stacked isomers in the systems are also calculated with the relationship 3:

$$\%(\text{MLA})_{\text{HI}} = [100 * K_1 / (1 + K_1)] \quad (3)$$

The values of K_1 and % (MLA)_{H1} for these systems are presented in Table 3. The perusal of parameters associated with hydrophobic interactions reveal that stabilization in ternary complexes with respect to amino acids follow the increasing order :

Straight chain:

α -aminobutyric acid < Norvaline < Norleucine

Branched chain

Isoleucine < Valine < Leucine

It is obvious from the above results that the extent of the intra-molecular hydrophobic interactions in these ternary complexes are dependent on a) length and b) possibly also on the bulkiness of the aliphatic side chain of the amino acid.

With increase in chain length (*viz.*, as propyl and butyl groups in norvaline or norleucine) there is better overlap between two ligands which results in maximum of hydrophobic interaction as reflected by their parameters.

Comparison of % stacked isomers formed (Table 3) for leucine and norvaline system reveal that leucine (having branched side chain) forms better stacked isomers than the norvaline, though both ligands have the same number of carbon atoms. This is an evidence that the bulkiness of aliphatic side chain of the amino acid play a role in enhancing the hydrophobic interactions in these ternary complexes.

Table 3— Parameters showing the extent of intramolecular hydrophobic interaction in ternary complexes
[$T = 30^\circ\text{C}$, $\mu = 0.1 \text{ mol dm}^{-3}$ (KNO_3), aqueous medium]

Secondary Ligands (A)	Parameters	Co(II)	Ni(II)	Cu(II)	Zn(II)
<i>Kojic acid as primary ligand (L)</i>					
α -aminobutyric acid	K_I	0.047	0.096	0.148	0.096
	%(MLA_{HI})	4.48	8.75	12.89	8.75
Norvaline	K_I	0.148	0.202	0.318	0.148
	%(MLA_{HI})	12.89	16.80	24.13	12.89
Norleucine	K_I	0.258	0.348	0.412	0.230
	%(MLA_{HI})	20.50	25.82	29.17	18.70
Valine	K_I	0.148	0.230	0.318	0.258
	%(MLA_{HI})	12.89	18.70	24.13	20.50
Leucine	K_I	0.318	0.412	0.479	0.348
	%(MLA_{st})	24.13	29.178	32.38	25.82

Table 3 Contd

Table 3 Contd

Isoleucine	K_I	0.071	0.122	0.202	0.122
	%(MLA_{HI})	6.67	10.87	16.80	10.87
<i>Maltol as primary ligand (L)</i>					
α -aminobutyric acid	K_I	0.071	0.122	0.202	0.148
	%(MLA_{HI})	6.67	10.87	16.80	12.89
Norvaline	K_I	0.174	0.230	0.3182	0.258
	%(MLA_{HI})	14.82	18.70	24.13	20.50
Norleucine	K_I	0.318	0.30	0.445	0.318
	%(MLA_{HI})	24.13	27.54	30.79	24.13
Valine	K_I	0.258	0.318	0.445	0.513
	%(MLA_{HI})	20.50	24.13	30.79	33.91
Leucine	K_I	0.380	0.513	0.622	0.445
	%(MLA_{HI})	27.54	33.91	38.35	30.79
Isoleucine	K_I	0.148	0.202	0.258	0.230
	%(MLA_{HI})	12.89	16.80	20.50	18.70

Further, the values of % stacked isomers of isoleucine complexes are more or less same as that of values of α -aminobutyric acid complexes, indicating that though isoleucine has branched side chain it behaves as α -aminobutyric acid in ternary complexes (i.e. it appears to react as an ethyl substituted α -aminobutyric acid). Hence it is concluded that in hydrophobic interactions, steric restriction does exist. The order with respect to primary ligands (*maltol* > *kojic acid*) is in line with basicity of the ligands. Again order with respect to metals is in conformity with Irving Williams natural order of stabilities¹⁰.

Acknowledgements

Mohd. Zakee thanks the U.G.C. and the Principal, Mumtaz College for awarding teacher fellowship under F.I.P.

References

- 1 Frieden, E J (1975) *J Chem Educ* **52** 754
- 2 Scheraga, H A (1979) *Acc Chem Res* **12** 7
- 3 Fischer, B E , & Sigel, H (1980) *J Am Chem Soc* **102** . 2998
- 4 Sigel, H (1989) *Pure & Appl Chem* **61**(5) . 923
- 5 Rani Usha, G. & Manwal, Deva Das (2000) *J Electrochem Soc India* **49**(1) 17
- 6 Rani Usha , G. & Manwal, Deva Das (2001) *J Electrochem Soc India* **50**(1) . 27
- 7 Martin, R B (1979) *Met ions Biol Syst* **9** 1
- 8 Schwarzenbach (1957) *Complexometric titration*, Interscience, New York, p 77
- 9 Motekaitis, R J & Martell, A E (1982) *Can J Chem* **60** 168 & 2403
- 10 Irving, H & Williams, R J P , (1953) *J Chem Soc* 3192

Synthesis and characterization of Mn(II), Cr(III) and Fe(III) complexes with 4,4'-diaminostilbene-2,2'-disulphonate Schiff bases

K. SIDDAPPA* and S. D. ANGADI

Department of Chemistry, Gulbarga University, Gulbarga- 585 106, Karnataka, India.

E-mail : siddappa_k1@rediffmail.com

**Author for correspondence*

Received January 25, 2003; Revised April 17, 2003, Accepted September 18, 2003

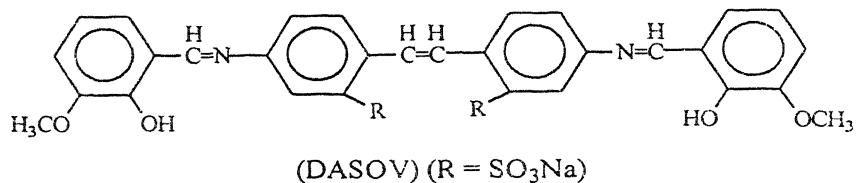
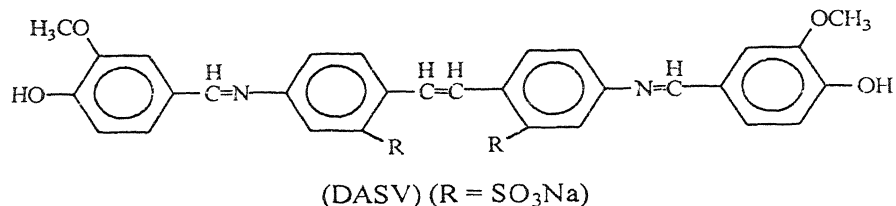
Abstract

A few Mn(II), Cr(III) and Fe(III) complexes have been prepared from 4,4'-diaminostilbene-2,2'-disulphonate (DAS) with anillin ($L = DASV$) and o-vanillin ($L' = DASOV$) Schiff bases. These complexes confine to stoichiometry of the type $[Mn_2L_2Cl_4(H_2O)_4]$, $[Fe_2L_2Cl_6(H_2O)_2]$, $[Cr_2L_2Cl_6(H_2O)_2]$ and $[Mn L'_2(H_2O)_4]$, $[Fe_2 L'_2Cl_2(H_2O)_2]$, $[Cr_2 L'_2(H_2O)_2]$. The complexes have been characterized by elemental, conductance, magnetic and spectral data. The infrared spectra of the complexes suggest that nitrogen and oxygen are involved in the bonding in case of DASOV ligand. However in DASV ligand the OH groups are not involved in bond formation. The magnetic and electronic spectra indicate that Mn(II), Cr(III) and Fe(III) complexes have octahedral configuration.

(Keywords IR/UV/stilbenediamine Schiff bases/Mn(II), Cr(III)/Fe(III))

Introduction

There have been a number of studies on metal complexes of Schiff bases formed from salicylaldehyde, substituted salicylaldehydes with various aromatic amines¹⁻⁵. 4,4'-diaminostilbene-2,2'-disulphonate and its derivatives with vanillin and o-vanillin constitute a very important class of compounds because they are biologically important. Substituted stilbene diamine derivatives have been found to possess antiviral activity⁶. The literature⁷ study shows that there appears no reports on corresponding chelates of Mn(II), Cr(III) and Fe(III) with ligands of stilbene diamines. Consequently the present work deals with the study of nature of metal-ligand bonding by spectrochemical and magnetochemical data with the following ligands (DASV and DASOV).



Materials and Method

The chemicals used in the preparation of ligands were of reagent grade. The following metal salts ($MnCl_2 \cdot 4H_2O$, $FeCl_3 \cdot 6H_2O$, $CrCl_3 \cdot 6H_2O$) were used for preparation of metal complexes.

Preparation of ligands : In a typical preparation to methanol solution of (0.04 mole) vanillin was added 0.02 mole of 4,4'-diaminostilbene-2,2'-disulphonate and the reaction mixture was refluxed for about 2 h. The Schiff base (DASV) separated after cooling was filtered and recrystallised from ethanol. The same procedure was followed for o-vanillin Schiff base (DASOV).

Preparation of metal complexes : To an ethanolic solution of 0.01 mole of DASV / DASOV was added 0.01 mole of Metal(II / III) chloride and the reaction mixture was refluxed for about 1 h and then sodium acetate (2g) was added to the reaction mixture and the refluxing was continued for about 3 h. The complex so obtained was filtered, washed with water and then with alcohol and finally dried in vacuum over fused calcium chloride.

Analysis : The complexes were analyzed for their metal, chloride and nitrogen contents by standard methods⁸. The results of the elemental analysis are shown in Table 1.

Physical Measurements : The molar conductance measurements of the complexes in DMF at a concentration $\sim 10^{-3}$ M were taken with an ELICO conductivity bridge having a cell of cell constant 0.829 cm⁻¹ manufactured by Electronic Industrial Instruments Co., Hyderabad. The magnetic measurements were taken at room temperature on a Gouy balance with glass tube calibrated for diamagnetism. The electronic spectra were obtained with a Beckman DB-2 recording spectrometer using 1 cm glass cell in the region 350-1200 nm. The weighed samples were dissolved in DMF and diluted to the required concentration $\sim 10^{-4}$ M. The IR spectra of the ligands and the complexes in KBr pellets were recorded in a Perkin Elmer 621 spectrophotometer in the range 4000 - 400 cm⁻¹. The low region IR spectra in the range of 450 - 250 cm⁻¹ were recorded in polyethelene pellets.

Results and Discussion

The Mn(II) and Fe(III) complexes were reddish brown, where as those of Cr(III) were reddish in colour. All these complexes have 1:1 stoichiometry (Table 1). They were insoluble in common organic solvents. The molecular weight of these complexes could not be determined because of their insolubility in nitrobenzene. However, they were soluble to a limited extent in DMF, DMSO and pyridine. The molar conductance values in DMF were too low to account for any dissociation. Hence, they can be regarded as non-electrolytes⁹.

Magnetic data : The magnetic moments obtained at room temperature for these complexes are listed in Table 1.

The magnetic moments for manganese(II) complexes are in the range of 5.35 to 5.85 B.M. suggesting the formation of spin-free complexes. This closely agrees with the expected value of about 5.90 B.M for Mn(II) complexes¹⁰.

The chromium(III) complexes exhibit magnetic moments in the range of 3.55-3.87 B.M agreeable to spin only value of chromium(III) complexes with octahedral configuration, viz., 3.88 B.M¹¹.

The iron(III) complexes are expected¹² to possess magnetic moments very close to spin only value of 5.92 B.M. The magnetic moments obtained for these iron(III) complexes were in the range of 5.89-5.90 B.M. All these complexes have lower than the spin-only values because of polymerization.

238
Table 1—Elemental analysis, colour, conductance, magnetic and electronic spectral data for DASV and DASOV and their met. complexes

Sl No	Empirical formula of ligand/complex	Colour		% Analysis found (calculated)			$\gamma_{\text{in}} \Omega^{-1}$ (mole ⁻¹ . cm ⁻¹)	μ_{eff} (B M)	Bands (cm ⁻¹)
		C	H	N	M	Cl			
1	$L = (\text{DASV})$ $(C_{30}H_{24}N_2S_2O_{10}Na_2)$	Light pink	52.65 (52.78)	3.46 (3.51)	4.01 (4.10)	-	-	-	35000
2	$[\text{Mn}_2(C_{30}H_{24}N_2S_2O_{10}Na_2)_2$ $Cl_4 2H_2O]$	Light brown	44.42 (42.67)	2.88 (3.08)	3.29 (3.31)	6.32 (6.46)	8.32 (8.41)	10.0	5.85 22480 21176 19230
3.	$[\text{Fe}_2(C_{30}H_{24}N_2S_2O_{10}Na_2)_2$ $Cl_6 2H_2O]$	Brown	41.62 (41.75)	2.89 (3.01)	3.12 (3.21)	6.36 (6.45)	12.17 (12.32)	14.0	5.89 11200 16680
4.	$[\text{Cr}_2(C_{30}H_{24}N_2S_2O_{10}Na_2)_2$ $Cl_6 2H_2O]$	Brick red	41.86 (41.94)	2.81 (3.02)	3.15 (3.26)	5.96 (6.05)	12.19 (12.38)	22.0	3.55 18200 22800
5	$L' = (\text{DASOV})$ $(C_{30}H_{24}N_2S_2O_{10}Na_2)$	Yellow w	52.71 (52.78)	3.47 (3.51)	4.02 (4.10)	-	-	-	38000
6	$[\text{Mn}_2(C_{30}H_{22}N_2S_2O_{10}Na_2)_2$ $4H_2O]$	Dark red	45.65 (46.72)	3.13 (3.37)	3.52 (3.63)	7.98 (7.12)	-	15.4	5.35 13200 20000 24200
7.	$[\text{Fe}_2(C_{30}H_{22}N_2S_2O_{10}Na_2)_2$ $Cl_2 2H_2O]$	Dark brown	45.56 (45.62)	3.01 (3.04)	3.46 (3.54)	7.02 (7.07)	4.41 (4.49)	30.5	5.90 20000 30000
8	$[\text{Cr}_2(C_{30}H_{22}N_2S_2O_{10}Na_2)_2$ $Cl_2 2H_2O]$	Brick red	48.78 (48.94)	3.05 (3.26)	3.69 (3.80)	6.87 (7.07)	4.69 (4.82)	12.5	3.87 18400 24400 34400

K. SIDDAPPA and S. D. ANGADI

Electronic spectra : The observed band maxima for the complexes are listed in Table 1. The electronic spectra of manganese(II) complexes show high intensity band maxima observed in the 24000-22480 cm⁻¹ region which has been regarded as ligand metal charge transfer band. The remaining *d-d* bands are observed in the region 20000-19000 and 13000 cm⁻¹¹³. The Fe(III) complexes show a high intensity band around 25000 cm⁻¹ due to the ligand metal charge transfer, this obscures the other *d-d* transitions in the visible region¹⁴. It has been observed in the diffuse reflectance spectra that iron(III) complexes exhibit two bands in the 12500-10640 and 20000-16670 cm⁻¹ regions attributable to $^6A_{1g} \rightarrow ^4T_{1g}(G)$ and $^6A_{1g} \rightarrow ^4A_{1g}(G)$ transitions respectively¹⁵. In these complexes we observe weak and broad band maxima in the regions 12500-11750 cm⁻¹ and 16140-16000 cm⁻¹ and these can be attributed to the $^6A_{1g} \rightarrow ^4T_{1g}(G)$ and $^6A_{1g} \rightarrow ^4A_{1g}(G)$ transitions.

Octahedral chromium(III) generally exhibits two spin allowed bands in the visible region¹⁶. The low energy transition $^4A_{2g} \rightarrow ^4T_{2g}$ occurs in the 17000-19000 cm⁻¹ regions and another band due to $^4A_{2g} \rightarrow ^4T_{1g}(F)$ transition is present in the region 27000-30000 cm⁻¹. In these complexes of chromium(III), we observe two bands in the following regions 25000-21720 cm⁻¹ and 18400-19230 cm⁻¹. These have been attributed respectively to $^4A_{2g} \rightarrow ^4T_{1g}(F)$ and $^4A_{2g} \rightarrow ^4T_{2g}$ transitions. The high intensity of the first band may be due to overlaying of the charge transfer band.

Infrared spectra : Important infrared frequencies of ligands and their complexes are set out in Table 2. It is shown¹⁷ that free hydroxy group gives rise to stretching band in the region 3600-3500 cm⁻¹. This band shifts to lower frequency on hydrogen bond formation. The intermolecular hydrogen bonding shifts it further to the lower frequency and causes broadening. The intramolecular hydrogen bonding further shifts it to the lower frequency. Hence, the band becomes weak and broad taking these observation into consideration and an analogy with salicylideneaniline, the weak broad band observed around 2650 cm⁻¹ is assigned to H-bonded -OH.

Considering the previous assignments¹⁸ the strong band observed around 1620 cm⁻¹ for Schiff base has been assign to $\nu(C=N)$ vibration. In all these complexes this band appears at lower frequency region 1620-1600 cm⁻¹ indicating that the coordinate bond is formed between the nitrogen of the azomethine group and metal ion.

There are three bands of high intensity in the range 1600-1550 cm⁻¹ which are attributed to the aromatic ring vibrations¹⁹. These bands show remarkable changes in frequencies on going from the ligand to metal complexes.

Table 2- Important infrared frequencies (cm^{-1}) of DASV and DASOV and their metal complexes

Sl No	Empirical formula of Ligand / Complexes	$\nu(\text{OH})$	$\nu(\text{C}=\text{N})$	$\nu(\text{C}=\text{C})$	$\nu(\text{C}-\text{O})$	$\nu(\text{M}-\text{N})$	$\nu(\text{M}-\text{O})$	$\nu(\text{M}-\text{Cl})$
1.	[DASV] ($\text{C}_{30}\text{H}_{24}\text{N}_2\text{S}_2\text{O}_{10}\text{Na}_2$)	3420	1610	1592	1280	-	-	-
2	[$\text{Mn}_2(\text{C}_{30}\text{H}_{24}\text{N}_2\text{S}_2\text{O}_{10}\text{Na}_2)_2$ $\text{Cl}_4\text{2H}_2\text{O}]$	3422	1600	1543	1334	523	-	334
3	[$\text{Fe}_2(\text{C}_{30}\text{H}_{24}\text{N}_2\text{S}_2\text{O}_{10}\text{Na}_2)_2$ $\text{Cl}_6\text{2H}_2\text{O}]$	3425	1598	1547	1335	534	-	342
4.	[$\text{Cr}_2(\text{C}_{30}\text{H}_{24}\text{N}_2\text{S}_2\text{O}_{10}\text{Na}_2)_2$ $\text{Cl}_6\text{2H}_2\text{O}]$	3420	1599	1542	1372	543	-	336
5	[DASOV] ($\text{C}_{30}\text{H}_{24}\text{N}_2\text{S}_2\text{O}_{10}\text{Na}_2$)	2650*	1620	1590	1280	-	-	-
6	[$\text{Mn}_2(\text{C}_{30}\text{H}_{22}\text{N}_2\text{S}_2\text{O}_{10}\text{Na}_2)_2$ $\text{4H}_2\text{O}]$	-	1630	1560	1315	530	460	-
7.	[$\text{Fe}_2(\text{C}_{30}\text{H}_{22}\text{N}_2\text{S}_2\text{O}_{10}\text{Na}_2)_2$ $\text{Cl}_2\text{2H}_2\text{O}]$	-	1632	1545	1310	535	465	318
8	[$\text{Cr}_2(\text{C}_{30}\text{H}_{22}\text{N}_2\text{S}_2\text{O}_{10}\text{Na}_2)_2$ $\text{Cl}_2\text{2H}_2\text{O}]$	-	1635	1555	1320	580	440	325

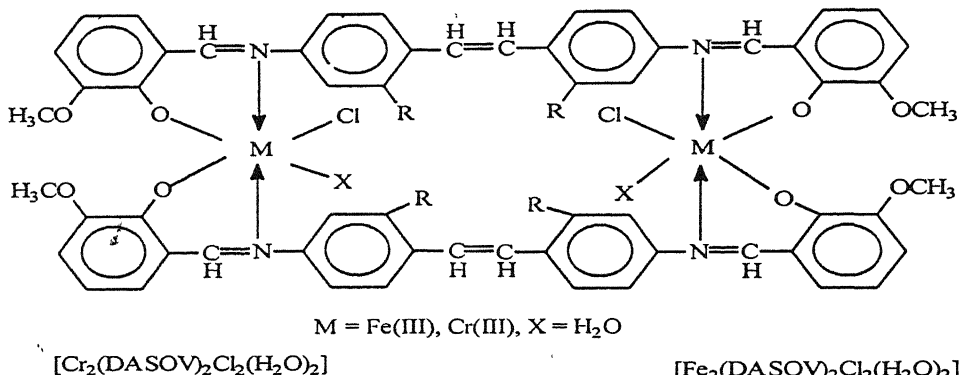
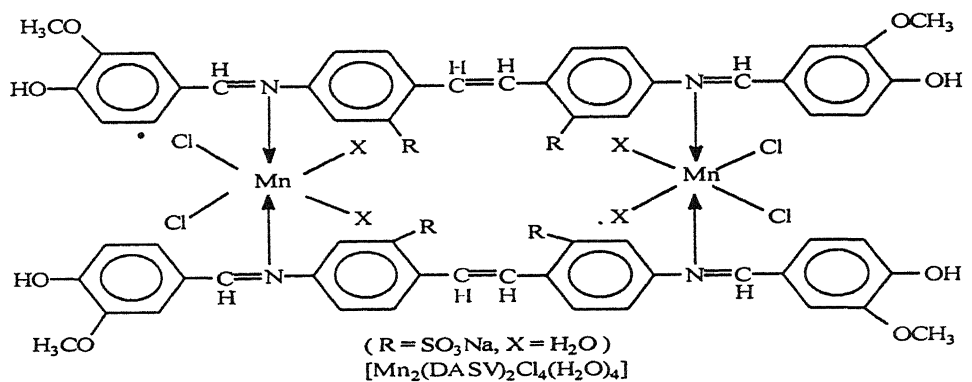
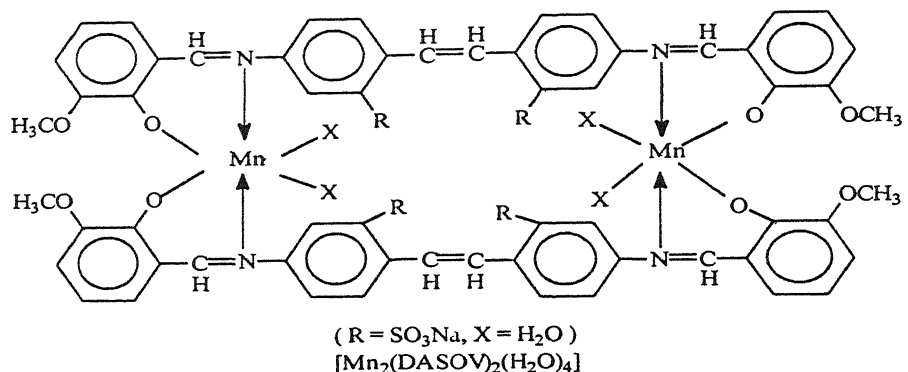
* Intramolecular -H-bonded -OH

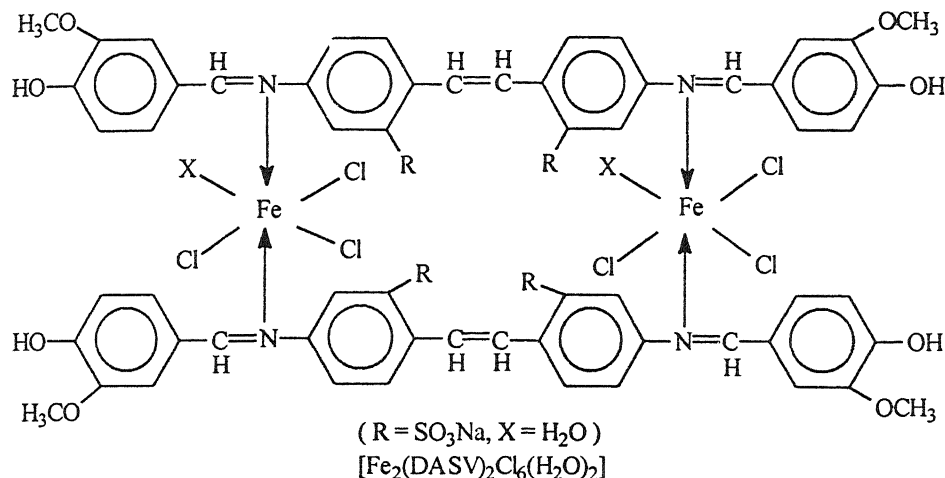
A strong intensity band observed in the region 1280 cm^{-1} of Schiff base ligand (DASV) has been assigned to the phenolic $\nu(\text{C}-\text{O})$ vibration. This band does not show any perturbation in the complexes indicating non involvement of OH groups in the bond formation. These observations emphasize that the ligand (DASV) has not undergone deprotonation while reacting with metal(II/III) chlorides. Analytical data also support this view. The asymmetric $\nu(\text{C}-\text{O})$ vibrations of the $-\text{OCH}_3$ group of the ligands at 1320 cm^{-1} remains inert to the complex formation indicating non involvement of OCH_3 group of ligand in coordination to the metal ion.

However a strong intensity band observed in the region 1280 cm^{-1} of Schiff base ligand (DASOV) has been assigned to phenolic $\nu(\text{C}-\text{O})$ vibration. In view of the previous²⁰ assignments, the H-bonded -OH band around 2700 cm^{-1} has been assigned to the intramolecular -H bonded -OH in this ligand. Further the assignment of the band is confirmed by comparing the spectra of the benziledene aniline and anisilidene aniline with that of DASOV ligand. The band due to intramolecular -H bonded -OH is absent in the model compounds. This band disappears in the spectra of complexes indicating reaction through oxygen *via* deprotonation. Further, the band at 1280 cm^{-1} attributed to $\nu(\text{C}-\text{O})$ has been shifted to higher frequency and is found in the region $1340\text{-}1305\text{ cm}^{-1}$ for these complexes. This confirms the involvement of phenolic -OH in the complex formation. The complexes display a broad intense band centered around 3400 cm^{-1} attributed to water molecules. No loss in weight was observed even after drying the complexes at 105°C for 2 h. The infrared spectra of the dried complexes also exhibit broad intense band around 3400 cm^{-1} and $\sim 830\text{ cm}^{-1}$.

The high intensity bands appearing in the region often interfere with M-L bands. Thus assignments of the bands to various $\nu(\text{M}-\text{N})$, $\nu(\text{M}-\text{O})$, $\nu(\text{M}-\text{Cl})$ vibrations in this region become much complicated. However, the assignments of the bands to various modes have been made by comparing the spectra of the complexes with those of ligands. Taking into consideration of previous reports²¹ the non-ligands bands in the region $543\text{-}520\text{ cm}^{-1}$, $460\text{-}440\text{ cm}^{-1}$ and $348\text{-}318\text{ cm}^{-1}$ have been assigned to $\nu(\text{M}-\text{N})$, $\nu(\text{M}-\text{O})$ and $\nu(\text{M}-\text{Cl})$ vibrations respectively.

The elemental analysis, magnetic study, electronic and IR spectral observations project the following structures of coordination number six for these complexes.





Acknowledgements

The authors thank Professor and Chairman, Department of Chemistry, Gulbarga University, Gulbarga for providing basic facilities.

References

- 1 Sacconi, L (1964) *Experientia Suppl* **9** 148.
- 2 Sacconi, L. (1966) *Coor Chem Rev* **1** : 126, 127
- 3 Yamada, S (1960) *Coor Chem Rev* **1** . 415
- 4 Tandon, J P. & Singh, R V. (1984) *Quart Chem Rev* **1** 88
5. Parihart, R. K. & Patil, R. K. (1999) *J Indian Chem Soc* **76** · 258
- 6 Crossely, M L Northey, E H & Hultquist, N G (1938) *Amer Chem Soc* **60** : 2217
- 7 Kenatomy, H & Murase, I (1976) *J Inorg Nucl Chem* **38** . 1465.
- 8 Vogel, A. I. (1969) *A Text Book of Quantitative Inorganic Analysis*, ELBS, Third Edition, Longmans Green, London.
- 9 Geary, W J. (1971) *Coord Chem Rev* **7** 81.
- 10 Bartlett, R. J & James, B R (1988) *Mobility and bioavailability of Chromium in soils*, John Wiley and Sons Inc., p 267
11. Srivastav, S. Prakash, S & Srivastav, M M. (1999) *Indian J Chem* **38A** : 514.

- 12 Figgis, B N (1961) *Trans Faraday Soc* **37** 199
- 13 Lever, A B P (1968) *Inorganic Electronic Spectroscopy*, Elsevier, Amsterdam
- 14 Pure, M & Verma, R D (1984) *Indian J Chem* **23A** 612
- 15 Sharp, D W A , Brown, D H , Moss, K C & Baillie, M J (1968) *J Chem Soc A* 3110
- 16 Gaur, M , Mathur, P K & Kapoor, S. N (1984) *Indian J Chem* **23A** 774
- 17 Rao, C N R (1967) *Chemical Application of Infrared Spectroscopy*, Academic Press, New York
- 18 Kovacic, J E (1967) *Spectrochim Acta* **23A** 183
- 19 King, R B (1966) *Inorg Chem* **5** 300
- 20 Nakamoto, K , Udovich, C & Takamoto, J (1970) *J Amer Chem Soc* **92** 3973
- 21 Ali, A , Livingstone, M S E & Phillips, D J (1971) *Inorg Chem Acta* **5** 119, 493

Speciation studies of calcium(II) and magnesium(II) complexes of L-glutamine and succinic acid in acetonitrile-water mixture

G NAGESWARA RAO and S.B. RONALD

*Bio-inorganic Chemistry Laboratories, School of Chemistry, Andhra University,
Visakhapatnam-530 003, India*

Received August 16, 2001, Revised December 16, 2002, Re-Revised September 6, 2003
Accepted November 13, 2003

Abstract

A computer assisted pH metric investigation has been made on the speciation of Ca(II) and Mg(II) complexes of glutamine and succinic acid in varying concentrations (0-60% v/v) of acetonitrile-water solutions at an ionic strength of 0.16 mol dm⁻³ (NaCl) and 303 K temperature. The predominant species detected for Ca(II) and Mg(II) complexes of glutamine are ML₂, ML₂H⁺ and of succinic acid are ML₂²⁻, MLH⁺ and ML₂H. The variation in values of stability constants with the change in dielectric constant of medium is attributed to the electrostatic and non-electrostatic interactions.

(Keywords speciation study/complex equilibria/acetonitrile/L-glutamine/ succinic acid/speciation)

Introduction

The physiological activities of Gln, Suc, Ca(II) and Mg(II) are associated with the metabolic processes in liver; hence, their speciation has been studied in varying compositions of acetonitrile-water mixtures. The protonation equilibria of Gln and Suc in acetonitrile-water have been reported earlier¹.

Materials and Method

Solutions of L-glutamine, succinic acid, calcium(II) and of magnesium(II) chlorides (E. Merck, Germany) were prepared in triple distilled water. 99.5% pure acetonitrile (E. Merck) was used. The strength of alkali and the acid present in the metal ion solutions was determined using the Gran plot method². The titrations were carried out in the medium containing varying concentrations (10-60% v/v) of acetonitrile in water maintaining an ionic strength of 0.16 mol dm⁻³ with NaCl at

303.0 ± 0.1 K using a Systronic (model 335) pH meter of 0.01 readability. In each of the titrations, the titrand consisted of mineral acid of approximately 1 mmol in a total volume 50 cm³. Titrations were carried out with 0.4 mol dm⁻³ sodium hydroxide. Other experimental details are given elsewhere³. The best fit chemical models for each system investigated were arrived at using a non-linear least squares computer program MINIQUAD75⁴

Results and Discussion

Refinement of species: The final models refined for Gln and Suc complexes contained ML_2 and ML_2H^+ and ML_2 , MLH^+ and ML_2H^- , respectively (Tables 1 and 2). A very low standard deviation in $\log \beta$ values indicates the precision of the parameters. The deviation of residuals from Gaussian distribution is reflected by the statistical parameters, skewness and kurtosis. Skewness indicates whether the residuals are concentrated to the left or to the right of the mean. Kurtosis indicates the peaked ness of the residual curve. For an ideal normal distribution, the values of kurtosis and skewness should be three and zero, respectively. The kurtosis values of most of the systems indicate that the residuals form platykurtic pattern. The values of skewness evince that the residuals of many systems form a part of normal distribution. The sufficiency of the model is further evident from the low crystallographic R values.

Effect of errors in influential parameters like the concentrations of ingredients on the stability constants is studied and the data show that the order of affecting the magnitudes of stability constant is due to errors in the concentrations of alkali> ligand> acid> metal.

Solute-solvent interactions: The linear variation of $\log K$ values of Ca(II) and Mg(II) complexes of L-glutamine and succinic acid with I/D indicates that electrostatic forces are dominating the equilibrium process under the present¹ experimental conditions. The decrease in the stability constants of Mg(II) complexes of succinic acid at 60% may be due to the competition of solvent molecules with the ligand for coordination position of metal ion in higher percent of acetonitrile-water mixture. Since complex formation can be viewed as a competition between the pure and solvated forms of ligand and the metal ion, the solute-solvent interactions, relative thermodynamic stabilities and kinetic labilities are also expected to play an important role. Different types of electrostatic forces dominate in different ranges of the composition of acetonitrile-water mixtures. The deviation from linearity in Ca(II)-Suc indicates the blend of both electrostatic and non-electrostatic interactions.

Table 1— Best fit chemical models of Ca(II) and Mg(II) complexes of L-glutamine in acetonitrile-water mixtures.

No. of titrations in each percentage = 4

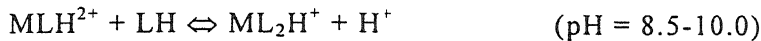
% v/v AN	120	121	NP	$U_{\text{corr}} X$ 10^7	Skewness	Kurtosis	χ^2	R
<u>Ca(II)- Glutamine (pH range : 8.5-11.0)</u>								
00.0	3.54(5)	13.46(7)	28	2.577	-0.17	7.8	35.41	0.015
10.0	3.46(7)	13.91(1)	27	2.874	-1.77	10.04	31.30	0.012
20.0	3.80(1)	13.86(9)	28	3.790	-2.94	17.96	76.00	0.013
30.0	3.72(6)	13.90(8)	28	2.824	-3.14	18.30	60.95	0.011
40.0	3.89(7)	13.85(2)	27	5.192	-2.14	9.04	28.33	0.015
50.0	4.01(1)	14.26(1)	28	2.902	3.52	-21.59	96.38	0.012
60.0	3.96(9)	14.41(8)	28	2.167	-3.01	18.40	46.29	0.010
<u>Mg(II)-Glutamine (pH range : 8.3 - 10.6)</u>								
00.0	3.40(5)	12.92(9)	28	8.185	-0.11	6.4	67.38	0.025
10.0	3.42(2)	13.55(1)	28	1.826	-1.48	14.88	78.86	0.009
20.0	3.61(4)	13.62(3)	27	0.503	-0.61	6.46	30.70	0.004
30.0	3.23(8)	13.72(4)	26	0.369	-0.24	5.36	15.13	0.004
40.0	3.73(7)	13.78(8)	28	1.348	-1.90	9.26	42.10	0.008
50.0	4.07(5)	14.10(6)	27	1.154	-1.92	8.53	40.78	0.007
60.0	3.36(2)	14.21(3)	27	0.296	1.94	14.07	73.17	0.003

Table 2- Best fit chemical models of Ca(II) and Mg(II) complexes of succinic acid in acetonitrile -water mixtures

No of titrations in each percentage = 4

% v/v AN		$\log \beta_{mlh}$ (SD)		NP	$U_{corr} X$ 10^7	Skewness	Kurtosis	χ^2	R
<u>Ca(II)- Succinic acid (pH range 3.0-9.0)</u>									
00.0	3.40	6.36(5)	9.61(8)	621.61(8)	1.626	-0.06	6.1	62.78	0.034
10.0	Rejected	Rejected	9.74(9)	61	3.200	-2.22	13.22	57.66	0.008
20.0	4.00(7)	7.18(2)	9.99(7)	62	1.406	-0.57	4.37	45.05	0.006
30.0	4.43(4)	7.64(4)	10.51(5)	57	0.948	-0.97	6.87	43.78	0.005
40.0	3.65(7)	7.71(3)	10.27(7)	58	1.531	-0.31	5.84	57.45	0.006
50.0	3.61(6)	Rejected	10.66(6)	59	1.025	-1.17	6.65	68.83	0.005
60.0	4.24(4)	8.17(3)	11.00(4)	60	0.586	-1.23	6.74	43.82	0.004
<u>Mg(II)-Succinic acid (pH range 3.0 - 9.0)</u>									
00.0	3.66(4)	7.16(1)	9.61	62	4.498	-3.76	23.48	109.7	0.016
10.0	Rejected	Rejected	9.64(6)	61	8.136	-1.46	8.95	118.6	0.014
20.0	4.23(5)	7.49(1)	10.06(6)	62	1.337	-0.82	5.14	41.18	0.005
30.0	3.96(5)	Rejected	10.11(1)	57	2.316	-1.50	8.06	59.22	0.008
40.0	4.22(3)	7.62(3)	10.41(4)	59	0.576	-0.75	5.98	57.80	0.004
50.0	4.21(2)	8.06(6)	10.78(2)	60	0.268	-1.75	10.20	56.80	0.002
60.0	3.67(3)	Rejected	10.76(4)	61	0.562	-1.77	12.23	85.20	0.003

Distribution diagrams : Different forms of Gln are LH_2^+ , LH, L^- in the pH regions 1.5-4.5, 1.5-9.5 and 8.0-11.0, respectively¹. The present study is confined to the pH range 8.3 -10.6 and 8.5 - 11 for Ca(II) and Mg(II) complexes of Gln, respectively. In this pH range the ligand is expected to be present in the form of LH and L^- . Hence the plausible metal-ligand species are ML_2 , MLH^{2+} , ML_2H^+ , which are confirmed by MINIQUAD75. The equilibria in these pH ranges can be represented as follows :



The various forms of suc can be given as LH_2 , LH^- and L^{2-} in the pH ranges 3.0-6.5, 3.0-7.0 and 4.5-7.0, respectively. The pH range of present study is 3.0-9.0 where the active forms of ligand are LH^- and LH_2 . The species confirmed in the pH range are ML_2^- , MLH^+ , ML_2H^- , MLH^+ . The formation equilibria can be represented as



The variation of species concentration with pH is shown in Fig. 1 for some typical systems. In glutamine complexes the concentrations of ML_2 and ML_2H^+ are almost same. But in succinate complexes ML_2^{2-} is the predominant species compared to MLH^+ and ML_2H^- . Another important observation is that the concentration of free metal ion in the presence of Gln is negligible where as there is still considerable amount of free metal in the presence of succinic acid. This indicates that Gln is a stronger complexing agent than Suc.

Biological relevance of present study: The polarity at the active-site cavities in enzymes/proteins is less compared to that of bulk water. The presence of acetonitrile in aqueous solution considerably decreases the dielectric constant and these solutions are expected to mimic the physiological conditions. This equivalent solution dielectric constant⁵ for protein cavities should be generally applicable when it is possible to compare ligand binding to the metal ion in protein and in mixed solvent environments. The studies carried out on these systems under the present experimental conditions are

useful to understand 1) the role played by the active site cavities in biological molecules, 2) the type of complex formed by the metal ion, and 3) the bonding behaviour of the protein residue with the metal ion. Hence, the various species detected in the present study and their concentrations can be extrapolated to the biological systems under similar conditions.

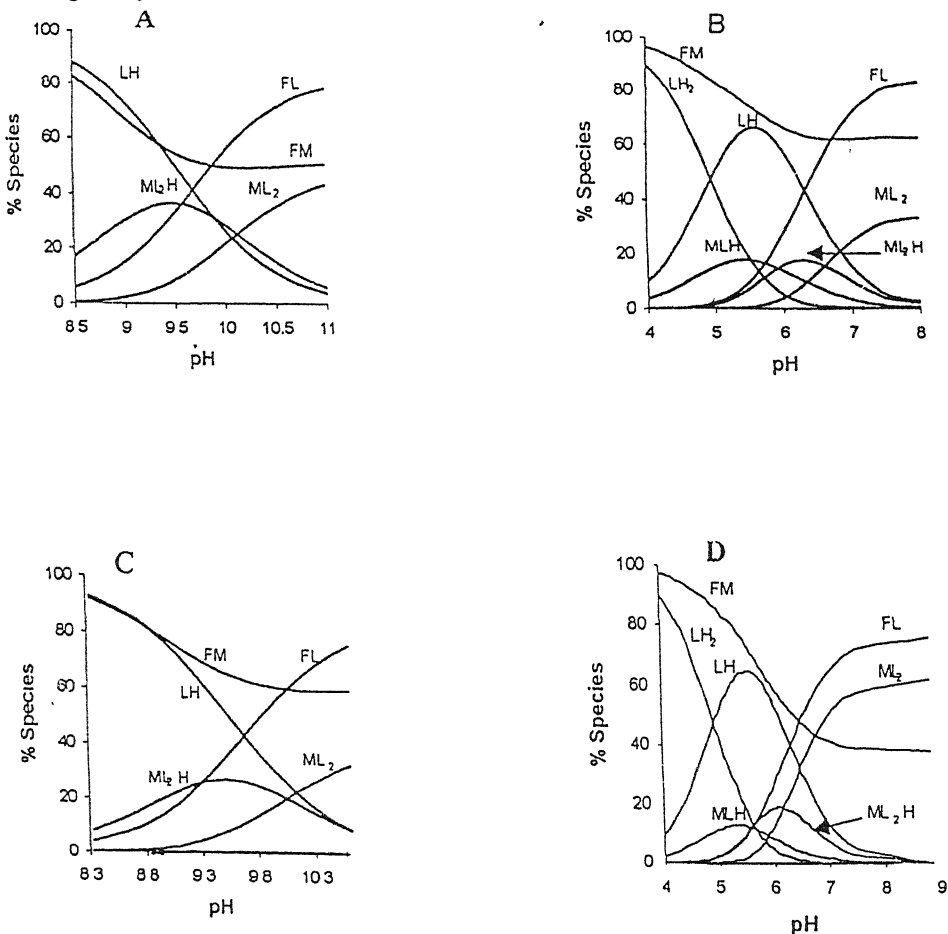


Fig 1—Species distribution diagrams in 40% acetonitrile-water mixture

A) Ca(II)-Gln, B) Ca(II)-Suc, C) Mg(II)-Gln, D) Mg(II)-Suc

References

1 Rao, G N & Ronald, S B (2002) *J Indian Chem Soc.* 79 416

- 2 Gran, G (1952) *Analyst* **77** 661 , (1988) *Anal Chem Acta* **206** 111
- 3 Padmaja, N , Babu, M S , Rao, G N , Rao R S & Ramana, K V (1990) *Polyhedron* **9** 2497
- 4 Gans, P Sabatini, A & Vacca, A (1976) *Inorg Chem Acta* **18** 237
- 5 Sigel, H Martin, R B , Tribolet, R , Haring, U K & Malini Balakrishnan, R (1985) *Eur J Biochem* **152** 187

Charge transfer interactions of L-aminoacids with chloranil : Conductometric studies*

H. S. RANDHAWA, P. PATYAR and B. S. SEKHON

Department of Chemistry, Punjab Agricultural University, Ludhiana-141004, India

Received December 10, 2001, Revised September 30, 2002, Re-Revised March 31, 2003,
Accepted December 6, 2003

Abstract

The charge transfer interactions of ten L-aminoacids namely isoleucine, leucine, phenylalanine, tryptophan, valine, asparagines, glycine threonine, histidinemonohydrochloride, lysinemonohydrochloride with chloranil has been studied in 50% aqueous ethanol by conductometric technique employing the models of Gutmann and Keyzer and Randhawa and Lakhani. Conductometric titration indicates 1:1 stoichiometry of these complexes. The equilibrium constant K and other thermodynamic functions have been determined and compared with those reported in the literature on the basis of spectroscopic and non-spectroscopic methods and models.

(Keywords charge transfer/conductance/L-aminoacids- chloranil systems)

Introduction

Charge transfer complexes are of importance as reaction intermediates¹ and in the field of drug-receptor binding mechanism². The stability constants of chloranil with various acids involving studies on weak interactions were reported³⁻⁴. In the present communication the charge transfer between ten L-amino acids namely isoleucine, leucine, phenylalanine, tryptophan, valine, asparagine, glycine, threonine, histidinemonohydrochloride, lysine and chloranil by the conductometric method of Gutmann and Keyzer⁵⁻⁷ and a model reported earlier from our laboratory⁸ is reported.

Materials and Method

Two sets of experiments were performed, one to determine the composition and second to determine formation constants of the complexes. In order to determine the stoichiometric ratio of CT complex, equimolar stock solutions (5×10^{-4} M) of D and A in 50% aqueous ethyl alcohol, were mixed in the conductivity cell, keeping the total volume constant by varying the volumes of D and A. In the second set of experiments,

*This work was presented at the International Symposium on Trends in Medicinal Chemistry and Biocatalysis held at University of Delhi from 26-29 January, 2000.

the stock solutions of donors with concentration 5×10^{-2} M and acceptor with 5×10^{-4} M except in case of tryptophan - chloranil system i.e. 5×10^{-3} M and 5×10^{-5} M were prepared in 50% aqueous ethanol, respectively. In order to determine K the concentration of D was varied while keeping the concentration of A fixed. The conductance measurements were made at three different temperatures i.e. 293, 303 and 313 ± 0.01 K on a Philipps PR9500 conductivity bridge using a conductivity cell pre standardized fitted with platinized platinum electrodes. The methodology to determine conductivity data and stoichiometry⁵⁻⁷, formation constants⁸ and thermodynamic functions have been reported in the literature and the data so obtained are listed in Tables (1-3).

Results and Discussion

The present conductometric results on the composition of amino acid - chloranil complexes in 50% aqueous ethanol except lysine monohydrochloride conforms to the spectrophotometric studies⁹⁻¹⁰. However, in case of lysine monohydrochloride, we failed to observe a break at 1:2 (D:A), since one of the amino groups of lysine is blocked in lysine monohydrochloride. Further, conductometric data (Table 1) reveal that there exists no definite relationship between the values of σ_p , σ_M and $E^\#$ as well as with pK_1 of amino acids as expected. This may be attributed to small variation of pK_1 (± 0.34) and pK_2 (± 0.74) values of amino acids. The absence of any definite relationship between K , $\ln K$ and $p\delta$ (Table 2) with σ_p , $E^\#$ and pK_1 (Table 1) may also be due to the above mentioned reason. A close look at Table 3 reveals that K values not only depend on temperature, the dielectric constant and pH of the medium, the nature of the method but also on the type of the model employed. One of the reasons for the difference between K values determined by spectral and conductance methods may be due to the fact that concentration manifests in spectral while activity in conductance method.

The dipole moment of the complex always depends upon the total polarizability of the complex. However, in the calculation of the dipole moment of the complex, the depolarizability is ignored on the basis that the polarizability is equal to the sum of the individual components. But from the depolarizability data in Table 2, it is evident that depolarizability increases over that of the additive values of the individual molecules. Thus to obtain the exact value of dipole moment, the depolarizability should be taken into account also. Further the inspection of Table 2 (columns, 8-10) shows that p_d , the depolarization constant grows with the growth of temperature which is reverse to the behaviour of K values with temperature as expected.

Table 1- Conductance(σ) data for 1 : 1 CT complexes of L-aminoacid donors with chloranil acceptor in aqueous ethanol (50%) at 293K

Donor	$pK_1(a)$ (α -COOH)	$pK_2(a)$ (α -NH ₃ ⁺)	$pK_1(\text{amino}$ acid)	Conductance (μmhos)			$E^\#$ (kJ mol ⁻¹)
				σ_p	σ_0	σ_M	
Isoleucine	2.32	9.76	6.04	69.0	44.0	56818	12.62
Leucine	2.33	9.74	6.035	66.2	52.5	10438	8.85
Phenylalanine	2.16	9.18	5.67	72.1	47.5	20715	7.75
Tryptophan	2.43	9.44	5.93	65.0	51.0	10980	6.64
Valine	2.29	9.74	6.01	62.0	49.0	10612	10.33
Asparagine	2.10	8.84	10.80	70.0	46.0	20869	8.45
Glycine	2.35	9.78	6.06	66.0	49.5	13333	11.62
Threonine	2.09	9.10	5.59	64.4	47.5	14231	9.06
Histidinemono- hydrochloride	1.80	9.30	7.65	70.0	50.0	16000	9.96
Lysinemono- Hydrochloride	2.20	9.20	9.70	64.5	48.5	13195	12.55

(a) ref(13)

Table 2- Thermodynamic functions for CT complexes of L-amino acid-chloramyl systems

Amino acid	K_{293} (dm ³ mol ⁻¹)	K_{303} (dm ³ mol ⁻¹)	K_{313} (dm ³ mol ⁻¹)	$-\Delta H$ (kJmol ⁻¹)	ΔS (Jmol ⁻¹ K ⁻¹)	$\ln K$	$\rho_d \times 10^5$ (μmhos dm ³ mol ⁻¹)	293K	303K	313K
Isoleucine	123.04	105.05	85.30	12.80	-3.80	4.81	2.44	3.05	3.91	
Leucine	153.62	149.65	144.38	2.74	+32.45	5.03	2.14	2.68		3.48
Phenylalanine	243.68	206.19	168.15	11.89	+5.05	5.49	2.52	3.17		4.33
Tryptophan	295.59	189.24	125.77	32.00	-61.97	5.68	43.41	54.64		78.81
Valine	298.17	266.40	234.43	9.81	+13.82	5.69	1.96	2.38		3.20
Asparagine	161.64	145.05	131.91	6.90	+18.66	5.08	2.06	2.38		2.76
Glycine	106.83	72.87	46.32	37.75	-90.00	4.67	2.61	3.15		5.30
Threonine	362.58	341.71	322.58	5.19	+31.23	5.89	2.13	2.30		2.50
Histidinmono-hydrochloride	116.38	80.16	52.32	30.26	-63.78	4.75	20.36	27.24		39.53
Lysinmono-Hydrochloride	737.05	691.21	613.36	5.49	+36.10	6.60	9.83	11.52		14.29

Table 3—Comparison of stability constants of L-amino acid - chloromethyl systems from different techniques and models

(a)-20% EtOH, (b) - ref (9), (c) - ref (10), (d) - ref (11). The values under refractometric method are from different models

The present values of K and other thermodynamic functions have been compared with the literature values¹¹ (Table 4) The sign of literature values of ΔH which is a true measure of strength of interaction and ΔS do not seem to be a typographical mistake, since these values do not fit into Gibbs-Helmholtz equation. In view of this we do not trust the literature values of thermodynamic functions determined from conductance data by Sahai and Singh¹¹ The equation used by Sahai and Singh¹¹ is quadratic in K and will give two roots. The authors have not given any justification for choosing value of K for further calculations and investigations whereas in the model employed in the present studies, only one value of K is obtained and hence there is no such ambiguity as above for further investigations. Further from the equilibrium constant data it is clear that the interaction is stronger in case of tryptophan than in case of phenylalanine. Theoretical calculation of Pullman reveals that tryptophan having an indole nucleus should behave as a better electron donor than phenylalanine¹².

Table 4— A comparison of thermodynamic functions of tryptophan - , and phenylalanine - chloranil systems

Donor	Literature values(a) (295 K)			Present studies (293 K)		
	K	ΔH	ΔS	K	$-\Delta H$	ΔS
Tryptophan	1 77 77	22 99	79 33	295 99	32.00	-62 01
		(-22 99)	(-34 88)			
Phenylalanine	133 33	22 23	72 77	243 68	11 89	+5 05
		(-22 23)	(-34 71)			

a - ref (11). The quantities within parenthesis are the redetermined values

References

- Roy, T., Dutta, K , Nayek, M K , Mukherjee, A K , Mukherjee, M & Seal, B K. (2000) *J Chem Soc Perkin Trans 2* 531
- Mandal, R & Lahiri, S C (1999) *J Indian Chem Soc* 73 163
- Majumdar, K , Majumdar, K & Lahiri, S C (2002) *J Indian Chem Soc* 79 . 811
- Abdel-Gawad, F M., Issa, Y M , Fahmy, H M & Hussein, H N (1998) *Mikrochim Acta* 130 35
- Gutmann, F & Keyzer, H (1966) *Electrochim Acta* 11 555, 1163
- Gutmann, F & Keyzer, H (1967) *Electrochim Acta* 12 . 1255.
- Gutmann, F (1967) *J Sci Ind Res* 26 19

- 8 Randhawa, H S & Lakhani, R (1993) *Colln Czech Chem Commun* **58** 783
- 9 Birks, J B & Slifkin, M A (1963) *Nature* **197** 42
10. Lin, B Y & Cheng, K L (1980) *Anal Chim Acta* **120** 335
- 11 Sahai, R. & Singh, V (1980) *Ind J Pure and Appl Phys* **18** 504
- 12 Puiiman, B. (1968) "Molecular association in Biology", Academic Press, New York
- 13 Murray, R K , Granner, D K , Moyes, P A. & Rodwell, V. W (1996) "Harper's Biochemistry" Prentice - Hall, London

New sensitive methods for the spectrophotometric determination of some catecholamine derivatives

R A. VASANTHA, P NAGARAJA* and H.S YATHIRAJAN

Department of Studies in Chemistry, University of Mysore, Manasagangotri, Mysore-570 006, India

email nagarajap@mailcity.com

Received April 30, 2002, Accepted December 26, 2003

Abstract

Rapid, simple and sensitive spectrophotometric methods for the determination of pyrocatechol, dopamine hydrochloride, levo dopa, methyl dopa and adrenaline hydrochloride in either pure form or its pharmaceutical preparations is described. The first method is based on the interaction of catecholamine derivatives with iron(III) and subsequent reaction with ferricyanide in presence of hydrochloric acid medium to yield prussian blue coloured complex with λ_{max} of 730 nm. In the second method, the interaction of nitrite ions with the catecholamines in neutral medium in presence of aluminium ions to yield a red product in alkaline medium with λ_{max} of 500-510 nm. The optical characteristics, interference studies and application to pharmaceutical preparations have been reported.

(Keywords catecholamines/spectrophotometry/aluminium ions/ferricyanide/pharmaceuticals)

Introduction

Catecholamine derivatives are aromatic vic-diols in which either the 3- or 4-position is unsubstituted and these positions are not sterically blocked. These derivatives are used as drugs and have wide application¹. There are various instrumental techniques for the determination of these catecholamine derivatives. We have already reported different spectrophotometric procedure²⁻⁶ for the determination of catecholamines. In continuation of our work in this field, we are reporting two more sensitive and rapid methods for the spectrophotometric determination of pyrocatechol (PCL), dopamine hydrochloride (DPH), levo dopa (LDP), methyl dopa (MDP) and adrenaline hydrochloride (ADH) in pure form as well as in its pharmaceutical formulations. Optical characteristics like Beer's law range, molar absorptivity, Sandell's sensitivity etc., have been reported. Commonly used excipients do not interfere in the present methods. Reaction mechanisms are discussed.

Materials and Method

A JASCO model UVIEC-610 spectrophotometer with 1.0 cm matched cells was used for absorbance measurements. Pharmaceutical grade PCL, DPH, LDP, MDP and ADH were purchased from Sigma Chemical Co. (USA). Aluminium chloride was purchased from Merck (Darmstadt, Germany). All other chemicals and solvents used were of analytical reagent grade. Commercial dosage forms were purchased from local sources. Deionized water was used throughout.

Stock solutions of catecholamine derivatives were prepared by dissolving 0.05 g of each drug in 100 ml of water. The working standard solutions of the drug were prepared by further dilution. A 1 % aqueous sodium nitrite, 0.2% aluminium chloride, 1M sodium hydroxide, 0.002M potassium ferricyanide, 0.1 M ferric chloride and 5M hydrochloric acid solutions were used for the experiments.

General procedure: *Method A* : Aliquots of standard solutions of PCL (2.5-140 µg), DPH (6.25-275 µg), LDP (2.5-100 µg), MDP (6.25-500 µg) or ADH (5-650 µg) were transferred into a series of 25 ml calibrated flasks. To each of the flasks, 1.0 ml of 1% sodium nitrite and 0.5 ml of 0.2% aluminium chloride were added. After 5 min. 2.0 ml of 1M sodium hydroxide was added, made upto the mark and shaken well. The absorbances of the red coloured products were measured at 500-510 nm against a reagent blank and calibration graphs were constructed. Optimum ranges are given in Table 1. *Method B* : Aliquots of standard solutions of PCL (2.5-80 µg), DPH (2.5-80 µg), LDP (2.5-60 µg), MDP (1.25-25 µg) and ADH (2.5-80 µg) were transferred into a series of 25 ml calibrated flasks. Requisite amounts of potassium ferricyanide and iron(III) were added as shown in Table 1 and left for 5 min. Then, 1.0 ml of 5M hydrochloric acid was added and diluted with water upto the mark. The contents were mixed thoroughly and the absorbance values were recorded at 730 nm against the reagent blank. Calibration graphs were constructed.

Table 1- Experimental conditions.

Catechol derivatives	Optimum reagent concentrations				
	1 % NaNO ₂	0.2% AlCl ₃	1 M NaOH	Iron(III)	Potassium ferricyanide
PCL	*1 ml *(0.5-3 ml)	0.5 ml (0.3-3ml)	2ml (1-4ml)	0.05 M 5ml (1-7 ml)	0.001 M 4 ml (1-5 ml)
DPH	1 ml (0.5-3 ml)	0.5 ml (0.3-3ml)	2ml (1-4ml)	0.1 M 3 ml (2-8ml)	0.002 M 3 ml (2-8 ml)

Table 1 Contd

Table 1 Contd

LDP	1 ml (0.5-3 ml)	0.5 ml (0.3-3 ml)	2ml (1-4ml)	0.05 M 4ml (1-5 ml)	0.01 M 4 ml (1-5 ml)
MDP	1 ml (0.5-3 ml)	0.5 ml (0.3-3 ml)	2ml (1-4ml)	0.1 M 5 ml (1-7ml)	0.002 M 5 ml (1-7 ml)
ADH	1 ml (0.5-3 ml)	0.5 ml (0.3-3 ml)	2ml (1-4ml)	0.05 M 4 ml (1-5ml)	0.001 M 4 ml (1-5 ml)

^aUsed in the proposed procedure

^bRange for maximum absorption and stability (values in parenthesis)

Procedure for the assay of pharmaceutic samples Fifteen tablets were weighed and finely powdered. The powder amount equivalent to 50 mg of LDP or MDP (for injection of PH or AH, an appropriate volume of the sample) was dissolved in water and filtered. The filterate was made upto 100 ml and an appropriate aliquot of the drug solutions were treated as described in the general procedure.

Results and Discussion

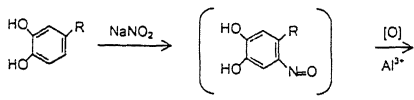
The optical characteristics and precision data for both the methods are given in Tables (2 & 3). Method A involves the reaction of catechol derivatives with sodium nitrite in neutral medium in presence of aluminium ions to produce an intense yellow coloured product which turns to deep red after addition of NaOH. It is presumed that anhydrous aluminium chloride not only acts as lewis acid for the nitration of catechols, but in higher concentration, it stabilizes the nitro derivatives by complex formation, which readily gets decomposed in alkaline medium. A bathochromic shift from 420 nm to 500-510 nm in alkaline medium is noticed. The probable mechanism is shown in Scheme 1. Method B involves the reduction of iron(III) in aqueous medium to form iron(II), which subsequently chelate with ferricyanide to form prussian blue coloured product.

Both the reactions are completed within 5 min. at room temperature ($26 \pm 1^\circ\text{C}$). The proposed methods were found to be free from the interference of commonly encountered excipients and additives such as sodium chloride, talc, starch, stearic acid, gelatin, gumacacia, glucose, lactose, sucrose and sodium alginate. Vitamin-B₆ and vitamin-C (upto 4000 ppm) do not interfere in method A, while any reducing agent interferes in method B. Some typical analysis of the results of tablets and injections are presented in Table 4.

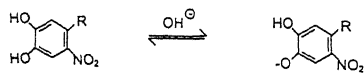
Table 2— Optical characteristics and precision data for method A

Characteristics / Parameter	PCL	DPH	LDP	MDP	ADH
Colour	Red	Red	Red	Red	Red
λ_{max} (nm)	510	505	500	500	500
Stability (h)	20	22	18	10	10
B-L range ($\mu\text{g/ml}$)	0.1-6.4	0.25-11	0.1-6.8	0.25-20	0.2-26
LOD ($\mu\text{g/ml}$)	0.0544	0.0918	0.0379	0.2148	0.1523
LOQ ($\mu\text{g/ml}$)	0.1815	0.3059	0.1266	0.7161	0.5077
Optimum photometric range ($\mu\text{g/ml}$)	0.5-5.2	0.75-10	0.5-5.5	0.75-18	0.8-24
Molar absorptivity ($1 \text{ mol}^{-1} \text{ cm}^{-1}$)	1.35×10^4	9.4×10^3	2.1×10^4	6.45×10^3	6.2×10^3
Sandell's sensitivity ($\mu\text{g/cm}^2$)	0.0085	0.0162	0.0094	0.032	0.029
Regression equation (Y)*	0.04798	0.0568	0.1031	0.0304	0.0257
Slope (a)					
Intercept (b)	-0.0075	0.0049	-0.0105	-0.0013	0.0138
Correlation coefficient (r)	0.9986	0.9987	0.9969	0.9998	0.9995
RSD % ($n=5$)	0.84	1.1	1.2	1.3	1.4
% Range of error ($n=5$) at 95% confidence limit	± 0.30	± 0.42	± 0.38	± 0.50	± 0.52

* $Y = ax + b$, where x is the concentration of catecholamines in $\mu\text{g/ml}$



Nitroso derivative

Nitro catechols
(yellow)

(Red)

where R = H → PCL, -CH₂CH₂NH₂ (DPH), -CH₂C(CH₃)₂-NH₂COOH → (MDP),
-CH₂-CH(NH₂)-COOH → (LDP), -CH(OH)-CH₂NHCH₃ → (ADH)

Scheme 1—Reaction sequence for method A

Table 3— Optical characteristics and precision data for method B

Characteristics / Parameters	PCL	DPH	LDP	MDP	ADII
Colour	Blue	Blue	Blue	Blue	Blue
λ_{max} (nm)	730	730	730	730	730
Stability (h)	1	1	1	1.5	1
B-L range ($\mu\text{g/ml}$)	0.1-3.2	0.1-2.0	0.1-2.4	0.05-1.0	0.1-3.2
LOD ($\mu\text{g/ml}$)	0.0501	0.0335	0.0301	0.0026	0.0456
LOQ ($\mu\text{g/ml}$)	0.1671	0.1116	0.1004	0.0087	0.1523
Molar absorptivity ($1 \text{ mol}^{-1} \text{ cm}^{-1}$)	5.3×10^4	7.2×10^4	1.45×10^5	1.14×10^5	4.4×10^4
Sandell's sensitivity ($\mu\text{g/cm}^2$)	0.0020	0.0026	0.0014	0.0018	0.0042
Optimum photometric range ($\mu\text{g/ml}$)	0.21-2.8	0.2-1.8	0.21-2.0	0.1-0.8	0.2-2.8
Regression equation (Y)*					
Slope (a)	0.2087	0.2733	0.2604	0.5013	0.1716
Intercept (b)	0.0314	0.0241	0.0772	-0.0053	0.0238
Correlation coefficient (r)	0.9971	0.9796	0.9836	0.9980	0.9959
RSD % (n=5)	0.5746	0.747	0.7699	0.2795	0.3462
% Range of error (n=5) at 95% confidence limit	± 0.7977	± 1.038	± 1.068	± 0.3882	± 0.4805

* $Y = ax + b$, where x is the concentration of catecholamines in $\mu\text{g/ml}$

Table 4— Determination of catechol derivatives in pharmaceutical preparations

Drug	Label claim (mg)	% Recovery \pm % RSD *		
		BP Method ⁷	Method A	Method B
Injections				
DPH ^a	200/5 ml	98.85 \pm 1.25	99.80 \pm 0.40	99.90 \pm 0.42
DPH ^b	200/5 ml	99.20 \pm 0.82	99.75 \pm 0.50	99.85 \pm 0.75

Table 4 Contd

Table 4 Contd

ADH ^c	200/5 ml	99.40 ± 0.55	98.95 ± 0.50	98.85 ± 0.65
ADH ^d	200/5 ml	100.00 ± 0.90	99.6 ± 0.80	99.4 ± 0.95
Tablets				
LDP ^e	500	98.78 ± 1.10	99.2 ± 0.70	99.80 ± 0.90
MDP ^f	250	98.78 ± 1.10	98.30 ± 1.3	98.84 ± 1.02

*_n = 5, Marketed by ^aTTK Pharma, ^bTroika Paren; ^cHarson Laboratories, ^dWallace Pharma, ^eSun Pharma; ^fMerind Pharma

Conclusions

The proposed methods are found to be simple, rapid and sensitive than most of the available methods in literature. Heating or extraction is avoided and compounds like resorcinol, phloroglucinol, hydroquinone and pyrogallol do not give the colour reaction for method A. The statistical parameters and the recovery study data clearly indicate the reproducibility and accuracy of the methods. Thus the methods can be adopted as an alternative to the existing methods.

Acknowledgements

One of the authors (R.A.V.) thanks the University of Mysore for the laboratory facilities and the financial assistance from the UGC, New Delhi, in the form of a fellowship under the Faculty Improvement Programme.

References

1. Barnum, D W. (1977) *Anal. Chem. Acta* **89** : 157.
2. Nagaraja, P., Murthy, K.C.S., Yathirajan, H.S. & Mohan B M (1998) *Ind. J. Pharm. Sci.* **60** 99
3. Nagaraja, P., Murthy, K.C.S., Rangappa, K.S. & Madegowda, N.M. (1998) *Talanta* **46** : 39.
4. Nagaraja, P., Vasantha, R.A. & Sunitha, K.R. (2001) *J. Pharm. Biomed. Anal.* **25** : 417.
5. Nagaraja, P., Vasantha, R.A. & Sunitha, K.R. (2001) *Talanta* **55** : 1039.
6. Nagaraja, P., Vasantha, R.A., Murthy, K.C.S. & Rangappa, K.S. (2001) *Chem. Anal.* **46** : 569.
7. *British Pharmacopoeia* (1998) HM Stationery Office, London, Vol. 1, p. 44, 509, 783.

Spectrophotometric determination of nickel with di(o-ethylphenyl) carbazole using the synergistic effect with 1,10-phenanthroline

T. SURESH

Department of Industrial Chemistry Gulbarga University P. G. Centre, Vinayakanagar, Bellary - 583 104, India.

Received July 8, 2002, Revised June 3, 2003; Accepted February 12, 2004

Abstract

A simple, convenient and highly sensitive method of determination of micro amount of nickel has been developed. The coloured complex formed on reaction of di(o-ethylphenyl) carbazole with nickel(II) to give 1 : 2 complex in presence of 1,10-phenanthroline. It is found that the extractability of the nickel di(o-ethylphenyl) carbazonate into chloroform can be increased by the addition of phenanthroline. Synergistic effect for nickel di(o-ethylphenyl) carbazonate with phenanthroline has been investigated.

(Keywords : spectrophotometry/synergistic effect/nickel adducts)

Introduction

In continuation of our studies on substituted diphenylcarbazones and dithizone as analytical reagent¹⁻³, we have examined the synergic extraction of nickel(II) chelate employing bidentate chelating agent di(o-ethylphenyl) carbazole in the presence of an adduct forming substance, 1,10-phenanthroline has received the considerable attention for the spectrophotometric determination of nickel(II)⁴⁻⁵. The method is elegant, sensitive and simple for extractive-photometric determination of micro amount of nickel.

In our present investigation it has been found that the extractability of the nickel(II) di(o-ethylphenyl) carbazole complex, Ni(OEPC)₂, into chloroform can be increased by the addition of phenanthroline and the extracted complex is stable for 6 h which is sufficient to perform analysis. Such synergistic effects are due to an increase in the distribution ratio of a metal chelate on addition of a base such as phenanthroline to the metal chelate. The detailed mechanism of synergistic effects for various metal chelates in presence of neutral bases has been investigated extensively⁶ and a few applications to analytical chemistry have also been reported⁷. In general, the

mechanism seems to involve the formation of a base adduct of a metal chelate. The synergistic effect in the present extraction results from the formation and the preferential extraction of a phenanthroline adduct of Ni(OEPC)_2 .

Materials and Method

The reagent di(o-ethylphenyl) carbazole was prepared by the reported method⁸ involving persulphate oxidation of the corresponding carbazole and then purified⁹. Chloroform (B.D.H.) was purified by the method suggested by Vogel¹⁰. The constant boiling fraction was collected and used. Nickel perchlorate and 1,10-phenanthroline (Fisher Reagent Grade) were used as received. The absorbances were measured by using the Baush and Lomb Spectronic 2000 recording spectrophotometer.

To 10ml of a solution containing from 0.1 to 10 μg of nickel (upto 25 μg may be accommodated) were added 5ml of phthalate or acetate buffer of pH 6.0 (or dilute ammonia may be used) followed by 15ml of a chloroform solution containing $7 \times 10^{-5}\text{M}$ Ni(OEPC)_2 and $3 \times 10^{-5}\text{M}$ phenanthroline. The two phases were shaken for 5 min. phases were separated after allowing them to settle. The chloroform layer was back extracted with 10ml of 0.1M sodium hydroxide shaking vigorously for about 1 min. The organic layer was separated and the absorbance of the extract was measured at 515nm against the reagent blank. The nickel content in unknown solutions was computed from the standard calibration curve.

Typical results are tabulated below :

Ni taken μg	Absorbance at 515nm	Ni found, μg
0.71	0.13	0.73
1.46	0.27	1.47
2.28	0.42	2.31
3.04	0.56	3.01
3.37	0.62	3.29
3.86	0.71	3.87
4.84	0.89	4.91

Results and Discussion

The nickel(II) di(o-ethylphenyl) carbazolephenanthroline adduct system exhibits maximum absorbance at 515nm when measured against the reagent blank and obeys Beer's Law over the range of 0.1-0.25mg of Ni¹¹. The Sandell's sensitivity of the colour reaction is 0.00049 μ g cm⁻² and molar absorptivity 5.33x10⁴lit. mole⁻¹cm⁻¹ at 515nm.

The results of extraction studies of nickel(II) di(o-ethylphenyl) carbazole system shows that nickel can be quantitatively extracted into chloroform in the pH range 6.0-11.0. Below and above the pH range, the extraction of nickel was incomplete. The extracted species exhibited constant and maximum absorption, when the pH of the aqueous phase was maintained with this range.

Various solvents such as benzene, toluene, amyl alcohol, carbon tetrachloride and chloroform were tested for the extraction of nickel complex, but chloroform was found to be the most effective. With 10ml of chloroform, the complex was recovered to the extent of 99.98% by a single extraction, whereas with other solvents, it was found to be less than 95%. For complete extraction of the complex, 5 min. shaking was adequate.

The mixed ligand complex is sufficiently stable to permit the removal of excess of di(o-ethylphenyl) carbazole by back - extraction with 0.1M sodium hydroxide, so a 'monocolour' method is applicable. The molar absorptivity of this complex is 5.33x10⁴ I mole⁻¹cm⁻¹ which makes a method based on this reaction about four times as sensitive as the dimethylglyoxime method used as oxidising agent¹¹.

References

- 1 Suresh, T & Kulkarni, V.H (1994) *Asian J Chem* **6** : 690.
- 2 Suresh, T. (1994) *Acta Cienica Indica* **XXC** : 58
- 3 Suresh, T. & Kulkarni, V.H. (1995) *J Indian Chem Soc.* **72** : 887.
4. Suresh, T., Kulkarni, V.H. & Hippalagi, S S (1994) *Nat Acad. Sci. Letters* **17** : 141.
- 5 Suresh, T. & Basavaraj, B. (1998) *Proc Nat Acad Sci India* **68(A)** : 121.
6. Healy, T.V (1961) *J Inorg Nucl Chem.* **19** : 328.
7. Taketatsu, T. & Banks, C.V. (1966) *Anal. Chem.* **38** : 1524, Akaiwa, H. & Kawamoto, H (1967) *Jpn Analyst*, **16** : 359, Math, K.S., Bhatki, K.S. & Frciscr, H. (1969) *Talanta* **16** : 412.
- 8 Hubbard, D.M. & Scott, E.W. (1953) *J Am Chem. Soc.* **65** : 2390.

- 9 Ghosh, N.N & Ray, J N (1960) *J Indian Chem Soc* **37** : 650
- 10 Vogel, A I (1964) *Text Book of Practical Organic Chemistry*, 3rd Ed , Longmans Press, London, p 176
11. Sandell, E B (1959) *Colorimetric Determination of Traces of Metals*, Interscience Publication, New York, p 669.

Titrimetric and spectrophotometric methods for the assay of albendazole in non-aqueous medium

K. BASAVAIAH¹, P.NAGEGOWDA¹ and V. RAMAKRISHNA²

¹*Department of Chemistry, University of Mysore, Manasagangotri, Mysore-570006 India*

²*Department of Pharmaceutical Chemistry, Government College of Pharmacy, Bangalore-560027, India*

Received December 22, 2003, Accepted February 17, 2004

Abstract

Three simple, rapid and cost-effective methods based on titrimetry and spectrophotometry are described for the determination of albendazole in pure form and in dosage forms. In titrimetry, the drug is dissolved in glacial acetic acid and titrated with acetous perchloric acid with visual and potentiometric end point detection, crystal violet being used as indicator for visual titration. Spectrophotometry involves adding different amounts of drug to a fixed amount of perchloric acid-crystal violet mixture and measuring the increase in absorbance at 570 nm. Both the titrimetric methods are applicable over 2-20 mg range, and in spectrophotometry, Beer's law is obeyed over range 5-60 $\mu\text{g ml}^{-1}$. The apparent molar absorptivity is calculated to be $2.18 \times 10^3 \text{ l mol}^{-1} \text{ cm}^{-1}$ with a Sandell sensitivity of 121.9 ng cm^{-2} . The limits of detection and quantification are calculated to be 1.02 and 3.39 $\mu\text{g ml}^{-1}$, respectively. The methods when applied to the assay of albendazole in tablet gave satisfactory results (97.26 to 102.53%). The accuracy and reliability of the methods were further ascertained by parallel determination by a reference method and by recovery studies via standard-addition technique.

Keywords : Albendazole/determination/titrimetry/spectrophotometry/non-aqueous medium/formulations

Introduction

Albendazole, chemically, 5-propyl thio-1H benzimidazole methyl carbamate¹ (Fig. 1) which in therapeutics is known as anthelmintic drug having a wide spectrum of activity². The therapeutic importance of albendazole justifies research to develop analytical methods for its determination in biological samples and in pharmaceuticals. The most widely used technique for the assay of albendazole has been the high performance liquid chromatography (HPLC) and has been used for the determination of the drug in biological fluids^{3,4}, plasma⁵⁻⁹, veterinary formulations¹⁰ and meat samples¹¹. Ion-pair liquid chromatography with uv-detection has been applied to the determination of the drug residus in milk and drug metabolites¹², and in cattle feed¹³.

The same technique with fluorescence detection has been used for drug in milk¹⁴. Liquid chromatography (LC) with fluorescence detection¹⁵ and uv-detection¹⁶ has found applications in the quantification of albendazole residues in cattle liver and in pork muscle tissue, respectively. Even-hyphenated techniques such as LC-MS and GC-MS have found use in the determination of drug residues in food products¹⁷ and in cattle liver¹⁸, respectively.

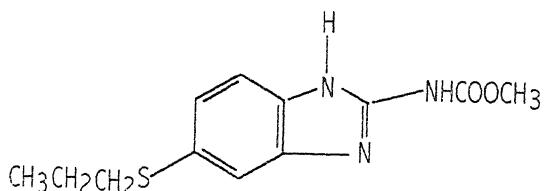


Fig 1– Structure of albendazole

Not many methods are found in the literature for the determination of albendazole in pharmaceutical products. Five methods based on the use of HPLC¹⁹⁻²³ have been proposed for bulk drug and for formulations and are less sensitive with linear ranges being 20-100 µg ml⁻¹¹⁹ 0.1-0.4 mg ml⁻¹²⁰ and 50-300 µg ml⁻¹²¹. The drug in tablets has been assayed by voltammetry²⁴ and uv-spectrophotometry^{25,26}. Two visible spectrophotometric methods, one based on ion-pair complex formation between the drug and acid dyes such as bromocresol green, bromophenol blue, bromophenol red and bromothymol blue followed by extraction into chloroform and absorbance measurement at 420 nm has been proposed by Sane *et. al.*²⁷ A similar reaction but involving picric acid²⁸ as the ion-pair reagent has served as the basis for the spectrophotometric determination of albendazole. Zarapkar and Deshpande have reported a redox method using Folin-Ciolteau reagent²⁹ for the assay of albendazole in tablets and syrup. Another redox method involves the treatment of the drug with a known excess of N-bromosuccinimide (NBS)³⁰ followed by the determination of the surplus oxidant spectrophotometrically based on charge-transfer complex reaction or using the dye Celestine Blue. One of the present authors³¹ has recently reported three procedures using bromate-bromide mixture and methyl orange dye, based on oxidation-bromination reaction, for the assay of drug both in pure form and in formulations. Though the procedures are fairly sensitive, they suffer from such disadvantages as extraction step^{27,28}, lack of selectivity^{29,31}, and use of an unstable reagent³⁰.

The present paper describes three methods based on the basic property of the drug molecule. In titrimetric procedures, the drug solution in glacial acetic acid is titrated

directly with acetoic perchloric acid, the end point being determined either visually using crystal violet indicator or potentiometrically using combined glass-modified SCE system. Spectrophotometry involves the treatment of a fixed amount of perchloric acid-crystal violet mixture with drug and measurement of absorbance at 570 nm. The increase in absorbance is related to drug concentration.

Materials and Method

Apparatus All absorbance measurements were made with a Systronics Model 106 digital spectrophotometer provided with matched 1-cm quartz cells. Potentiometric titration was performed with an Elico-120 digital pH meter provided with a combined glass-SCE system, the KCl of the salt bridge being replaced with 0.1M lithium perchlorate solution in glacial acetic acid.

Reagents and standards All chemicals used were of analytical reagent grade. All solutions were made in glacial acetic acid unless specified otherwise.

Perchloric acid (0.01 M) To 4.5 ml of 70 % perchloric acid (S. d. Fine Chem, Mumbai, India) was added 150 ml of glacial acetic acid, mixed well; added 10.5 ml of acetic anhydride and allowed the solution to cool for 30 min; finally diluted to 500 ml with glacial acetic acid and allowed to stand overnight. This perchloric acid (~0.1 M) was diluted to get 0.01 M acid with glacial acetic acid and standardized with pure potassium biphthalate and crystal violet indicator.

Crystal violet indicator. Prepared by dissolving 0.1 g of dye in 100 ml glacial acetic acid.

Perchloric acid-crystal violet mixture (1.5 mM HClO₄ - 0.25 mM crystal violet) Prepared by mixing 15 ml of 0.01 M perchloric acid and 10 ml of 1000 µg ml⁻¹ crystal violet solutions and diluting to 100 ml with glacial acetic acid.

Standard drug solution Pharmaceutical grade albendazole was procured from Cipla India Ltd., Mumbai, as gift, and was used as received. A stock standard solution containing 2 mg ml⁻¹ albendazole was prepared by dissolving 500 mg of pure drug in glacial acetic acid and diluting to the mark in a 250 ml calibrated flask. This solution (2 mg ml⁻¹) was used for titrimetric work, and for spectrophotometric work, the same was diluted appropriately with glacial acetic acid to get 100 µg ml⁻¹ working concentration.

Procedures

Visual titration (Method A). A 10 ml aliquot of standard drug solution containing 2-20 mg of albendazole was pipetted out into a clean and dry 100 ml titration flask, 2

drops of crystal violet indicator was added and titrated with standard 0.01 M perchloric acid to an emerald green end point. The amount of drug in the measured aliquot was calculated from

$$\text{Amount (mg)} = VMR$$

where V = volume of perchloric acid required, ml

M = relative molecular mass of drug,

R = molarity of perchloric acid.

Potentiometric titration (Method B) A 10 ml aliquot of standard drug solution equivalent to 2-20 mg of albendazole was pipetted out into a clean and dry 100 ml beaker and the solution was diluted to 30 ml by adding glacial acetic acid. A combined glass-SCE (modified) system was dipped in the solution. The contents were stirred magnetically and the titrant (0.01M HClO_4) was added from a micro burette. Near the equivalence point, the titrant was added in 0.2 ml increments. After each addition of titrant, the solution was stirred magnetically for 30 S and the steady potential was noted. The addition of titrant was continued until there was no significant change in potential on further addition of titrant. The equivalence point was determined by applying the graphical Gran's plot method. The amount of drug in the measured aliquot was calculated as described under visual titration.

Spectrophotometric assay (Method C) Different aliquots (0.5 - 6.0 ml) of standard $100 \mu\text{g ml}^{-1}$ drug solution were accurately transferred into a series of 10 ml calibrated flasks. An exactly measured (2 ml) perchloric acid-crystal violet mixture was added to each flask and the volume was diluted to the mark with glacial acetic acid, mixed well and absorbance was measured at 570 nm against a reagent blank. The increasing absorbance values at 570 nm were plotted against the concentration of drug to obtain the calibration graph. The concentration of the unknown was read from the calibration graph or calculated from the regression equation obtained from Beer's law data.

Procedure for tablets. Twenty tablets were weighed and ground into a fine powder. An amount of powder equivalent to 500 mg of albendazole was weighed accurately into 250 ml calibrated flask, 150 ml of glacial acetic acid added and shaken for about 20 min. Then, the volume was made up to the mark, mixed well and filtered using a quantitative filter paper. First 10 ml portion of the filtrate was discarded and a suitable aliquot was then subjected to analysis by titrimetry. The filtrate equivalent to 2 mg ml^{-1} was diluted appropriately to obtain $100 \mu\text{g ml}^{-1}$ drug solution and analysed by spectrophotometry as described under the general procedure.

Results and Discussion

Several titrimetric³¹, voltammetric²⁴ and spectrophotometric^{30,31} methods have been described for the determination of albendazole based on latter's redox property. A couple of extraction spectrophotometric methods^{27,28} utilizing the tertiary nitrogen of the drug molecule have also been proposed. The present methods are based on the basic property of albendazole employing two techniques. The methods are based on the principle that substances, which are too weakly basic in aqueous medium, exhibit enhanced basicity in non-aqueous solvents thus allowing their easy determination. In the present titrimetric methods, the weakly basic property of albendazole was enhanced due to the non leveling effect of glacial acetic acid and titrated with perchloric acid with visual and potentiometric end point detection. Crystal violet gave highly satisfactory end point for the concentrations of analyte and titrant employed. A steep rise in the potential was observed at the equivalence point with potentiometric end point detection (Fig 2). The Gran's plot method was applied to ascertain the equivalence point (Fig 3). With both methods of equivalence point detection, a reaction stoichiometry of 1: 1 (drug: titrant) was obtained which served as the basis for quantitation. Using 0.01 M perchloric acid, 2-20 mg of albendazole was conveniently determined. The relationship between the drug amount and the titration end point was examined. The linearity between two parameters is apparent from the correlation coefficients of 0.9983 and 0.9996 obtained by the method of least squares for visual and potentiometric methods, respectively. From this, it is implied that the reaction between albendazole and perchloric acid proceeds stoichiometrically in the ratio 1 : 1 in the range studied.

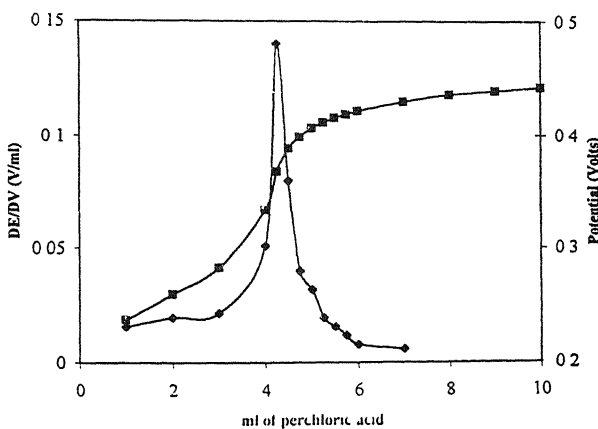


Fig. 2— Potentiometric end point point.

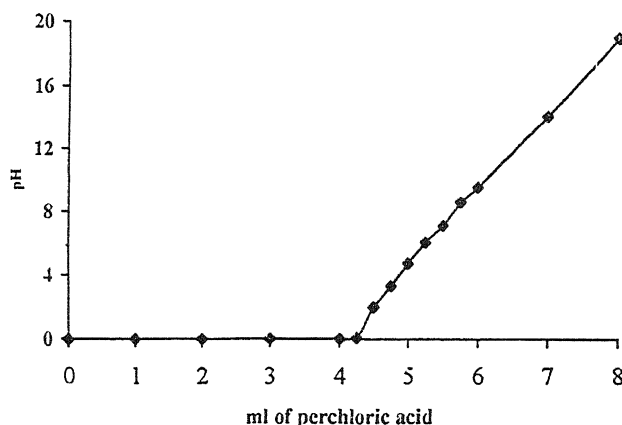


Fig. 3—Gran's plot

Crystal violet is a dye exhibiting violet colour in the base form and emerald green in the acid form. The present spectrophotometric method is based on the facts that the colour of the dye is dependent on the pH of the solution and that the colour change is not sudden but occurs continuously as the pH changes over a definite range. To a fixed amount of acid-dye mixture where the dye is in the acid form (emerald green), different amounts albendazole were added. This caused a progressive increase in pH of the solution because of neutralization of acid by the added drug (base), and as a result, the concentration of the acid form of the dye increases. This is shown by the proportional increase in the absorbance of the solution at 570 nm (Fig 4) which is corroborated by the correlation coefficient of 0.9982.

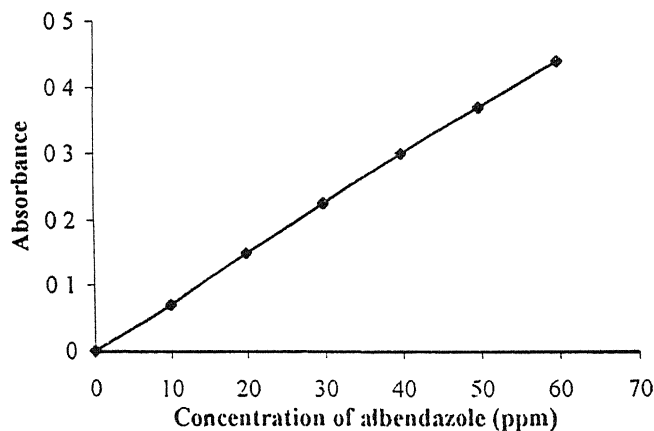


Fig. 4—Calibration graph

In a preliminary study, 20 $\mu\text{g ml}^{-1}$ crystal violet in basic medium was found to exhibit a convenient absorbance at 570 nm. In the presence of 2 ml of 1.5 mM perchloric acid in a total volume of 10 ml, this absorbance decreased to a constant minimum. Hence, different amounts of drug were treated with a fixed amount of acid-dye mixture i.e., 2 ml of 1.5 mM HClO_4 - 0.25 mM crystal violet ($100 \mu\text{g ml}^{-1}$) to determine the concentration range of the drug that could be determined by the method of absorbance transitions of the dye accompanying the pH changes. The dye colour was found to be stable for several hours, and the order of addition of reactants was not critical.

The increasing absorbance values at 570 nm were plotted against the increasing concentration of drug to obtain a calibration graph. Beer's law is obeyed over the concentration range 5-60 $\mu\text{g ml}^{-1}$, the equation of the line being

$$A = 0.013 + 0.007 C$$

where A is absorbance and C concentration in $\mu\text{g ml}^{-1}$. The correlation coefficient of the calibration plot was calculated to be 0.9982 ($n=7$) confirming a linear increase in absorbance with increasing concentration of albendazole. The calculated molar absorptivity was found to be $2.2 \times 10^3 \text{ l mol}^{-1} \text{ ml}^{-1}$ at 570 nm and the Sandell sensitivity was 122 ng cm^{-2} . The limits of detection and quantification were calculated from the standard deviation of the absorbance measurements obtained from a series of seven blank solutions. The limits of detection and quantification established according to IUPAC definitions³² were 1.02 and 3.39 $\mu\text{g ml}^{-1}$, respectively.

Accuracy and precision

The accuracy and precision of the methods were established by analyzing the pure drug solution at three different levels. The relative error (%), which is a measure of accuracy, is < 2% revealing high accuracy of the methods. The coefficient of variation, which is an indicator of precision, is less than 1.5 % and speaks of excellent precision of the methods. The results of the study are complied in Table 1.

Application

The proposed methods were successfully applied to determine albendazole in tablets. The same batch tablets were analysed by an established procedure for comparison. The results obtained by the proposed methods agree well with these of reference method and with the label claim.

Table 1—Evaluation of accuracy and precision of the methods

	Method A				Method B				Method C			
	Amount taken, mg	Amount found*, mg	Relative error, %	RSD, %	Amount taken, mg	Amount found**, mg	Relative error, %	RSD, %	Conc taken, μg ml ⁻¹	Conc found* μg ml ⁻¹	Relative error, %	RSD, %
10.00	10.14	1.40	0.48	10.00	10.13	1.30	0.11	10.00	10.07	0.70	0.86	
15.00	15.08	0.53	0.86	15.00	15.28	1.86	0.67	30.00	30.45	1.50	0.83	
20.00	19.66	1.69	0.73	20.00	20.22	1.10	0.38	50.00	14.42	1.16	0.76	

*Average value of seven determinations

**Average value of three determinations

RSD - Relative standard deviation.

The results were also compared statistically by a Student's t-test for accuracy and a variance ratio F-test for precision with those of the reference method³³ at 95% confidence level as summarized in Table 2. The results showed that the calculated t- and F- values did not exceed the tabulated values inferring that proposed methods are as accurate and precise as the reference method³³.

Table 2- Results of assay of tablets by the proposed methods

Tablet brand name*	Nominal value (mg)	Method A ^ψ	Method B ^{\$}	Method C ^ψ	Official method
Alminth ^a	200	99.86 ± 1.25 t=1.63 F=1.88	100.24 ± 0.68 t=1.26 F=1.79	102.36 ± 1.54 t=1.78 F=2.86	100.98 ± 0.92
Albazole ^b	400	100.76 ± 1.06 t=2.58 F=2.29	100.42 ± 1.18 t=1.60 F=2.84	97.63 ± 0.85 t=1.41 F=1.47	99.32 ± 0.70
Dispel ^c	400	98.62 ± 1.36 t=2.31 F=2.23	100.63 ± 0.58 t=0.64 F=2.46	99.28 ± 1.16 t=1.52 F=1.62	100.28 ± 0.91
Nopar ^d	50	99.83 ± 0.97 t=1.72 F=3.59	99.88 ± 1.28 t=1.30 F=2.07	102.28 ± 0.82 t=1.09 F=5.03	101.36 ± 1.84

*Marketed by a. Torrent Pharmaceuticals,

b · Wings Pharma; c · Indchemie; d · Malladi Drugs ,

Tabulated t-value at 95% confidence level is 2.77 A & C, 2.37 for method B

Tabulated F-value at 95% confidence level is 6.39 A & C, 9.28 for method B.

ψ · Mean value of five determinations

\$: Mean value of three determinations

Table 3—Results of recovery study by standard addition method.

Preparation studies	Amount of drug in tablet, mg	Amount of pure drug added, mg	Method A			Method B			Method C		
			Total found, mg	Recovery* of pure drug, %	Amount of drug in tablet, mg	Total found, mg	Recovery* of pure drug, %	Amount of drug in tablet, mg	Total found, mg	Recovery* of pure drug, %	Amount of drug added, mg
Alminth (200 mg)	4.98	4.0	8.89	97.75	8.08	4.00	12.19	102.75	100.06	200.0	305.12
			12.90	99.00	8.08	6.00	13.91	97.16	100.06	300.0	400.36
Albazole (400 mg)	4.98	12.0	17.07	100.75	8.08	8.00	15.83	96.87	100.06	400.0	506.30
			10.28	102.50	9.86	4.00	14.00	103.20	149.88	200.0	348.60
Dispel (400 mg)	6.18	8.0	14.05	98.37	9.86	6.00	16.02	102.67	149.88	300.0	451.53
			17.80	96.83	9.86	8.00	17.94	101.00	149.88	400.0	549.88
	8.21	4.0	12.17	99.00	12.21	4.00	16.23	100.50	200.2	200.0	397.40
			16.23	100.25	12.21	6.00	18.13	98.67	200.2	300.0	498.76
	8.21	12.0	20.28	100.58	12.21	8.00	20.03	97.75	200.2	400.0	593.88
											98.42

*Mean value of three determinations

Accuracy and reliability of the methods were further ascertained by performing recovery experiments. To a fixed amount of the drug in tablet (pre-analysed), pure drug at three different levels was added, and the total was found by the proposed methods. Each test was repeated three times. The results compiled in Table 3 show that the recoveries were in the range 96.8 – 103.2% indicating that commonly added excipients to tablets such as talc, starch, gelatin, sodium alginate, magnesium stearate, calcium gluconate, calcium dihydrogenorthophosphate etc, did not interfere in the determination.

Conclusions

Albendazole has been determined in tablets using three different techniques. The developed methods are rapid, simple and accurate. The proposed spectrophotometric method is comparable in sensitivity to many of the existing methods including HPLC procedures. The procedure is free from tedious steps like extraction or heating and involves least number of experimental variables which is reflected in high precision. All the three methods are applicable over long dynamic concentration range and can serve as useful reference methods which could be used for a specific albendazole assay.

Acknowledgement

The authors thank the Quality Control Manger, Cipla India Ltd., Mumbai, India for gifting pure albendazole. Two of the authors (PN and VRK) thank the University of Mysore, Mysore for providing research facilities.

References

- 1 Reynolds, J. E F & Martindale (1989) *The Extra Pharmacopoeia*, 29th ed , The Pharmaceutical Press, London, p 47.
- 2 Goodmann & Giaian, *The Pharmaceutical Basis of Therapeutics*, 7th ed , MacMillan Publishing Company, New York, Chapter 44, p 102
- 3 Del Revero, L. M., Jung, H , Castillo, R & Campos, H A (1998) *J Chromatogr Biomed Appl* 712 : 237.
- 4 Hoaksey, P E., Awadzzi, K., Ward, S A, Conventry, P. A, Oreme, M.L.E. & Edwards, G (1991) *J Chromatogr. Biomed Appl.* 104 : 244.
5. Lan Chote, V.L., Camarques, M.P., Takayanagu, O.M , De Carvalho, R , Paixas, F O. & Bonato, P.S. (1998) *J Chromatogr Biomed. Appl.* 709 : 273.

- 6 Botsoglou, N A , Fletouris, D J , Psomas, I E & Mants, A I (1997) *Anal Chim Acta* **354** : 115
- 7 Hurtado, M , Medina, M T , Sotelo, J & Jung, H (1989) *J Chromatogr Biomed Appl* **494** : 403.
- 8 Zeugin, T , Zysset, T & Cotting, J (1990) *Ther Drug Monitor.* **12** 187
- 9 Polo, S R., Torrado, T , Bolas, F & Torrado, S (1998) *J Liq Chromatogr Rel Technol* **21** : 2327
- 10 Vantonder, E C , De Villers, M M , Handford, J S , Malan, C E P. & Du Preez, A V (1996) *J Chromatogr* **729** . 627
- 11 Mart, A M , Mooser, A E & Koch, H (1990) *J Chromatogr* **498** · 145
- 12 Fletouris, D J., Botsoglou, N A & Psomas, I E (1997) *Anal Chim Acta* **345** 111.
- 13 Botsoglou, N A , Fletouris, D J , & Psomas, I E (1999) *J Liq Chromatogr Relat Technol* **22** . 2297
- 14 Fletouris, D J , Botsoglou, N.A , Psomas, I E. & Mahtis, A I (1997) *Anal Chim. Acta* **345** . 111
- 15 Markus, J. & Sherma, J (1992) *J Assoc off Anal Chem Int* **75** 1129
- 16 Long, A R , Hsech, L C, Malbrough, M S , Short, C R & Barker, S.A (1990) *J Food Compos Anal* **3** : 20
- 17 Casetta, B., Cozzani, R , Cinquina, A L. & Dimarzio, S (1996) *Rapid Commun Mass Spectrom* **10** : 1497.
- 18 Markus, J. & Sherma, J (1992) *J Assoc off. Anal Chem Int* **75** 1135.
- 19 Maian, C.E P., De Utiliers M M & Loetter, A.P (1997) *Drug. Dev Ind Pharm* **23** : 533.
- 20 Sane, R T , Samant, R.S , Joshi, M D , Parandare, S M., Tembe, P.B & Nayak, U G. (1989) *Indian Drugs* **26** · 494.
- 21 Liawruangrath, B. & Liawruangrath, S. (1998) *ACGC Chem Res Commun* **8** 45.
- 22 Krishnaiah, Y S.R., Latha, K., Karthikeyan, R S. & Sathyanarayana, V (2002) *Asian J. Chem* **14** : 67.
- 23 Gomes, A R. & Nagaraju, V. (2001) *J Pharm Biomed Anal* **26** : 919
24. De Oliveira, M.F & Stradiotta, N.R. (2001) *Anal Lett* **34** : 377
25. Mandal, S.C , Bhattacharya, M., Marty, A K , Gupta, B R. & Ghoshal, S.K. (1992) *Indian Drugs* **29** . 323
26. Wu, Y., Liu, F. & Li, C. (1991) *Zhongguo Yao Gongye Zazhi* **22** : 75
27. Sane, R.T., Gangal, D.P., Tendolkar, R.V., Ladage, K.D. & Kotharkar, A.M. (1989) *Indian Drugs* **26** . 632.
28. Senthil, K.N., Gana, S V., & Lalitha, R K.G (1998) *East Pharm* **41** : 125.

- 29 Zarapkar, S S & Deshpande, D M (1998) *Indian J Pharm Sci* **50** 296
- 30 Sastry, C S P , Sarma, V A N , Prasad, U V & Lakshmi, C S R (1997) *Indian J Pharm Sci* **59** 161
- 31 Basavaiah, K & Prameela, H C (2003) *Anal Bioanal Chem* **376** 879
- 32 IUPAC (1978) *Spectrochim Acta*, Part 13, **33** 242
- 33 *United States Pharmacopoeia* (1993) 25th ed , National Formulary, p 54

Weak-waves in reacting gases

K PANDEY and R. CHATURVEDI

*Department of Mathematics & Astronomy Lucknow University, Lucknow-226 007,
India*

Received July 15, 2002, Revised April 4, 2003, Accepted July 12, 2003

Abstract

In the present paper an attempt has been made to obtain and discuss the growth and decay of weak discontinuities in characteristic plane for reacting gases, when chemical reaction between n species are taken as the source of non-equilibrium effects. The critical amplitude of the initial compressive-disturbance has been determined and it is shown that any compressive-wave with an initial amplitude greater than critical one will terminate into a shock-wave, while compressive-wave with an initial amplitude less than the critical one will result in a decay. With the help of Laplace-transformation exact solutions and solution upto first order of small quantities have been obtained and discussed for expansion-wave.

(Keywords weak-wave/non-equilibrium flow/reacting gases)

Introduction

Bauer and Bass¹ have demonstrated that gas maintained in ambient vibrational and, radiative non-equilibrium by thermal radiation can amplify acoustic-waves. Using gas dynamic approach Srinivasan and Vincenti² have obtained a criteria for acoustic instability in a gas with ambient vibrational and radiative-non-equilibrium. Ram and Singh³ have discussed the growth and decay of weak discontinuities in relativistic fluids with vibrational-relaxation. Johnnesen⁴ has analysed the vibrational relaxation region by Rayleigh method. Ram and Pandey⁵ have discussed the growth and decay of acceleration-waves in transient gas flows with vibrational-relaxation. Wegener *et al.*⁶ have discussed weak-waves in relaxing flows with a single relaxing process. Sharma⁷ had obtained explicit criteria for the breaking or non-breaking of acceleration-waves in plane, axially or spherically symmetric flow of a relaxing gas by taking into account a general relaxing gas model. Sharma *et al.*⁸ have discussed the behaviour of discontinuity at the wave head propagating through a relaxing gas. Clark *et al.*⁹ have discussed the dynamics of relaxing gas. Rarity¹⁰ has investigated the break-down of characteristic solutions in flow with vibrational-relaxation. Moore and Gibson¹¹ have studied the propagation of weak-disturbances in a gas subject to

relaxation effect Shuler¹² has analysed the relaxation processes in multistate systems Sharma¹³ has investigated the growth and decay properties of first order discontinuities headed by wave-front of arbitrary shape in non-equilibrium flows of relaxing gas. Borer¹⁴ has discussed the method of characteristics for the computation of supersonic flow field in a reacting gas under equilibrium condition Chu¹⁵ has discussed the wave propagation in reacting mixture Coleman and Gurtin¹⁶ have discussed growth and decay of discontinuities in fluids with internal state variables Pandey and Saxena¹⁷ have discussed weak-waves in dissociating gases

Having such rich back-ground of non-equilibrium flows, in this paper an attempt has been made to discuss growth and decay of weak-discontinuity for reacting gases, where chemical reaction between n -species has been taken as the source of non-equilibrium effect.

Equation of Motion in Characteristic Plane and Behaviour at Wave-Front

Neglecting viscosity, heat-conduction and body forces, equations governing one-dimensional motion of reacting gases are given by

$$U_t + BU_x + D = 0 \quad (1)$$

where U is a column matrix of order $(n+3) \times 1$ with elements $p, u, s, c_1, c_2, \dots, c_n$. B is a square matrix of order $n+3$, with elements $b_{12} = \rho a_f^2, b_{12} = \frac{1}{\rho}, b_n = u$ and other elements zero, D is a column matrix of order $(n+3) \times 1$ with elements

$$d_1 = a_f^2 \sum_{i=1}^n \left(\frac{\rho_s}{T} A_i + \rho c_i \right) \dot{c}_i + \frac{\nu u \rho}{x} a_f^2, \quad d_2 = 0$$

$$d_3 = -\frac{1}{T} \sum_{i=1}^n A_i \dot{c}_i, \quad d_i = \frac{\omega_i}{\rho} (i = 1, \dots, n)$$

ρ, u, p, s, T being density, velocity, pressure entropy and temperature of gas, a_f is frozen sound speed and A_i, c_i and ω_i are affinity, concentration and rate of production

of i th species $\nu = 0, 1, 2$ for planer, cylindrical and spherical symmetry. A comma followed by an index denotes partial derivatives with respect to that index. 0 is a null matrix of order $n+3$ and \dot{c}_i is material derivative (i taking values 1 to n).

A function $U(x,t)$ satisfying equation (1), every where except at the characteristic curve $\Sigma(t)$ is said to be a weak-discontinuity at this curve and propagate along the characteristics, where U is continuous and $U_{,t}$ and $U_{,x}$ may suffer a finite jump. There are $(n+3)$ families of characteristics of equation two of which

$$\frac{dx}{dt} = u \pm a_f \quad (2)$$

represent the wave propagation in $\pm x$ direction with an effective local-speed of sound a_f and

$$\frac{dx}{dt} = u \quad (3)$$

repeated for $(n+1)$ times represent the particle path.

In studying the wave phenomenon governed by hyperbolic equations, it is usually more natural and convenient to use the characteristics of governing system as the reference coordinate system. Following Chu¹⁵ and introducing two characteristic variables α and ψ , equations of motion in characteristic plane are given by

$$(p_{,\alpha} - a_f \rho u_{,\alpha}) t_{,\psi} - p_{,\psi} t_{,\alpha} = 0 \quad (4)$$

$$T s_{,\alpha} - \left(\sum_{i=1}^n A_i \dot{c}_i \right) t_{,\alpha} = 0 \quad (5)$$

$$c_{i,\alpha} - c_i t_{,\alpha} = 0, (i = 1, \dots, n), \quad (6)$$

$$P_{,\psi} + \rho a_f u_{,\psi} + a_f^2 \left\{ \sum_{i=1}^n \left(\frac{\rho_s}{T} A_i + \rho c_i \right) \dot{c}_i + \frac{\nu \rho u}{x} \right\} t_{,\psi} = 0 \quad (7)$$

The boundary conditions at the characteristic wave front $\alpha = 0$ are

$$p_{,\psi} = u_{,\psi} = \rho_{,\psi} = c_{i,\psi} = 0. (i=1, \dots, n)$$

$$t_{,\psi} = 1$$

$$p_{,\alpha} = \rho_0 \quad a_{f0} \quad u_{,\alpha} = c_{i,\psi} = 0, (i = 1, \dots, n)$$

$$x_{,\alpha} = 0$$

$$x_{,\psi} = a_{f0}$$

where flow variables associated with the undisturbed medium ahead of the wave signified by the subscript 'o'.

At wave-front, $\alpha = 0$

$$u_{,x} = -\frac{u_{,\alpha}}{a_{f0}, t_{,\alpha}} \stackrel{\text{def}}{=} \bar{\alpha}.$$

Introducing dimensionless parameters

$$\bar{\delta} = \frac{\bar{\alpha}}{\bar{\alpha}^*}, \quad \eta = \frac{\Psi - \Psi^*}{2\Psi^*}$$

$$\lambda = (\Gamma_0 + 1)\bar{\alpha}^* \Psi^*$$

$$\sigma = a_{f0}^2 \Psi^* \sum_{i=1}^n \left\{ \rho_{,c_{i0}} \left(c_{i,P} \right)_0 \right\}$$

fundamental equation for the evaluation of a weak-wave reduces to

$$\frac{d\bar{\delta}}{d\eta} + \left(\sigma + \frac{\nu}{2\eta+1} \right) \bar{\delta} + \lambda \bar{\delta}^2 = 0 \quad (8)$$

Solution of equation (8) is

$$\bar{\delta} = \left[(1+2\eta)^{\nu/2} e^{\sigma\eta} \{1 + \lambda W(\eta)\} \right]^{-1}, \quad (9)$$

where

$$W(\eta) = \int_0^\eta \frac{e^{-(\sigma\eta)}}{(1+2\eta)^{\nu/2}} d\eta$$

and

$$\Gamma = 1 + (\alpha_f^2)_{,p}$$

The function $W(\eta)$ plays an important role in the breakdown of the characteristic solution. As $W(\eta) \geq 0$, only compressive-wave front may terminate into a shock-wave.

(i) Plan-Wave-Front

For plane-wave-front, $\nu = 0$, hence

$$u_{,\alpha\psi} = -\Omega u_{,\alpha}, \quad (10)$$

$$\text{where } \Omega = \frac{\alpha_{f0}^2}{2} \sum_{i=1}^n \left\{ p_{,c_{i0}} \left(c_{i,p} \right)_o \right\}$$

From equation (10), we have

$$u_{,\alpha} = u_{,\alpha}^* e^{-\Omega(\psi-\psi^*)} \quad (11)$$

which gives dependence of $u_{,\alpha}$ at the wave front on time. Since at wave front, $t = \psi$, $u^*_{,\alpha}$ is value of $u_{,\alpha}$ at $t = t^*$

For unconstrained equilibrium case,

$$\Omega = \sum_{i=1}^n \left\{ \frac{1}{2\tau_i} \left(\frac{a_{f0}^2}{a_{e0}^2} - 1 \right) \right\}$$

The critical time for shock-formation is given by

$$t_c = t^* + \frac{2t^*}{\sigma} \left\{ \frac{(\Gamma_o + 1)\bar{\alpha}^* t^*}{(\Gamma_o + 1)\bar{\alpha}^* t^* + \sigma} \right\}$$

Velocity gradient $u_{,x}$ is given by

$$u_{,x} = \frac{u^*_{,x} e^{-\Omega(t-t^*)}}{1 + \frac{\Gamma_o + 1}{2} u^*_{,x} \left(\frac{1 - e^{-\Omega(t-t^*)}}{\Omega} \right)} \quad (12)$$

which in dimensionless form can be written as

$$\bar{\delta} = \left\{ e^{\sigma\eta} + \frac{\lambda}{\sigma} (e^{\sigma\eta} - 1) \right\}^{-1} \quad (13)$$

For rarefaction wave-front, velocity-gradient at an instant t^* is positive and will decrease exponentially and damped out ultimately. This nature is exhibited by curve 'd' and 'e' in Fig. 1. For compressive-wave front, velocity gradient at the wave front will be steepen up into a shock-wave as shown by curves 'c' and 'i' in Fig. 1. However, if

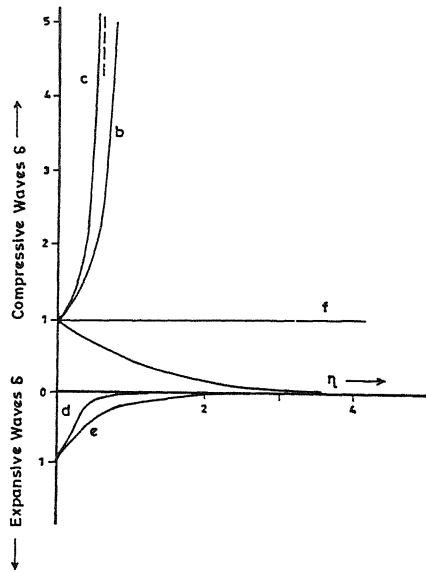


Fig 1—Growth and decay of non-linear waves with planar symmetry

$$u_{,x} = -\frac{2\Omega}{\Gamma_0 + 1}$$

velocity gradient at the wave-front will remain constant in time.

(ii) Particular cases

Case I - for $n = 0$, we have, law of propagation for ordinary gas

Case II - for $n = 1$, we have law of propagation for single relaxation mode discussed by Clark⁹ and Rarity¹⁰

Case III - for $n = 2$, case for disociation and vibrational mode can be discussed.

(iii) Cylindrical and spherical wave-front

For cylindrical and spherical wave front, we put $\nu=1$ and 2 in equation (9) respectively and accordingly have equations

$$\bar{\delta} = [(1 + 2\eta)^{1/2} e^{\sigma\eta} \{1 + \lambda W(\eta)\}]^{-1}$$

and

$$\bar{\delta} = [(1 + 2\eta)e^{\sigma\eta}\{1 + \lambda W(\eta)\}]^{-1}$$

respectively. Nature of cylindrical and spherical wave-fronts are almost similar to that for plane-wave front.

Weak Non-Linear Wave

Here we discuss certain properties of weak-non linear wave in reacting-gases for planer-wave front and obtain exact solution with the help of Laplace-transformation.

Following Chu¹⁵ governing equations in this case are

$$P_{,\alpha}^{(1)} - u_{,\alpha}^{(1)} - p_{,\psi}^{(1)} = 0 \quad (14)$$

$$c_{i,\alpha}^{(1)} = -\frac{1}{\tau_i} \left\{ c_i^{(1)} - \bar{c}_i^{(1)} \right\} \quad i = 1, \dots, n \quad (15)$$

$$p_{,\psi}^{(1)} + u_{,\psi}^{(1)} = \sum_{i=1}^n \left\{ \frac{\rho_{,c_{i0}}}{\tau_i} \left(c_i^{(1)} - \bar{c}_i^{(1)} \right) \right\} \quad (16)$$

$$x_{,\alpha}^{(1)} = u \quad (17)$$

$$x_{,\psi}^{(1)} = u^{(1)} + a_f^{(1)} + t_{,\psi}^{(1)} \quad (18)$$

Applying Laplace-transformation and initial boundary conditions to equations (14) to (18) and on inversion, we have

$$u(\alpha, \psi) = \frac{\epsilon}{2\pi i} \int_{-\infty}^{\ell+i\infty} \hat{f}(\xi) e^{(\xi\alpha - \lambda\psi)} d\xi + O(\epsilon^2) \quad (19)$$

$$u(\alpha, \psi) = \psi + \frac{\epsilon}{2\pi i} \int_{-\infty}^{\ell+\infty} \hat{f}(\xi) e^{(\xi\alpha - \lambda\psi)} d\xi + O(\epsilon^2) \quad (20)$$

$$\begin{aligned} t(\alpha, \psi) &= \alpha + \psi + \frac{\epsilon}{2\pi i} \left[\int_{\ell-\infty}^{\ell+\infty} \frac{\xi \hat{f}(\xi)}{\lambda} \left\{ \frac{\Gamma + 2 + \sum_{i=1}^n \frac{a_f^2}{\xi \tau_i + 1} \left(\frac{1}{a_e^2} - \frac{1}{a_f^2} \right)}{1 + \sum_{i=1}^n \frac{a_f^2}{(\tau_i \xi + 1)} \left(\frac{1}{a_e^2} - \frac{1}{a_f^2} \right)} \right\} e^{(\xi\alpha - \lambda\psi)} d\xi \right] \\ &= 0(\epsilon^2) \end{aligned} \quad (21)$$

where ℓ is a positive number which satisfies the condition that all the singularities of these integrals are to the left of line $\xi = \ell$ in complex ξ -plane. Inverting equations (20) and (21), we have

$$\alpha = \alpha(x, t) \text{ and } \psi = \psi(x, t),$$

which give the trajectories of an outgoing wave and particle path in (x, t) plane.

Thus

$$\left. \begin{aligned} \alpha &= t - x + \epsilon \alpha^{(1)}(x, t) + O(\epsilon^2) \\ \psi &= x + \epsilon \psi^{(1)}(x, t) + O(\epsilon^2) \end{aligned} \right\} \quad (22)$$

Equations (19) to (21) describe the trajectories of an outgoing wave and particle paths in (x, t) plane. The formation of shock is characterized by $t_{,\alpha} = 0$.

Central Expansion Fan

We consider the expansive action of a receding piston with

$$f(t) = \begin{cases} -\beta \frac{t^2}{2} & \text{for } t < 1/\beta \\ g(t) & \text{for } t \geq 1/\beta \end{cases} \quad (23)$$

where $g(1/\beta) = -1/2 \beta$, $g'(1/\beta) = -1$ and β is dimensionless piston acceleration. Here we consider a particular case in which the piston velocity changes from 0 at $t = 0$, to $-\epsilon$ as $\beta \rightarrow \infty$

Introducing a new characteristic level z defined by $z = \beta\alpha$, for $\alpha < 1/\beta$, we see that as α varies from 0 to $1/\beta$, z will change from 0 to 1. As we are interested in a solution to the problem in which an abrupt change in piston velocity generates expansion-wave, following Chu¹⁵, we have

$$\left. \begin{aligned} x_{,z}^{(1)} &= \frac{u^{(1)}}{z} \\ x_{,\Psi}^{(1)} &= u^{(1)} + a_f^{(1)} + t_{,\Psi}^{(1)} \end{aligned} \right\} \quad (24)$$

$$p_{,z}^{(1)} - u_{,z}^{(1)} - \frac{1}{\beta} p_{,\Psi}^{(1)} = 0 \quad (25)$$

$$\bar{c}_i^{(1)} = \bar{c}_{i,po} p^{(1)}, \quad i = 1, 2, \dots, n \quad (26)$$

$$p_{,\Psi}^{(1)} + u_{,\Psi}^{(1)} = \sum_{i=1}^n \frac{\rho_{,ci_0}}{\tau_i} \left\{ c_i^{(1)} - \bar{c}_i^{(1)} \right\} \quad (27)$$

$$c_{i,z}^{(1)} = -\frac{1}{\beta \tau_i} \left\{ c_i^{(1)} - \bar{c}_i^{(1)} \right\} \quad i = 1, 2, \dots, n \quad (28)$$

$$a_f^{(1)} = (a_{f,p})_o^{(1)} p^{(1)} + \sum_{i=1}^n (a_{f,c_i})_o^{(1)} c_i^{(1)}. \quad (29)$$

Solutions of equations (24) to (29) in limit when $\beta \rightarrow \infty$, can be written as

$$\left. \begin{aligned} u^{(1)} &= p^{(1)} = -\beta e^{-\Omega\Psi} \\ x^{(1)} &= c_i^{(1)} = 0, \quad i = 1, \dots, n \\ t^{(1)} &= \frac{\Gamma_o + 1}{2} \frac{\beta}{\Omega} (1 - e^{-\Omega\Psi}) \end{aligned} \right\}, \quad (30)$$

where Γ and Ω have the same meaning as before. Thus complete solution in expansion fan valid upto first order in ϵ is

$$\left. \begin{array}{l} p = p_o - \epsilon \beta e^{-\Omega \Psi} + O(\epsilon^2) \\ u = - \epsilon \beta e^{-\Omega \Psi} + O(\epsilon^2) \\ S = S_o + O(\epsilon^2) \\ c_i = c_{io} + O(\epsilon^2), i = 1, 2, \dots, n \\ x = \Psi + O(\epsilon^2) \\ t = \Psi + \frac{\Gamma_o + 1}{2} \frac{\epsilon \beta}{\Omega} (1 - e^{-\Omega \Psi}) + O(\epsilon^2) \end{array} \right\} \quad (31)$$

The characteristic for this case is given as

$$t = x + \frac{\Gamma_o + 1}{2} \frac{\epsilon \beta}{\Omega} (1 - e^{-\Omega \Psi}) + O(\epsilon^2) \quad (32)$$

For $x \Omega \ll 1$, i.e. for time small compared to the relaxation time, we have

$$x = t \left\{ 1 + \frac{\Gamma_o + 1}{2} \epsilon \beta \right\}^{-1} + O(\epsilon^2) \quad (33)$$

For $x \Omega \gg 1$, characteristic in expansion fan becomes

$$t = x + \frac{\Gamma_o + 1}{2} \frac{\epsilon \beta}{\Omega} + O(\epsilon^2). \quad (34)$$

The velocity field in the physical space for this case is given by

$$u = \left(\frac{2}{\Gamma_o + 1} \right) \left\{ \frac{\Omega e^{-\Omega x} (x - t)}{1 - e^{-\Omega x}} \right\} + O(\epsilon^2). \quad (35)$$

Thus, velocity gradient at leading wave front $x = t$, is given by

$$u_{xx} = \frac{2}{\Gamma_0 + 1} \left\{ \frac{\Omega e^{-\Omega x}}{1 - e^{-\Omega x}} \right\} + O(\epsilon^2) \quad (36)$$

In limit when $\tau_o \rightarrow \infty, \Omega \rightarrow 0$, and we have

$$u(x, t) = \frac{2}{\Gamma_0 + 1} \left(\frac{\Omega e^{-\Omega t}}{1 - e^{-\Omega t}} \right) + O(\epsilon^2) \quad (36)$$

Acknowledgements

Authors thank the referee for his valuable suggestions for improving the paper

References

- 1 Bauer, H J & Bass, H E (1973) *The Physics of Fluids* 16(7) 988
- 2 Srinivasan, J & Vincenti, W G (1975) *The Physics of Fluids* 18(12) 1670
- 3 Ram, R & Singh, H N. (1979) *Acta Physica Acad Sci Hung Tomus* 46(3). 157
- 4 Johannesen, H N. (1961) *J. Fluid Mech* 10 25
- 5 Ram, R & Pandey, B D (1979) *Acta Mechanica* 33 171
- 6 Wegner, P P , Chu, B T & Klikoff, W V (1965) *J Fluid Mech* 23 (4) 787.
- 7 Sharma, V D (1982) *Acta Mechanica* 44 121
- 8 Sharma, J , Shyam, R & Sharma, V D (1982) *Acta Mechanica* 43 27
- 9 Clark, J F & McChesney, M (1976) *Dynamics of Relaxing Gases*, Butterworths
- 10 Rarity, B S H (1979) *J Fluid Mech* 27(1) . 49
- 11 Moore, F K & Gibson, W E (1960) *J Aero Space Sci* 22 117
- 12 Shuier, KE (1959) *The Physics of Fluids* 2(4) 442
- 13 Sharma, V D (1979) *Quart. J Mech Appl Maths* 32(4) 331
- 14 Broer, L J F (1958) *J Fluid Mech*. 4(3) 276
- 15 Chu, B T (1958) *Proc. Heat Transfer and Fluid Mech Inst.*, Standford University Press
- 16 Coleman, B D. & Gurtin, M E (1967) *The Physics of Fluids* 10(7) 1454
- 17 Pandey, K & Saxena, M. (1991) *Indian J Pure Appl. Maths* 22(6) 513.

PROC. NAT ACAD SCI INDIA, 74 (A), III, 2004

Turbulent free jet with suspended particulate matter (SPM)

T.C.PANDA^{**}, S K.MISHRA^{*} and A.K. DAS

^{**}*Author for correspondence :*

Department of Mathematics, Berhampur University, Berhampur - 760 007, Orissa, India,

E-mail tc_panda@yahoo.com

**Department of Mathematics, R C M. Science College, Khallikote- 761 030 , Orissa, India.*

Department of Mathematics, U.C.P School of Engineering, Berhampur- 760 010, Orissa, India

Received July 9, 2002, Revised January 23, 2003, Accepted July 15, 2003

Abstract

Mathematical model analysis of turbulent free jet envisaging the physical processes like Brownian diffusion, drag force and volume fraction in relation to dust loading in the atmosphere has been studied for better monitoring and prediction. The analysis presented the modified form of Reynolds equations for turbulent boundary layer to account for the interactions due to physical processes that arise due to presence of SPM. Crank-Nicholson implicit finite difference scheme has been employed for model validation. The model prediction depicts the interdependence of SPM and mixing length. The analysis is in good agreement with Schlichting and experimental results of Reichardt. Consideration of volume fraction and Brownian diffusion of SPM helps in the migration of SPM through a longer distance.

(Keywords turbulent free jet/suspended particulate matter)

Introduction

Flow of fluids with SPM has been the focus of the study of engineers and meteorologists for its wide range of applications. Most of the practical fluid flow problems involve turbulence. There are a number of laminar flow problems for which the equations of motion have been solved exactly and many more for which the equations can be solved by certain approximations without greatly affecting the validity of the results. However there does not seem to have exact solution for turbulent flow. The approximate equations describing turbulent flow depend on so

many assumptions that it is difficult to say whether agreement with experiment is the result of reasonable simplifications or of fortuitous cancellations of the errors arising from the assumptions. In spite of the difficulties of obtaining a complete theoretical solution of the turbulent flow problem, useful quantitative relations have been obtained by a combination of theoretical reasoning and empiricism.

Kriegel³ and Soo⁴ have excluded turbulence in their studies of dynamics of fluid with SPM. Rose⁵, Soo⁶ and Wen *et al.*⁷ have studied similar problems with empiricism. Soo⁸ has studied the fully developed turbulent pipe flow by extending the 1/7th velocity distributions of Schlichting¹ to the gas solid suspension. Soo⁹ and Ryhming¹⁰ have considered two dimensional jet mixings of dusty fluid with a clear fluid. While Soo⁹ did not consider the diffusion of SPM in his analysis, neither Soo⁹ nor Ryhming¹⁰ considered the Stokes drag terms in the fluid momentum equations.

The present work proposes to study the turbulent boundary layer equations governing the jet flow with SPM in two different approaches. In the first approach, mixing length is assumed to be unaffected by the presence of SPM. In the 2nd approach, when SPM is assumed to affect the mixing length, the Reynolds stress terms are replaced by Boussinesq approximations. The interactions of SPM with the carrier fluid, which is summarized as those forces like drag-forces due to slip, transverse forces due to slip shear, lift forces due to Brownian motion of the SPM, have been considered. In addition to these forces, volume fraction of SPM, which plays an important role, has been considered. Brownian diffusion of SPM is also considered due to small size of particles. Prandtl's boundary layer approximation for simplifying Reynolds equations for a turbulent boundary layer flow and Prandtl's mixing length theory and Boussinesq approximations have been adopted to close the system.

Mathematical Formulation

Typically, the jet is turbulent and is characterized by a uniform velocity profile at the nozzle exit. However with increasing distance from the exit, momentum exchange between the jet and the ambient causes the free boundary of the jet to broaden and the potential core, within which the uniform exit velocity is retained, to contract. Downstream of the potential core the velocity profile is non-uniform over the entire jet cross-section and the maximum velocity (center) decreases with increasing distance from the nozzle exit. The region of the flow over which conditions are unaffected by the impingement surface is termed as the free jet.

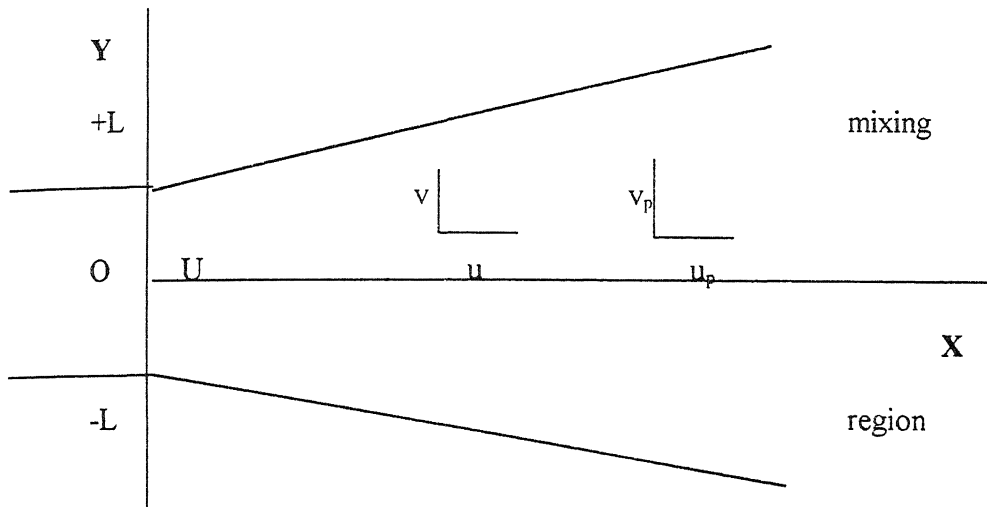


Fig 1- Schematic view of the two - dimensional jet flow

A realistic theory of the motion of fluid with SPM must account for (i) the solid fluid mixture is heterogeneous, (ii) the average velocity of the particles near the wall is not zero and the excess of particle velocity over the fluid velocity is positive near the wall, (iii) the concentration of the solid particles is not uniform because the solid particles have greater density than fluid

Basically there have been two approaches to the problem of fluid-solid flow, *viz.* (i) extending the dynamics of a single particle to the case in a similar manner as is done in case of molecular theory, (ii) modifying the continuum approach to account for the particles in the fluid phase. In the second approach, the dispersed solid phase is viewed as a continuum despite the discreteness of the particles. Following the second approach, a number of authors *viz.* Soo⁴, Marble^{11,12}, Saffman¹³, Batchelor¹⁴, Hinze¹⁵ and others, have presented modified forms of N. S. equations for the fluid and particle phases.

In case of fluid velocity ranging from 15 to 30 meters per second, diameter of solid particles ranging from 100 to 200 microns (for glass beads) and solid to air mass ratios of 0.05 to 0.15, compressibility of fluid phase and the effect of gravity on the density distribution of solid particles are negligible and velocity distribution of fluid stream is not significantly affected by solid particles.

The equation of continuity for the pseudo fluid of SPM can be written as

$$\frac{\partial}{\partial x} (\phi \rho_{sp} u_p) + \frac{\partial}{\partial y} (\phi \rho_{sp} v_p) = 0 \quad (1)$$

$$\text{or} \quad \frac{\partial}{\partial x} (\rho_{sp} u_p) + \frac{\partial}{\partial y} (\rho_{sp} v_p) = 0$$

since ρ_{sp} is constant, the equation of continuity reduces to

$$\frac{\partial u_p}{\partial x} + \frac{\partial v_p}{\partial y} = 0 \quad (2)$$

The diffusion of the species of pseudo fluid of SPM will be governed by law of conservation of species and the Fick's Law can be used to determine the species diffusion rate at any point in the medium and the resulting equation could be solved for species concentration distribution. The species conservation equation is given by

$$u \frac{\partial c}{\partial x} + v \frac{\partial c}{\partial y} = D_p \left(\frac{\partial^2 c}{\partial x^2} + \frac{\partial^2 c}{\partial y^2} \right) \quad (3)$$

where $c = \frac{\rho_p}{\rho_m}$, ρ_p -density of particle phase, ρ_m -density of the mixture of fluid and particles

$$\text{so } \rho_m = \rho_p + \rho \left(1 - \frac{\rho_p}{\rho_{sp}} \right)$$

where $\frac{\rho_p}{\rho_{sp}} = \phi$ is the volume fraction.

Considering finite volume fraction and diffusion of SPM through carrier fluid, the governing Reynolds equations in two-dimensional cartesian coordinate system are given by

$$\frac{\partial u}{\partial x} + \frac{\partial v}{\partial y} = 0 \quad (4)$$

$$(1-\phi) \left[u \frac{\partial u}{\partial x} + v \frac{\partial u}{\partial y} \right] = -\frac{1}{\rho} \frac{\partial p}{\partial x} + v \left(\frac{\partial^2 u}{\partial y^2} \right) + \frac{\rho_p}{\rho \tau_p} (u_p - u) + (1-\phi) \left[\frac{\partial}{\partial y} \left(-\bar{u'v'} \right) \right] \quad (5)$$

$$\phi \left[u_p \frac{\partial u_p}{\partial x} + v_p \frac{\partial u_p}{\partial y} \right] = -\frac{1}{\tau_p} (u_p - u) + \phi \left[\frac{\partial}{\partial y} \left(-\bar{u'_p v'_p} \right) \right] - v_p \frac{\partial^2 u_p}{\partial y^2} \quad (6)$$

$$\phi \left[u_p \frac{\partial v_p}{\partial x} + v_p \frac{\partial v_p}{\partial y} \right] = -\frac{1}{\tau_p} (v_p - v) + \phi \left[\frac{\partial}{\partial y} \left(-\bar{v'_p} \right) \right] - v_p \frac{\partial^2 v_p}{\partial y^2} \quad (7)$$

$$u \frac{\partial c}{\partial x} + v \frac{\partial c}{\partial y} = \frac{\partial}{\partial y} \left(D_p \frac{\partial c}{\partial y} - \bar{v'c'} \right) \quad (8)$$

where the variables $u, v, u_p, v_p, p, \rho, \rho_p, c$ etc represent the mean quantities.

In deriving the above equations the following considerations are accounted for

The terms $(u_p - u)$ and $(v_p - v)$ are negligible in comparison with $(\bar{u_p} - \bar{u})$ and $(\bar{v_p} - \bar{v})$

Since, by the time the flow becomes turbulent the SPM have had enough time to cover many times of the particle velocity relaxation length so that the slip velocity $(u_p - u)$ and $(v_p - v)$ become very small and the perturbation quantities u', u_p, v', v_p are such that we can assume $u_p = o(u')$, $v_p = o(v')$

As has been done in deriving boundary layer equations, where

$$\frac{\partial}{\partial x} \approx O\left(\frac{1}{L}\right) \ll \frac{\partial}{\partial y} \approx O\left(\frac{1}{\delta}\right)$$

The term, $\frac{\partial}{\partial x} \left(\overline{v'^2} - (1-\phi) \overline{r'^2} \right)$, can also be neglected

and
$$-\frac{1}{\rho} \frac{\partial \bar{p}}{\partial y} \approx O(\delta)$$

$$\frac{1}{\rho} \frac{\partial \bar{p}}{\partial y} \approx \frac{\partial}{\partial y} \left(-\overline{v'^2} \right) \Rightarrow \frac{1}{\rho} \frac{\partial \bar{p}}{\partial x} \approx \frac{\partial}{\partial x} \left(-\overline{v'^2} \right)$$

If we assume that the SPM does not affect the mixing length as the particle concentration is very lean, terms $\frac{\partial}{\partial y} \left(-\overline{u_p v_p} \right)$ and $\frac{\partial}{\partial y} \left(-\overline{v_p'^2} \right)$ can be neglected.

Using Prandtl's mixing length theory the Reynolds stress, $-\overline{u'v'}$, is replaced by $l^2 \left(\frac{\partial u}{\partial y} \right)^2$, where l is known as the mixing length which is the distance up to which migration of fluid elements is assumed to take place.

By analogy with Fick's Law of diffusion, we write

$$\overline{v'c'} = -K_c \frac{\partial \bar{c}}{\partial y}$$

in which K_c is the turbulent diffusivity or 'eddy diffusivity'.

After making the above mentioned replacements for the turbulent momentum flux and turbulent mass flux and introducing non dimensional variables

$$x^* = \frac{x}{\lambda}, y^* = \frac{y}{(\nu \tau_p)^{1/2}}, \lambda = \tau_p U$$

$$u^* = \frac{u}{U}, v^* = \nu \left(\frac{\tau_p}{v} \right)^{1/2}, u_p^* = \frac{u_p}{U}, v_p^* = \nu_p \left(\frac{\tau_p}{v} \right)^{1/2}, p^* = \frac{p}{\rho U^2}, \rho_p^* = \frac{\rho_p}{\rho_{p\infty}}$$

the eqn. (4) to (8) can be written as (after dropping the stars)

$$\frac{\partial u}{\partial x} + \frac{\partial v}{\partial y} = 0 \quad (9)$$

$$(1-\phi) \left(u \frac{\partial u}{\partial x} + v \frac{\partial u}{\partial y} \right) = - \frac{\partial p}{\partial x} + \alpha \rho_p (u_p - u) + \frac{\partial^2 u}{\partial y^2} + \text{Re} J^2 (1-\phi) \frac{\partial}{\partial y} \left(\frac{\partial u}{\partial y} \right)^2 \quad (10)$$

$$\phi \left(u_p \frac{\partial u_p}{\partial x} + v_p \frac{\partial u_p}{\partial y} \right) = -(u_p - u) - \frac{v_p}{v} \frac{\partial^2 u_p}{\partial y^2} \quad (11)$$

$$\phi \left(u_p \frac{\partial v_p}{\partial x} + v_p \frac{\partial v_p}{\partial y} \right) = -(v_p - v) - \frac{v_p}{v} \frac{\partial^2 v_p}{\partial y^2} \quad (12)$$

$$u \frac{\partial \rho_p}{\partial x} + v \frac{\partial \rho_p}{\partial y} = \frac{(\mathcal{D}_p + K_c)}{U \lambda} \text{Re} \cdot \frac{\partial^2 \rho_p}{\partial y^2} \quad (13)$$

The boundary conditions are

$$\begin{aligned} u(0, y) &= 1 & u_p(0, y) &= 1 & u_y(x, 0) &= 0 \\ u(x, \infty) &= 0 & u_p(x, \infty) &= 0 & u_{py}(x, 0) &= 0 \end{aligned} \quad (14)$$

the governing equations (9)-(13) are solved by using Crank-Nicholson finite difference scheme¹⁹.

However, if we assume that the SPM does affect the mixing length, the 2nd terms of right hand side of eqn (6) and (7) i.e $\frac{\partial}{\partial y} \left(-\overline{u'_p v'_p} \right) \frac{\partial}{\partial y} \left(-\overline{v'^2_p} \right)$ can not be neglected

Boussinesq, in 1877, had suggested that the turbulent stress in analogy to viscous stress can be related to the rate of strain, in case of incompressible flow, as

$$-\overline{u'_i u'_j} = K_m \left(\frac{\partial \overline{u_i}}{\partial x_j} + \frac{\partial \overline{u_j}}{\partial x_i} \right)$$

where K_m is the eddy diffusivity for momentum transfer for fluid phase. Boussnesq approximations for particle phase may be stated as follows

$$-\overline{u'_{p_i} u'_{p_j}} = K_{mp} \left(\frac{\partial \overline{u_{p_i}}}{\partial x_j} + \frac{\partial \overline{u_{p_j}}}{\partial x_i} \right)$$

where K_{mp} is the eddy diffusivity for momentum transfer for particle phase

Introducing non dimensional variables, as earlier, the eqn. (4) to (8) can be written as(after dropping the stars)

$$\frac{\partial u}{\partial x} + \frac{\partial v}{\partial y} = 0 \quad (15)$$

$$(1 - \phi) \left[u \frac{\partial u}{\partial x} + v \frac{\partial u}{\partial y} \right] = (1 + (1 - \phi) \epsilon_m \text{Re}) \frac{\partial^2 u}{\partial y^2} + \alpha \rho_p (u_p - u) \quad (16)$$

$$\phi \left[u_p \frac{\partial u_p}{\partial x} + v_p \frac{\partial u_p}{\partial y} \right] = -(u_p - u) + (\phi \epsilon_{mp} \text{Re} - \epsilon) \frac{\partial^2 u_p}{\partial y^2} \quad (17)$$

$$\phi \left[u_p \frac{\partial v_p}{\partial x} + v_p \frac{\partial v_p}{\partial y} \right] = -(v_p - v) + (2\phi \epsilon_{mp} \text{Re} - \epsilon) \frac{\partial^2 v_p}{\partial y^2} \quad (18)$$

$$u \frac{\partial \rho_p}{\partial x} + v \frac{\partial \rho_p}{\partial y} = \varepsilon'_c \text{Re} \frac{\partial^2 \rho_p}{\partial y^2} \quad (19)$$

where $\varepsilon = \frac{v_p}{v} \varepsilon_m = \frac{K_m}{U\lambda}$, $\varepsilon_{mp} = \frac{K_{mp}}{U\lambda}$, $\varepsilon_c' = \frac{(D_p + K_c)}{U\lambda}$

and are solved by using the Crank-Nicholson scheme.

Discussion of Results

The numerical results obtained suggest some of the characteristic features of gas particulate flow in the turbulent jet. The values used for numerical computations are presented in Table-2 which have been modified from the data used by Fenton and Stukel¹⁶, given in Table-1, using the following relations, to suit the present problem.

$$\lambda = \frac{2}{9} \left(\frac{\rho_s}{\rho} \right) \frac{a^2 U}{v}, \varepsilon_m = \frac{K_m}{Ud} \frac{d}{\lambda}, \varepsilon_{mp} = \frac{K_{mp}}{K_m} \frac{K_m}{U\lambda} = \frac{K_{mp}}{K_m} \varepsilon_m, \varepsilon_c = \frac{K_c}{K_m} \varepsilon_m$$

Table 1- Data used by Fenton and Stukel¹⁶

α	d (m)	ρ_s (Kgm^{-3})	a (micron)	U (ms^{-1})	$\frac{K_m}{Ud}$	$\frac{K_{mp}}{Ud}$	$\frac{K_c}{Ud}$
0.0141	0.003175	801	5.00E-05	12.68	0.0481	0.489	0.632
0.0141	0.003175	1602	5.00E-05	12.68	0.0481	0.489	0.632
0.00657	0.003175	801	5.00E-05	18.07	0.0481	0.469	0.675
0.00657	0.003175	1602	5.00E-05	18.07	0.0481	0.469	0.675
0.0157	0.003175	801	5.00E-05	18.26	0.0443	0.551	0.686
0.0157	0.003175	1602	5.00E-05	18.26	0.0443	0.551	0.686
0.0146	0.00635	801	5.00E-05	27	0.0418	0.608	0.804
0.0146	0.00635	1602	5.00E-05	27	0.0418	0.608	0.804

Table 2- Data used in the present analysis

α	ρ (Kgm ⁻³)	μ (Kgm ⁻³)	ρ (Kgm ⁻³)	a (m)	U (ms ⁻¹)	λ (m)	$\frac{K_m}{U\lambda} = \varepsilon_m$	$\frac{K_{mp}}{U\lambda} = \varepsilon_{mp}$	$\frac{K_c}{U\lambda} = \varepsilon_c$
0.0141	0.9752	1.54E-05	891	1.00E-04	12.68	1.46E+00	1.04E-04	5.10E-05	6.59E-05
0.0141	0.9752	1.54E-05	1602	1.00E-04	12.68	2.93E+00	5.22E-05	2.55E-05	3.30E-05
0.00657	0.9752	1.54E-05	801	1.00E-04	18.07	2.09E+00	7.32E-05	3.43E-05	4.94E-05
0.00657	0.9752	1.54E-05	8010	1.00E-04	18.07	2.09E+01	7.32E-06	3.43E-06	4.94E-06
0.0157	0.9752	1.54E-05	801	1.00E-04	18.26	2.11E+00	6.67E-05	3.68E-05	4.58E-05
0.0157	0.9752	1.54E-05	1602	1.00E-04	18.26	4.22E+00	3.34E-05	1.84E-05	2.29E-05
0.0146	0.9752	1.54E-05	801	1.00E-04	27	3.12E+00	8.51E-05	5.18E-05	6.85E-05
0.0146	0.9752	1.54E-05	1602	1.00E-04	27	6.24E+00	4.26E-05	2.59E-05	3.42E-05

Fig 2 compares velocity profile of carrier fluid, which is numerically computed and drawn against the velocity profile of Schlichting¹, viz.

$$u = \frac{\sqrt{3}}{2} \sqrt{\frac{k\sigma}{x}} (1 - \tanh^2 \eta), v = \frac{\sqrt{3}}{4} \sqrt{\frac{k}{x\sigma}} (2\eta(1 - \tanh^2 \eta) - \tanh \eta)$$

The computed profile agrees well in the core of the jet and differs from the profile outside the core due to the presence of SPM.

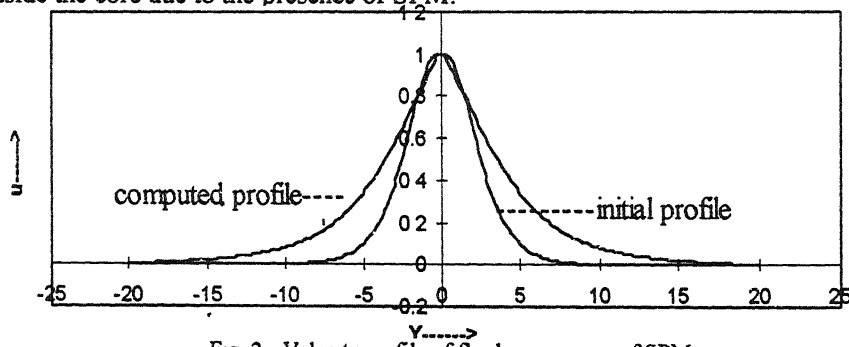


Fig. 2 - Velocity profile of fluid in presence of SPM

Fig 3 presents the velocity profile of SPM drawn against the mean velocity distribution of solid particles approximated by an equation analogous to the velocity profile of fluid. The computed results show that the particle velocity decreases monotonically from the value unity at the center of the jet to its asymptotic value in the free-stream

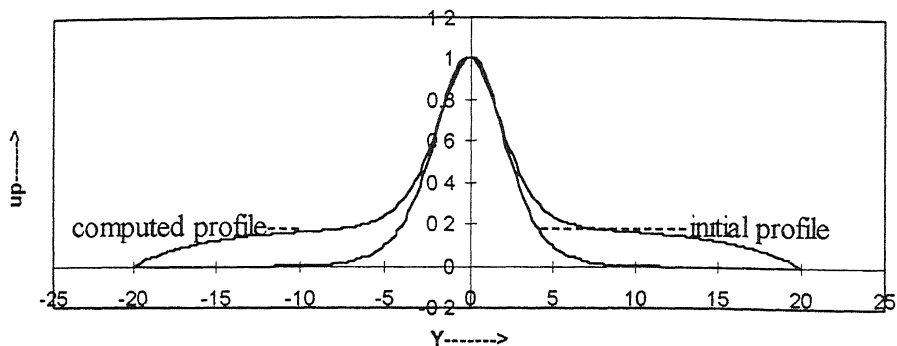


Fig 3 - Velocity profile of SPM

Fig 4 shows the computed density profile of SPM drawn against that akin to the postulated velocity profile of fluid. The density profile agrees well in the core of the jet but deviates outside the core

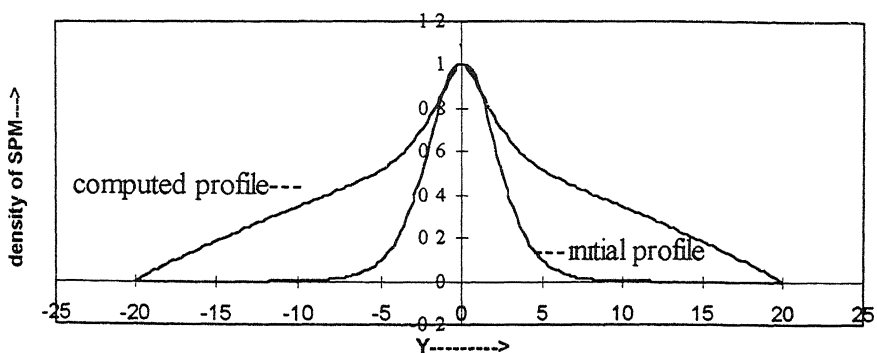


Fig 4- Density profile of SPM

Fig. 5 presents the velocity profile of carrier fluid in presence of SPM, which affects the mixing length. The Reynolds stress terms appearing in the governing equations have been approximated by quantities as predicted by Boussinesq. It is observed that when SPM affects the mixing length, the velocity profile of fluid deviates from the one, which have been computed using mixing length theory (Fig. 2). The fluid velocity falls sharply, from the maximum value of unity at the center of jet, inside the core of the jet and afterwards maintains a steady decline outside the core

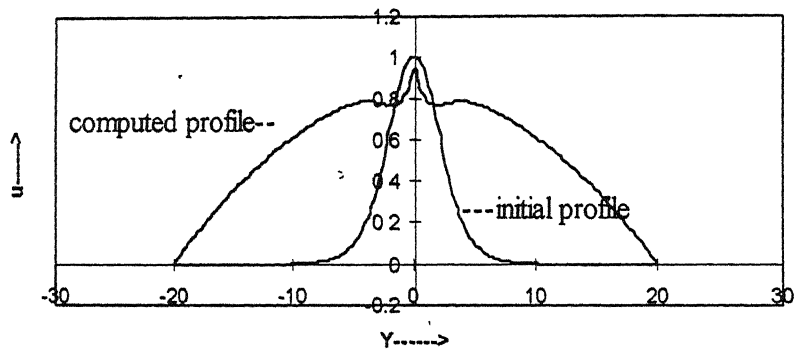


Fig. 5 - Velocity profile of fluid in presence of SPM when SPM affects mixing length

Fig. 6 makes a comparison of the velocity distribution of SPM and that of the postulated distribution when the mixing length is affected by SPM. In this case also, the velocity distribution differs from the one that have been computed using mixing length theory. The velocity falls monotonically from the maximum value at the center of jet to zero in the free-stream.

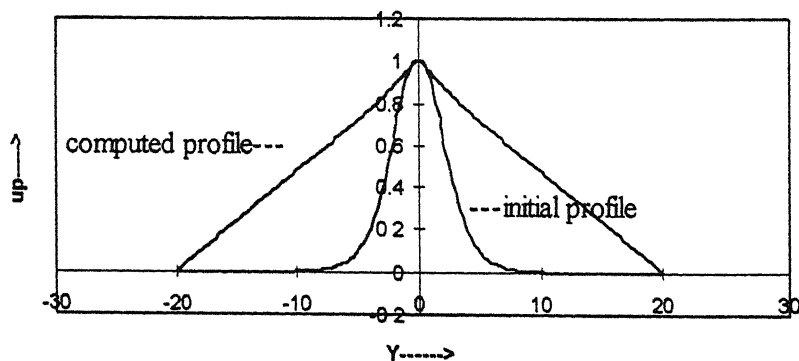


Fig. 6- Velocity profile of SPM when SPM affects mixing length

Fig. 7 depicts the density profile of SPM which when compared with that obtained in the 1st approach (Fig. 3) resembles well. No significant change is observed in the density profile in the two approaches.

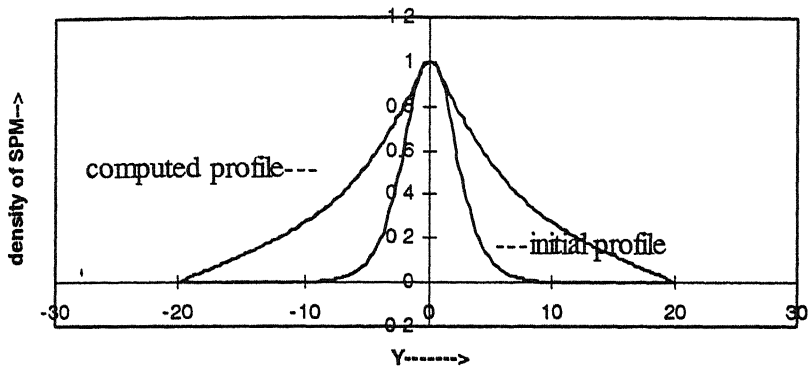


Fig 7- Density profile of SPM when SPM affects mixing length

Conclusions

A comparative study of the results obtained in both the approaches suggests that the first one, where mixing length theory has been used, gives a better structure of the boundary layer flow.

The deviations marked in the computed results from the experimental results might have been caused by the following factors

- Boundary layer assumptions
- Postulation of velocity and density distribution from experimental results
- Assumptions made to close the system

The shortcomings of the present result may be overcome by considering higher order closure schemes.

Acknowledgements

This work was supported by Office of Naval Research/Naval Research Laboratory, Washington, D.C., USA, under Grant No.-N00014 - 97 - 1 - 0905

References

- 1 Schlichting, H (1968) *Boundary Layer Theory*, Mc Graw-Hill Book Company
- 2 Reichardt, H (1951) *Gesetzmäßigkeiten der freien Turbulenz*, VDI - Forschungsheft, 2nd ed, 414,1942
- 3 Kliegel J R (1961) *Inst of Aerospace Science* 1913
- 4 Soo, S L (1961) *University of Illinois, Project Squid Report*, ILL-P
- 5 Rose, H E & Barnacle, H E (1957) *Engineer* **203** 898
- 6 Soo, S L & Hohnstreitj, G F *Project Squid Progress Report*
- 7 Wen, C Y & Simmons, H P (1959) *AI Ch E. Journal* **5** 263
- 8 Soo, S L (1962) *I and EC Fund* **3** 33
- 9 Soo, S L (1965) *EC Fund* **4** 426
- 10 Ryhming, I L (1971) *Acta Mech* **11** 1170
- 11 Marble, F E (1963) *Fifth AGARD Combustion and Propulsion Colloquium*, Pergamon Press, Oxford, England, 175
- 12 Marble, F E (1970) *Annual Review of Fluid Mechanics* **2**, Palo Alto, California, 397
- 13 Saffmann, P G (1973) *J Fluid Mech* **13**
- 14 Batchelor, G K (1977) *J Fluid Mech* **88** 97
- 15 Hinze, J O (1959) *Turbulence*, Mc Graw-Hill Book Company, Inc, New York.
- 16 Fenton, D L & Stukel, J J (1976) *Int J. Multiphase Flow* **3** 123
- 17 Panda, T C , Mishra, S K & Das, A K (1999) *Acta Ciencia Indica*, **25**(4) 365
- 18 Gupta, A S & Pop, I (1975) *Bull. Math de la RS de Rourmanie*, 291
- 19 Crank, J & Nicolson, P (1947) *Proc Camb Phil Soc. vol* **43** 50

Stability of superposed viscoelastic (Walters' B')-Newtonian fluids in porous medium

R C. SHARMA⁺, SUNIL^{*} and P.K. BHARTI^{*}

⁺*Department of Mathematics, Himachal Pradesh University, Summer Hill, Shimla (H.P.)-171 005, India*

^{*}*Department of Applied Sciences, National Institute of Technology (Deemed University), Hamirpur, (H.P.)-177 005, India*

* Author for correspondence

Received September 25, 2002, Accepted July 15, 2003

Abstract

The Rayleigh-Taylor instability of a Newtonian viscous fluid overlying Walters' (model B') viscoelastic fluid is considered. For the stable configuration, the system is found to be stable or

unstable if $v'_1 < \frac{k}{\varepsilon\alpha_1}$. The system is found to be unstable in the potentially unstable case. The variable horizontal magnetic field is also considered. For the stable configuration, in

the hydromagnetic case also, the system is found to be stable or unstable if $v'_1 < \frac{k}{\varepsilon\alpha_1}$. For

the unstable configuration, the system is unstable for the wave-number band $k < k^*$ or if $v'_1 >$

$\frac{k}{\varepsilon\alpha_1}$. The magnetic field has stabilizing effect and completely stabilizes the wave number band

$k > k^*$ if $v'_1 < \frac{k}{\varepsilon\alpha_1}$. This is in contrast to the stability of Newtonian superposed fluids in porous medium, where the system is always stable for the stable configuration.

(Keywords : viscoelastic (Walters' B')-Newtonian fluids/variable magnetic field/ porous medium)

Introduction

The stability derived from the character of the equilibrium of an incompressible heavy fluid of variable density (i.e. of a heterogeneous fluid) is termed as Rayleigh-Taylor instability. The Rayleigh-Taylor instability of a Newtonian fluid under varying assumptions of hydrodynamics and hydromagnetics has been studied by several authors, and Chandrasekhar¹, in his celebrated monograph, has given a detailed account of these investigations. The Rayleigh-Taylor instability problems arise in oceanography, limnology and engineering. The problem of Rayleigh-Taylor instability in fluids in a porous medium is of great importance in geophysics, soil sciences, ground water hydrology and astrophysics.

With the growing importance of non-Newtonian fluids in modern technology and industries, the investigations on such fluids are desirable. There are many elastico-viscous fluids that cannot be characterized by Maxwell's constitutive relations or Oldroyd's constitutive relations. One such class of elastico-viscous fluids is Walters' (model B') fluid. In recent years, the investigation of flow of fluids through porous media has become an important topic due to the recovery of crude oil from the pores of reservoir rocks. The flow through porous media is of considerable interest for petroleum engineers and for geophysical fluid dynamicists. A great number of applications in geophysics may be found in a book by Phillips². When the fluid permeates a porous material, the gross effect is represented by the Darcy's law. As a result of this macroscopic law, the usual viscous and viscoelastic terms in the equation of Walters' (model B') fluid motion are replaced by the resistance term $\left[-\frac{1}{k_1} \left(\mu - \mu' \frac{\partial}{\partial t} \right) \bar{u} \right]$, where μ and μ' are the viscosity and viscoelasticity of the Walters' (model B') fluid, k_1 is the medium permeability and \bar{u} is the Darcian (filter) velocity of the fluid. Sharma *et al.*^{3,4} have studied the thermosolutal convection in Walters' (model B') fluid in porous medium in the presence of magnetic field and rotation, respectively.

Generally, it is accepted that comets consist of a dusty 'snowball' of a mixture of frozen gases which, in the process of their journey, changes from solid to gas and vice-versa. The physical properties of comets, meteorites and interplanetary dust strongly suggest the importance of porosity in astrophysical context (McDonnell⁵). Wooding⁶ has considered the Rayleigh instability of a thermal boundary layer in flow through a porous medium. In stellar interiors and atmospheres, the magnetic field may be (and quite often is) variable (and non-uniform) and may altogether alter the nature of the instability. Sharma and Sunil⁷ have studied the Rayleigh-Taylor instability of a

partially ionized plasma in a porous medium in presence of a variable magnetic field. Sunil and Chand⁸ have studied the Rayleigh-Taylor instability of a plasma in the presence of a variable magnetic field and suspended particles in porous medium. There is growing importance of non-Newtonian fluids in chemical technology, industry and geophysical fluid dynamics.

Keeping in mind the importance of non-Newtonian fluids in modern technology and various applications mentioned above, the present paper is devoted to the consideration of the stability of superposed Newtonian-Walters' (model B') fluids in porous medium. The effect of variable horizontal magnetic field, bearing relevancy in geophysics, is also considered separately.

Formulation of the Problem and Perturbation Equations

Consider a static state in which an incompressible Walters' (model B') fluid layer of variable density is arranged in horizontal strata and the pressure p and density ρ are functions of the vertical coordinate z only. The character of the equilibrium of this initial state is determined by supposing that the system is slightly disturbed and then by following its further evolution. The fluid is under the action of gravity $\bar{g} (0, 0, -g)$. This fluid layer is assumed to be flowing through an isotropic and homogeneous porous medium of porosity ϵ and medium permeability k_l , where the porosity is defined as

$$\epsilon = (\text{volume of the voids}) / (\text{total volume}), \quad (0 < \epsilon < 1).$$

For very fluffy foam materials, ϵ is nearly one and in beds of packed spheres, ϵ is in the range 0.25-0.50.

Let p , ρ , μ , μ' and \bar{u} (u, v, w) denote, respectively, the pressure, density, viscosity, viscoelasticity and filter velocity of the pure Walters' (model B') fluid. Here g is the acceleration due to gravity, $\bar{x} = (x, y, z)$ and $\bar{\lambda} = (0, 0, 1)$. Then the equations of motion and continuity for the Walters' (model B') fluid are

$$\frac{\rho}{\epsilon} \left[\frac{\partial \bar{u}}{\partial t} + \frac{1}{\epsilon} (\bar{u} \cdot \nabla) \bar{u} \right] = -\nabla p - \rho g \bar{\lambda} - \frac{1}{k_l} \left(\mu - \mu' \frac{\partial}{\partial t} \right) \bar{u}, \quad (1)$$

$$\nabla \cdot \bar{u} = 0 \quad (2)$$

Since the density of a fluid particle remains unchanged as we follow it with its motion, we have

$$\varepsilon \frac{\partial \bar{u}}{\partial t} + (\bar{u}, \nabla) \rho = 0 \quad (3)$$

Consider a small perturbation on the steady state solution, and let δp , $\delta \rho$ and \bar{u} (u , v , w) denote, respectively, the perturbations in pressure p , density ρ and fluid velocity $(0,0,0)$. Then the linearized perturbation equations governing the motion of the Walters' (model B') fluid layer through porous medium are

$$\frac{\rho}{\varepsilon} \frac{\partial \bar{u}}{\partial t} = -\nabla \delta p - g \delta \rho \bar{\lambda} - \frac{1}{k_1} \left(\mu - \mu' \frac{\partial}{\partial t} \right) \bar{u}, \quad (4)$$

$$\nabla \bar{u} = 0, \quad (5)$$

$$\varepsilon \frac{\partial}{\partial t} \delta \rho = -w(D\rho) \quad (6)$$

Dispersion Relation

Analyzing the perturbations into normal modes, we assume that the perturbation quantities have an x , y and t dependence of the form

$$\exp(i k_x x + i k_y y + nt), \quad (7)$$

where k_x , k_y are the wave numbers along the x - and y - directions respectively, $k = \sqrt{(k_x^2 + k_y^2)}$ is the resultant wave number of disturbance and n is the growth rate which is, in general, a complex constant.

For perturbations of the form (7), eqns (4)-(6) give

$$\left[\frac{n}{\varepsilon} + \frac{1}{k_1} (\nu - \nu' n) \right] \rho u = -i k_x \delta p, \quad (8)$$

$$\left[\frac{n}{\varepsilon} + \frac{1}{k_1} (\nu - \nu' n) \right] \rho v = -i k_y \delta p, \quad (9)$$

$$\left[\frac{n}{\varepsilon} + \frac{1}{k_1} (\nu - \nu' n) \right] \rho w = -D \delta p - g \delta p, \quad (10)$$

$$ik_x u + ik_y v + Dw = 0, \quad (11)$$

$$\varepsilon n \delta \rho = -w(D\rho), \quad (12)$$

where $\nu = \frac{\mu}{\rho}$, $\nu' = \frac{\mu'}{\rho}$ and $D = \frac{d}{dz}$.

Multiplying (8) by $-ik_x$, (9) by $-ik_y$, adding and using (11), we obtain

$$\left[\frac{n}{\varepsilon} + \frac{1}{k_1} (\nu - \nu' n) \right] \rho Dw = -k^2 \delta p. \quad (13)$$

Eliminating δp between (10) and (13) and using (12), we get

$$\frac{n}{\varepsilon} [D(\rho Dw) - k^2 \rho w] + \frac{1}{k_1} [D\{(\mu - \mu' n) Dw\} - k^2 (\mu - \mu' n) w] + \frac{gk^2}{\varepsilon n} (D\rho) w = 0 \quad (14)$$

Two Uniform Newtonian and Viscoelastic (Walters' B') Fluids Separated by a Horizontal Boundary

We consider the case of two uniform fluids of densities, viscosities, viscoelasticities; $\rho_2, \mu_2, 0$ (upper newtonian fluid) and ρ_1, μ_1, μ'_1 (lower Walters' B' viscoelastic fluid) separated by a horizontal boundary at $z=0$. Then, in each region of constant ρ , constant μ and constant μ' , eqn. (14) becomes

$$(D^2 - k^2)w = 0 \quad (15)$$

The general solution of eqn. (15) is

$$w = A e^{+kz} + B e^{-kz}, \quad (16)$$

where A and B are arbitrary constants.

The boundary conditions to be satisfied in the present problem are :

- (i) The velocity w should vanish when $z \rightarrow +\infty$ (for the upper fluid) and $z \rightarrow -\infty$ (for the lower fluid)
- (ii) $w(z)$ is continuous at $z = 0$
- (iii) The jumps condition at the interface $z = 0$ between the fluids is obtained by integrating eqn (14) across the interface at $z = 0$ and is

$$\frac{n}{\varepsilon} [\rho_2 D w_2 - \rho_1 D w_1]_{z=0} + \frac{1}{k_1} [\mu_2 D w_2 - (\mu_1 - \mu'_1 n) D w_1]_{z=0} = -\frac{g k^2}{\varepsilon n} (\rho_2 - \rho_1) w_0, \quad (17)$$

remembering that upper fluid is Newtonian and lower fluid is Walters B' viscoelastic
Here w_0 is the common value of w at $z = 0$

Applying the boundary conditions (i) and (ii), we can write

$$w_1 = A e^{+kz}, \quad (z < 0), \quad (18)$$

$$w_2 = A e^{-kz}, \quad (z > 0), \quad (19)$$

where the same constant A has been chosen to ensure the continuity of w at $z = 0$

Applying the condition (17) to the solutions (18) and (19), we obtain

$$\left[1 - \frac{\varepsilon \nu'_1 \alpha_1}{k_1} \right] n^2 + \frac{\varepsilon}{k_1} (\nu_2 \alpha_2 + \nu_1 \alpha_1) n - g k (\alpha_2 - \alpha_1) = 0, \quad (20)$$

$$\text{where } \alpha_{1,2} = \frac{\rho_{1,2}}{\rho_1 + \rho_2}, \quad \nu_{1,2} = \frac{\mu_{1,2}}{\rho_{1,2}}, \quad \nu'_1 = \frac{\mu'_1}{\rho_1}$$

(a) *Stable case ($\rho_2 < \rho_1$)*

For the potentially stable arrangement ($\rho_2 < \rho_1$), the system is stable or unstable according as

$$v'_1 < \text{or} > \frac{k_1}{\epsilon \alpha_1} \quad (21)$$

(b) *Unstable case* ($\rho_2 > \rho_1$)

For the potentially unstable arrangement ($\rho_2 > \rho_1$), there is atleast one change of sign in eqn (20) and so this equation has one positive root. The occurrence of positive root implies that the system is unstable.

Effect of Variable Horizontal Magnetic Field

Here the problem and configuration is same as described above except that the incompressible Walters' (model B') fluid layer arranged in horizontal strata is acted on by a variable horizontal magnetic field \vec{H} ($H_0(z)$, 0, 0). Then the equations of motion and the Maxwell's equations are

$$\frac{\rho}{\epsilon} \left[\frac{\partial \vec{u}}{\partial t} + \frac{1}{\epsilon} (\vec{u} \cdot \nabla) \vec{u} \right] = -\nabla p - \rho g \vec{\lambda} - \frac{1}{k_1} \left(\mu - \mu' \frac{\partial}{\partial t} \right) \vec{u} + \frac{\mu_e}{4\pi} (\nabla \times \vec{H}) \times \vec{H}, \quad (22)$$

$$\nabla \cdot \vec{H} = 0, \quad (23)$$

$$\epsilon \frac{\partial \vec{H}}{\partial t} = (\vec{H} \cdot \nabla) \vec{u} - (\vec{u} \cdot \nabla) \vec{H}, \quad (24)$$

together with eqns. (2) and (3). here μ_e denotes the magnetic permeability.

Let \vec{h} (h_x, h_y, h_z) denotes the perturbation in the variable horizontal magnetic field \vec{H} ($H_0(z)$, 0, 0). Then the linearized perturbation equations, governing the motion of the Walters' (model B') fluid layer through porous medium in the presence of variable horizontal magnetic field are

$$\frac{\rho}{\epsilon} \frac{\partial \vec{u}}{\partial t} = -\nabla \delta p - g \delta \rho \vec{\lambda} - \frac{1}{k_1} \left(\mu - \mu' \frac{\partial}{\partial t} \right) \vec{u} + \frac{\mu_e}{4\pi} [(\nabla \times \vec{h}) \times \vec{H} + (\nabla \times \vec{H}) \times \vec{h}] \quad (25)$$

$$\nabla \cdot \vec{h} = 0, \quad (26)$$

$$\varepsilon \frac{\partial \vec{h}}{\partial t} = (\vec{H} \cdot \nabla) \vec{u} - (\vec{u} \cdot \nabla) \vec{H}, \quad (27)$$

together with eqns (5) and (6)

For perturbations of the form (7) eqns. (25)-(27) give

$$\left[\frac{n}{\varepsilon} + \frac{1}{k_1} (\nu - \nu' n) \right] \rho u = -ik_x \delta p + \frac{\mu_e}{4\pi} h_z (DH_0), \quad (28)$$

$$\left[\frac{n}{\varepsilon} + \frac{1}{k_1} (\nu - \nu' n) \right] \rho v = -ik_y \delta p + \frac{\mu_e H_0}{4\pi} (ik_x h_y - ik_y h_x), \quad (29)$$

$$\left[\frac{n}{\varepsilon} + \frac{1}{k_1} (\nu - \nu' n) \right] \rho w = -D \delta p + \frac{\mu_e H_0}{4\pi} \left(ik_x h_z - Dh_x - h_x \frac{DH_0}{H_0} \right) - g \delta \rho, \quad (30)$$

$$ik_x h_x + ik_y h_y + Dh_z = 0, \quad (31)$$

$$\varepsilon n h_x = ik_x H_0 u - w D H_0, \quad (32)$$

$$\varepsilon n h_y = ik_x H_0 v, \quad (33)$$

$$\varepsilon n h_z = ik_x H_0 w, \quad (34)$$

together with eqns. (11) and (12).

Equation (29), with the help of (32) and (33), becomes

$$\left[\frac{n}{\varepsilon} + \frac{1}{k_1} (\nu - \nu' n) \right] \rho v = -ik_y \delta p + \frac{\mu_e H_0}{4\pi \varepsilon n} (ik_x H_0 \zeta + ik_y w D H_0), \quad (35)$$

where $\zeta = ik_x v - ik_y u$ is the z-component of vorticity.

Multiplying (28) by $-ik_x$, (35) by $-ik_y$, adding and using (11), we obtain

$$\left[\frac{n}{\varepsilon} + \frac{1}{k_1} (\nu - \nu' n) \right] \rho D w = -k^2 \delta p + \frac{\mu_e k_x k_y H_0^2}{4\pi\varepsilon n} \zeta + \frac{\mu_e k_y^2 H_0}{4\pi\varepsilon n} (DH_0) w - \frac{i\mu_e k_x}{4\pi} h_z (DH_0) \quad (36)$$

Eliminating δp between (30) and (36) and using (11), (12) and (28)-(34), we get

$$\begin{aligned} & \frac{n}{\varepsilon} [D(\rho Dw) - k^2 \rho w] + \frac{1}{k_1} [D\{(\mu - \mu' n)\} - k^2 (\mu - \mu' n) w] \\ &= -\frac{\mu_e k_x^2}{4\pi\varepsilon n} [D(H_0^2 Dw) - H_0^2 k^2 w] - \frac{gk^2}{\varepsilon n} (D\rho) w \end{aligned} \quad (37)$$

Here also we consider the case of two uniform Newtonian and viscoelastic Walters' (model B') fluids separated by a horizontal boundary in hydromagnetics exactly as in previous section.

The jumps condition at the interface $z = 0$ between the fluids is obtained by integrating eqn. (37) across the interface at $z = 0$ and is

$$\begin{aligned} & \frac{n}{\varepsilon} [\rho_2 Dw_2 - \rho_1 Dw_1]_{z=0} + \frac{1}{k_1} [\mu_2 Dw_2 - (\mu_1 - \mu'_1 n) Dw_1]_{z=0} \\ &= -\frac{\mu_e k_x^2}{4\pi\varepsilon n} [H_0^2 Dw_2 - H_1^2 Dw_1]_{z=0} - \frac{gk^2}{\varepsilon n} (\rho_2 - \rho_1) w_0 \end{aligned} \quad (38)$$

Following the procedure as in previous section, we obtain

$$\left[1 - \frac{\varepsilon \nu'_1 \alpha}{k_1} \right] n^2 + \frac{\varepsilon}{k_1} (\nu_2 \alpha_2 + \nu_1 \alpha_1) n + [k_x^2 V_A^2 - gk(\alpha_2 - \alpha_1)] = 0 \quad (39)$$

where for the sake of simplicity, we have considered that the Alfvén velocities of the two fluids are the same, so that

$$V_A^2 = \frac{\mu_e H_1^2}{4\pi\rho_1} = \frac{\mu_e H_2^2}{4\pi\rho_2}$$

(a) *Stable case* ($\rho_2 < \rho_1$)

For the potentially stable arrangement ($\rho_2 < \rho_1$), the system is stable or unstable according as

$$v'_1 < \text{or} > \frac{k_1}{\varepsilon\alpha_1} \quad (40)$$

Thus, for two uniform Newtonian and viscoelastic Walters' (model B') fluids in porous medium in hydromagnetics and for the potentially stable case, the system is stable or unstable according as $v'_1 < \text{or} > \frac{k_1}{\varepsilon\alpha_1}$

This is in contrast to the stability of Newtonian superposed fluids in porous medium, where the system is always stable for the stable configuration

(b) *Unstable case* ($\rho_2 > \rho_1$)

For the potentially unstable arrangement ($\rho_2 > \rho_1$), if

$$k_x^2 V_A^2 > gk(\alpha_2 - \alpha_1) \text{ and } v'_1 < \frac{k_1}{\varepsilon\alpha_1} \quad (41)$$

Eqn (39) does not admit any change of sign and so has no positive root. Therefore, the system is stable. However, if

$$k_x^2 V_A^2 < gk(\alpha_2 - \alpha_1), \quad (42)$$

the constant term in eqn (39) is negative. Eqn. (39), therefore, allows one change in sign and so has one positive root. The occurrence of positive root implies that the system is unstable

Thus for the unstable case ($\rho_2 > \rho_1$) and $v'_1 < \frac{k_1}{\varepsilon\alpha_1}$, the magnetic field has got stabilizing effect and completely stabilize the system for all wave numbers which satisfy the inequality

$$k_x^2 V_A^2 > gk(\alpha_2 - \alpha_1), \quad (43)$$

i.e. $k > k^*$

$$\text{where } k^* = \frac{g(\alpha_2 - \alpha_1)}{V_A^2} \sec^2 \theta,$$

and θ is the angle between k and \vec{H} .

However, for the potentially unstable arrangement ($\rho_2 > \rho_1$), the system is unstable for the wave-number band $k < k^*$ or if $v'_1 > \frac{k_1}{\varepsilon\alpha_1}$.

Thus, for the potentially unstable configuration and for a uniform Newtonian fluid overlying a viscoelastic Walters' (model B') fluid in porous medium in hydrodynamics, the system is unstable for all wave numbers, whereas in hydromagnetics, the magnetic field has stabilizing effect and completely stabilizes the wave number band $k > k^*$, where $k^* = \frac{g(\alpha_2 - \alpha_1)}{V_A^2} \sec^2 \theta$

Acknowledgement

The financial assistance to Dr. Sunil in the form of a Research and Development Project [No. 25(0129)/02/EMR-II] of the Council of Scientific and Industrial Research (CSIR), New Delhi is gratefully acknowledged.

References

- 1 Chandrasekhar, S (1981) "Hydrodynamic and Hydromagnetic Stability", Dover Publication, New York
- 2 Phillips, O M (1991) "Flow and Reaction in Permeable Rocks", Cambridge University Press, Cambridge

- 3 Sharma, R C , Sunil & Chand, S (1998) *Applied Mechanics and Engineering* 3(1) 171
- 4 Sharma, R C , Sunil & Chand, S (1998) *Indian J. Pure Appl. Math.* 29(4) 433
- 5 McDonnell, J A M (1978) "Cosmic Dust", John Wiley and Sons, Toronto, p 330
- 6 Wooding, R A (1960) *J. Fluid Mech.* 9 183.
- 7 Sharma, R C & Sunil (1992) *Zeitschrift fur Naturforschung* 47a . 1227
- 8 Sunil & Chand, T (1997) *Ind. Jour. of Phys.* 71B(I) 95

Optimal implementation of parallel divide and conquer algorithm on de Bruijn networks

P K MISHRA and C.K. SHARMA*

*Department of Applied Mathematics, Birla Institute of Technology, Mesra, Ranchi
835 215, India*

Email . pkmishra_69@rediffmail.com, pkmishra@bitmesra.ac.in

**Department of Mathematical Sciences, APS University, Rewa 486 003, India*

Email cksharma5@rediffmail.com

Received October 17, 2001, Revised April 20, 2003; Accepted September 18, 2003

Abstract

We study the problem of optimal implementation of parallel divide-and-conquer algorithm on binary de Bruijn networks. A divide and conquer algorithm is modeled as a temporal complete binary tree computation structure. An important contraction property between two successive binary de Bruijn network is revealed. A twice-size compute binary is mapped to a de Bruijn network. Two nodes in the compute binary tree are mapped to a single node. The mapping is of dilation one, communication contention free and of good load balance.

(Keywords parallel divide/ conquer algorithm de Bruijn network/ parallel algorithms)

Introduction

Divide and Conquer method is an important parallel programming paradigm¹⁻³. The problem of implementation of such algorithms onto various parallel architectures such as hypercubes, tree machines, mesh connected computer, etc. has been studied. A de Bruijn network¹ consists of $n=2^k$ nodes. Let $a_{k-1}, a_{k-2}, \dots, a_1, a_0$ be the address of a node in the de Bruijn network. The two nodes reachable via directed edges from the node are

$$a_{k-2}, a_{k-3}, \dots, a_1, a_0 0$$

$$a_{k-2}, a_{k-3}, \dots, a_1, a_0 1.$$

The diameter of a de Bruijn network¹ with 2^k nodes is k , which is about half the diameter of a shuffle-exchange network with the same number of nodes. As an interconnection network, a de Bruijn network has many superior features such as bounded degree, logarithmic diameter and high connectivity. Recently, there has been increasing interest in exploring such networks for multiprocessor system².

In this paper, we model a divide and conquer algorithm as a complete binary tree. To improve the efficiency, we map two non conflicting nodes in a complete binary tree to a single node in the binary de Bruijn network. We present a mapping which achieves dilation one and communication contention free. This is accomplished by utilizing an important contraction property of binary de Bruijn networks.

The Model of Divide and Conquer

A classic task graph structure for a degree-2 divide and conquer algorithm is a complete binary tree⁴ where, the root first starts to divide the work into two approximately equal parts to its two children and once an interior node receives the work, it also divides it evenly to its children. After the leaves receives their work, they start to do compute and the results are aggregated level by level back to the root. We observe a very regular temporal activation pattern in such a computation : nodes and communication edges are active level by level .

Formally, a complete binary tree with 2^{n-1} nodes is denoted as $\text{CBT}(n)$. We call the communication in the dividing from level i to $i+1$ ($i=1,\dots,n-1$) i -th communication phase and cell edges from nodes in level i to nodes in level $i+1$ edges in level i to nodes in level $i+1$ edges in level i .

Four metrics are used to evaluate a mapping. For the computation, *Load Balancing* is a measure for the processors load, defined as the maximum number of tasks which are mapped to a single processor. *Processor Contention* measures the degree of the contention for a processor among tasks. We call a mapping *Processor Contention Free* if all tasks in a processor are active at different times. For the communication, *Maximum Dilation*⁵ is defined as the maximum length of the paths of the de Bruijn net chosen for the communication edges in the CBT. Communication Contention is used to measure the contention among message traffic. We call a mapping *Communication Contention Free* if paths of the de Bruijn network chosen for edges active at the same time are unoverlapped⁴.

The Binary de Bruijn Network

Definition . A binary de Bruijn network (graph) BDG(k)⁶ is an undirected graph with 2^k nodes. Each node is represented as a k -digit binary number $a_{k-1} a_{k-2} \dots a_0$ where $a_i \in \{0, \dots, r-1\}$. Every node $a_{k-1} a_{k-2} \dots a_0$ is connected to the nodes : $a_{k-2} \dots a_0x$ (by left shifting) and $xa_{k-1} a_{k-2} \dots a_1$ (by right shifting) where $x \in \{0,1\}$.

Property 1: A CBT(k) is a subgraph of a BDG(k).

Proof We construct a CBT as follows start with 10^{k-1} as the root of the CBT(k), right shift to 010^{k-2} to construct its left child, and right shift to 110^{k-2} to construct its right child. Inductively , any node $z10^m$, where $m>0$ and z is an arbitrary string of length $k-m-1$, has left child $0z10^{m-1}$ and right child $1z10^{m-1}$. This procedure can be repeated until we reach a string whose rightmost bit is 1, which is the leaf of the CBT to be constructed.

Nodes in the CBT ($n+1$) are labeled based on their labels in BDG ($n+1$). We call such a labeling of a complete binary tree de Bruijn labeling⁷.

We now reveal an important contraction existing between BDG (n) and BDG ($n-1$)

We define a function F as follows :

$$F(x_1 \dots x_{n-1} x_n) = x'_1 x'_2 \dots x'_{n-1} \quad (1)$$

where $x_i \in \{0,1\}$ and $x'_i = (x_i \oplus x_{i+1})$ for $i < n$. (2)

Lemma 1: F is a two -to -one function which maps both $x_1 \dots x_{n-1} x_n$ and its binary complement strings $\bar{x}_1 \dots \bar{x}_{n-1} \bar{x}_n$ to the same string .

Proof · It is easy to see that F maps both $x_1 \dots x_{n-1} x_n$ and $\bar{x}_1 \dots \bar{x}_{n-1} \bar{x}_n$ to the same string

$x'_1 x'_2 \dots x'_{n-1}$ where $x'_i = (x_i \oplus x_{i+1})$ for $i < n$ because $x \oplus y = \bar{x} \oplus \bar{y}$. Conversely, the strings $x_1 \dots x_{n-1} x_n$ which are mapped to $y_1 \dots y_{n-1}$ are the solutions to the system of equations

- 3 Cole, M I (1989) *Research Monographs in Parallel and Distributed Computing*, MIT Press
- 4 Lo, V M , Rajopadhye, S , Gupta, S , Kelsen, D , Mohammmd, M A & Telle, J (2000) in *Proceedings of International Conference on Parallel Processing*, Pages III 128
- 5 Mou, Z G & Hudak, P (1998) *Jour of Supercomputing* 2(3) 257
- 6 Samatham, M R & Pradhan D K (1989) *IEEE Transactions on Computers* 38 (4) . 567
- 7 Zhong, Xiaoxiong, Rajopadhye, Sanjay & Lo, Virginia (1992) in *Sixth International Parallel Processing Symposium (IPPS 92)*

PROC NAT ACAD SCI INDIA, 74 (A), III, 2004

Ramanujan number

BAIKUNTH PRASAD AMBASHT* and JAMUNA PRASAD AMBASHT

**Department of Mechanical Engineering, Bokaro Institute of Technology, 363 Sector 3B, Bokaro Skeel City 827001, India.*

Department of Mathematics and Computer Science, Benedict College, 34 Westpine Court, Columbia, South Carolina 29212-1703, U.S.A.

Received December 17, 2002, Revised August 25, 2003, Accepted October 23, 2003

Abstract

1729 is associated with the famous Indian Mathematician Ramanujan. This interesting number happened to be the number of the taxicab in which Professor Hardy visited him in the hospital and was astonished at Ramanujan's remark that 1729 was the smallest natural number expressible as sum of two cubes in two distinct ways involving relatively prime pairs

$$(1) A^3 + B^3 = C^3 + D^3 = N \text{ with } (A,B) = 1, (C,D) = 1, 1^3 + 12^3 = 9^3 + 10^3 = 1729$$

We propose to investigate (2) $x^3 + y^3 + z^3 + u^3 = 0$ for nonzero reals. Through this we run into (1) No mathematical proof that 1729 is indeed the smallest number of the form (1) is claimed

Introduction

We introduce the following notations :

$$\langle x, y \rangle = x^3 + y^3 \quad \underset{\vee}{\alpha} = \alpha_1 \alpha_2 \quad \hat{ab} = a_1 b_2 - a_2 b_1$$

$(n, m) = 1$ the natural numbers n, m have no common divisors.

$]u, w[$ open interval on the real axis.

$$S_1 = -0.70326$$

$$R =]-\infty, +\infty[$$

$$I =]-1, S_1[$$

$$\begin{array}{lll}
 S_2 = +2.36992 & C^* =] -\infty, S_3 [& J =] S_4, 1 [\\
 S_3 = -1.42195 & D^* =] S_4, +\infty [& \\
 S_4 = +0.42195 & E^* =] S_1, S_4 [& \\
 A^* =] -\infty, S_1 [& p^* =] S_3, S_1 [& \\
 B^* =] S_2, +\infty [& Q^* =] S_4, S_2 [&
 \end{array}$$

Section 1

If three real non-zero variables retain the same sign and one the opposite sign (2) takes the form

$$(3) \quad A^3 + B^3 + C^3 = D^3$$

Otherwise when two are of the same sign (2) becomes

$$(4) \quad A^3 + B^3 = C^3 + D^3$$

with A, B, C, D positive real numbers

Section 2

Let (x_j, y_j, Z_j, U_j) $j = 1, 2$ be arbitrary solution sets of (2)

(5) Then (x, y, z, u) with $x = x_1 + \lambda x_2$, etc can be a solution set of (2) provided.

$$(6) \quad \lambda = \frac{-x_1^2 x_2 + y_1^2 y_2 + z_1^2 z_2 + u_1^2 u_2}{K}$$

$$K \neq 0 \text{ with } K = x_1 x_2^2 + y_1 y_2^2 + z_1 z_2^2 + u_1 u_2^2$$

Substituting λ in (5) we have $x = E/K, y = F/K, z = G/K, u = H/K$

$$(7.1) \quad E = \underset{\vee}{y} \hat{x} \hat{y} + \underset{\vee}{z} \hat{x} \hat{z} + \underset{\vee}{u} \hat{x} \hat{u}$$

$$(7.2) \quad F = z \underset{\vee}{\hat{y}z} + u \underset{\vee}{\hat{yu}} + x \underset{\vee}{\hat{yx}}$$

$$(7.3) \quad G = u \underset{\vee}{\hat{zu}} + x \underset{\vee}{\hat{zx}} + y \underset{\vee}{\hat{zy}}$$

$$(7.4) \quad H = x \underset{\vee}{\hat{ux}} + y \underset{\vee}{\hat{uy}} + z \underset{\vee}{\hat{uz}}$$

$$(7.5) \quad K = x \underset{\vee}{x_2} + y \underset{\vee}{y_2} + z \underset{\vee}{z_2} + u \underset{\vee}{u},$$

Section 3

If $K \neq 0$, (E, F, G, H) will be a solution set for (2). (since $\langle 3, 4 \rangle + \langle 5, -6 \rangle = 0$, and $\langle p, q \rangle + \langle -p, -q \rangle = 0$)

Choose $(x_1, y_1, z_1, u_1) = (3, 4, 5, -6)$

$(x_2, y_2, z_2, u_2) = (p, q, -p, -q)$ with $p \neq 0, q \neq 0$

$$(8.1) \quad E = 40 p^2 + 20 pq - 6q^2$$

$$(8.2) \quad F = 32 p^2 + 16pq + 12 q^2$$

$$(8.3) \quad G = 24 p^2 - 20 pq - 10q^2$$

$$(8.4) \quad H = -48 p^2 - 16 pq - 8q^2$$

$$(8.5) \quad K = 8p^2 - 2q^2$$

Let $S = 2p/q$ then :

$$(8.1*) \quad e = 5S^2 + 5S - 3$$

$$(8.2*) \quad f = 4S^2 + 4S + 6$$

$$(8.3*) \quad g = 3S^2 - 5S - 5$$

$$(8 \ 4*) \quad h = -6S^2 - 4S - 4$$

$$(8 \ 5*) \quad k = S^2 - 1$$

$\{(x, y, z, u) = (g, f, e, h) \text{ satisfies (2) if } S \neq \pm I\}$

From g . the zeros of x are $S_1 = (5 - \sqrt{85})/6 = -0.70326$

$$\text{and } S_2 = \frac{5 + \sqrt{85}}{6} = +2.36992$$

From e the zeros of z are $S_3 = (-5 - \sqrt{85})/10 = -1.42195$ and

$$S_4 = \frac{-5 + \sqrt{85}}{10} = +0.42195.$$

Section 4

$(2S + 1)^2 + 5 = f > 0$ thus y is always positive.

$-6(S + 1/3)^2 - 10/3 = h < 0$ thus u is always negative.

On C^* UB^* , also on E^* three variables retain the same sign whereas one variable is of the opposite sign thus (2) takes the form (3). On p^* UQ^* two variables are of the same sign and the other two are of the opposite sign thus (2) takes the form (4).

$$(-e/S^2, -f/S^2, -g/S^2, -h/S^2) = (g^*, h^*, e^*, f^*)$$

Thus swapping S with $t = 1/S$ we still get solution set with the same constraints on t as on S . The range $-\infty \leq t < +\infty$ can be contracted to $-1 < t < +1$, since $S \neq \pm 1$. Thus we can choose S in $I \cup J$ in order to get the solution (2) in the form (4). By choosing rational $S = p/q$ with $(p, q) = 1$ in $I \cup J$ we can rid the equation (4) of fractions and get the solution as stipulated in (1) : $A^3 + B^3 = C^3 + D^3 = N$ where A, B, C, D are distinct natural numbers with no common divisors. Fifty solutions are appended in Table 1. Table 2 is actual verification $1 \leq N \leq 1729$.

Table 1

St=1	<A,B> =			<C,D> =		N
	S or t	A	B	C	D	
1/2, -3/4		1	12	9	10	1,729 (1)
2/3, -16/19		23	94	63	84	842,751 (2)
4/5, -10/11		35	98	59	92	984,067 (3)
10/17, -4/5		23	134	95	116	2,418,271 (4)
5/7, -13/15		51	178	115	162	5,772,403 (5)
3/4		57	180	113	166	6,017,193 (6)
13/20, -5/6		45	196	133	174	7,620,661 (7)
6/13, -8/11		9	210	161	172	9,261,729 (8)
3/5		45	246	173	214	14,978,061 (9)
-5/7		5	254	197	206	16,387,189 (10)
-6/7		73	270	177	244	20,072,017 (11)
7/8, -17/18		111	268	151	258	20,616,463 (12)
8/15, -10/13		35	298	219	252	26,506,467 (13)
9/16, -11/14		51	348	251	298	42,276,843 (14)
-7/8		107	356	227	326	46,343,059 (15)
7/11		89	410	281	362	69,625,969 (16)
3/7		3	414	323	334	70,957,971 (17)
-7/9		57	430	313	366	79,692,193 (18)
5/6		167	436	255	414	87,539,319 (19)
-8/9		147	454	283	420	96,753,187 (20)
-13/16		89	460	321	402	98,040,969 (21)

Table 1 Contd..

St=1	$\langle A, B \rangle =$		$\langle C, D \rangle =$		N
	A	B	C	D	
4/7	73	470	337	404	104,212,017 (22)
12/19, -14/17	111	522	359	460	143,604,279 (23)
10/11	229	522	285	508	154,245,637 (24)
8/13	111	562	391	492	178,871,959 (25)
-9/10	193	564	345	526	186,595,201 (26)
6/7	243	606	347	580	236,893,923 (27)
5/8	133	644	445	566	269,442,621 (28)
-9/11	133	654	453	574	282,078,901 (29)
4/9	17	694	537	564	334,260,297 (30)
11/13	271	690	399	658	348,411,511 (31)
-17/20	189	732	485	658	398,974,437 (32)
5/9	107	766	555	654	450,680,139 (33)
-11/12	303	820	487	774	579,186,127 (34)
13/14	389	860	461	842	694,919,869 (35)
11/16	239	908	599	818	762,265,231 (36)
-11/13	233	926	617	830	806,672,113 (37)
7/9	317	934	573	870	846,635,517 (38)
-12/13	367	966	567	916	950,859,559 (39)
5/11	37	1,046	805	854	1,144,495,989 (40)
8/9	437	1,030	573	996	1,176,180,453 (41)
7/10	295	1,076	703	974	1,271,439,351 (42)

Table 1 Contd

St=1	<A,B> =		<C, D> =		N	
	S or t	A	B	C		
13/17		361	1,098	681	1,018	1,370,799,073 (43)
6/11		147	1,134	827	964	1,461,450,627 (44)
-13/14		437	1,124	653	1,070	1503,488,077 (45)
11/19		189	1,162	829	1,002	1,575,734,797 1461
-11/15		63	1,174	895	966	1,618,346,071 (47)
9/10		555	1,284	707	1,246	2,287,828,179 (48)
-14/15		513	1,294	745	1,236	2,301,725,881 (49)
16/17		591	1,282	679	1,260	2,313,422,839 (50)

Table 2– List of natural numbers $1 \leq N \leq 1729$ expressible as the sum of cubes of two distinct natural numbers

For $x = 2, 3, 4, 5, 6, 7, 8, 9, 10, 11, 12$

$\langle 1, x \rangle = 9, 28, 65, 126, 217, 344, 513, 730, 1,001, 1,332, 1,729$, respectively

For $x = 3, 4, 5, 6, 7, 8, 9, 10, 11$

$\langle 2, x \rangle = 35, 72, 133, 224, 351, 520, 737, 1008, 1339$, respectively

For $x = 4, 5, 6, 7, 8, 9, 10, 11$

$\langle 3, x \rangle = 91, 152, 243, 370, 539, 756, 1027, 1358$, respectively

For $x = 5, 6, 7, 8, 9, 10, 11$

$\langle 4, x \rangle = 189, 280, 407, 576, 793, 1064, 1395$, respectively

For $x = 6, 7, 8, 9, 10, 11$

$\langle 5, x \rangle = 341, 468, 637, 854, 1125, 1456$, respectively

For $x = 7, 8, 9, 10, 11$

$\langle 6, x \rangle = 559, 728, 945, 1216, 1547$, respectively

Table 2 Contd

For $x = 8, 9, 10, 11$
 $\langle 7, x \rangle = 855, 1072, 1343, 1674$, respectively

For $x = 9, 10$
 $\langle 8, x \rangle = 1241, 1512$, respectively

Finally $\langle 9, 10 \rangle = 1729$

Acknowledgements

To the memory of our respected presents Tarawanti Devi and Guru Narain Lal, this humble work is dedicated Our parents set Ramanujan as our role model. For valuable suggestions, we are grateful to referee.

Remarks · This paper was presented at the annual session of the American Mathematical Society [A.M S. Vol. 14, No. 1 Abs Jan 1993, Issue 85]

References

Kanigel, Rebert, *The man who knew infinity*, Maxwell Macmillan Intl

PROC NAT ACAD SCI INDIA, 74 (A), III, 2004

A matrix-variate extension of inverted Dirichlet integral

K M KURIAN, BENNY KURIAN and *A M MATHAI

Department of Statistics, St Thomas College Palai Mahatma Gandhi University, Arunapuram P O., Palai, Kerala, India

**McGill University, Montreal, Canada, and Centre for Mathematical Sciences, Trivandrum, India*

Received August 30, 2003, Accepted October 23, 2003

Abstract

Type-2 or inverted multiple Dirichlet integral is extended for the real scalar variable case. Then the matrix-variate analogues of the extended Dirichlet integrals, the associated extended Dirichlet models and extended Dirichlet densities are considered. Various types of results are obtained which are mathematically and statistically interesting.

(Keywords : generalized Dirichlet model/real matrix-variate distributions/Jacobians of matrix transformation/type-2 model)

Introduction

The type-1 Dirichlet integral is given by

$$\int \dots \int_{0 < x_j < 1, 0 < x_1 + \dots + x_k < 1} x_1^{\alpha_1-1} \dots x_k^{\alpha_k-1} (1 - x_1 - \dots - x_k)^{\alpha_{k+1}-1} dx_1 \wedge \dots \wedge dx_k \\ = \frac{\Gamma(\alpha_1) \dots \Gamma(\alpha_{k+1})}{\Gamma(\alpha_1 + \dots + \alpha_{k+1})} \quad (1)$$

for $\Re(\alpha_j) > 0$, $j = 1, \dots, k+1$ where $\Re(\cdot)$ denotes the real part of (\cdot) . Hence the associated type-1 Dirichlet density is given by

$$f_1(x_1, \dots, x_k) = \frac{\Gamma(\alpha_1 + \dots + \alpha_{k+1})}{\Gamma(\alpha_1) \dots (\alpha_{k+1})} x_1^{\alpha_1-1} \dots x_k^{\alpha_k-1} (1 - x_1 - \dots - x_k)^{\alpha_{k+1}-1}, \quad (2)$$

$0 < x_j < 1, j = 1, \dots, k, 0 < x_1 + \dots + x_k < 1, \Re(\alpha_j) > 0, j = 1, \dots, k+1$, and $f_1(x_1, \dots, x_k) = 0$, elsewhere. The inverted Dirichlet or type-2 Dirichlet integral is given by

$$\int_0^\infty \dots \int_0^\infty x_1^{\alpha_1-1} \cdot x_k^{\alpha_k-1} (1+x_1+\dots+x_k)^{-(\alpha_1+\dots+\alpha_{k+1})} = \frac{\Gamma(\alpha_1) \dots \Gamma(\alpha_{k+1})}{\Gamma(\alpha_1 + \dots + \alpha_{k+1})} \quad (3)$$

for $\Re(\alpha_j) > 0, j = 1, \dots, k+1$, and the associated inverted Dirichlet or type-2 Dirichlet density is given by

$$f_2(x_1, \dots, x_k) = \frac{\Gamma(\alpha_1 + \dots + \alpha_{k+1})}{\Gamma(\alpha_1) \dots \Gamma(\alpha_{k+1})} x_1^{\alpha_1-1} \cdot x_k^{\alpha_k-1} (1+x_1+\dots+x_k)^{-(\alpha_1+\dots+\alpha_{k+1})} \quad (4)$$

for $0 \leq x_j < \infty, j = 1, \dots, k$ and $f_2(x_1, \dots, x_k) = 0$, elsewhere. The matrix-variate extensions of type-1 and type-2 Dirichlet densities or the matrix-variate analogues of (2) and (4) are available in the literature, see for example Mathai¹. They are the following :

$$f_3(X_1, \dots, X_k) = \frac{\Gamma_p(\alpha_1 + \dots + \alpha_{k+1})}{\Gamma_p(\alpha_1) \dots \Gamma_p(\alpha_{k+1})} |X_1|^{\alpha_1 - \frac{p+1}{2}} \dots |X_k|^{\alpha_k - \frac{p+1}{2}} |I - X_1 - \dots - X_k|^{\alpha_{k+1} - \frac{p+1}{2}} \quad (5)$$

for $0 < X_j = X'_j < I, 0 < X_1 + \dots + X_k < I, \Re(\alpha_j) > \frac{p-1}{2}, j = 1, \dots, k+1$ and zero elsewhere, where the following notations are used.

All the matrices appearing in this paper are real symmetric $p \times p$ matrices unless stated otherwise. A prime denotes a transpose, $|(\cdot)|$ denotes the determinant of (\cdot) , $\text{tr}(\cdot)$ denotes the trace of (\cdot) , $X_j = X'_j > 0$ means X_j is real symmetric positive definite. $0 < X_j < I$ means $X_j = X'_j > 0$ and $I - X_j > 0$ or that all the eigenvalues of X_j are in the open interval $(0, 1)$, and I denotes the identity matrix. The standard notation $\Gamma_p(\alpha)$ means matrix-variate real gamma or

$$\Gamma_p(\alpha) = \pi^{\frac{p(p-1)}{4}} \Gamma(\alpha) \Gamma\left(\alpha - \frac{1}{2}\right) \Gamma(\alpha - 1) \dots \Gamma\left(\alpha - \frac{p-1}{2}\right), \Re(\alpha) > \frac{p-1}{2} \quad (6)$$

$$= \int_{x=\lambda'>0} |X|^{\alpha - \frac{p+1}{2}} e^{-tr(X)} dX \quad (7)$$

where $dX = \wedge_{i \geq j=1}^p dx_i$ wedge product of the $\frac{p(p+1)}{2}$ differentials dx_i 's. Matrix-variate version of type-2 density is given by the following :

$$f_4(X_1, \dots, X_k) =$$

$$\frac{\Gamma_p(\alpha_1 + \dots + \alpha_{k+1})}{\Gamma_p(\alpha_1) \cdot \Gamma_p(\alpha_{k+1})} |X_1|^{\alpha_1 - \frac{p+1}{2}} \dots |X_k|^{\alpha_k - \frac{p+1}{2}} |I + X_1 + \dots + X_k|^{-(\alpha_1 + \dots + \alpha_{k+1})} \quad (8)$$

for $X_j = X'_j > 0, j = 1, \dots, k, \Re(\alpha_j) > \frac{p-1}{2}, j = 1, \dots, k+1$ and zero elsewhere.

Matrix-variate functions appear in a wide variety of problems in Statistics, Economics, Physics and so on. When dealing with non-null distributions of likelihood ratio criteria in testing statistical hypotheses on the parameters of one or more multivariate normal or Gaussian distributions, functions of matrix argument come in naturally. An example may be seen from Conradie and Troskie². Applications of matrix-variate functions in various areas may be seen from Mathai¹ and the references therein. Liouville models are generalizations of the scalar Dirichlet models. Matrix-variate analogues of Liouville models may be seen from Gupta and Richards³.

The model that we are going to consider in this paper is a generalization of (8), along with its various properties.

A Generalized Matrix-variate Type-2 Dirichlet Model

Let $X_j = X'_j > 0$ be $p \times p$ real symmetric positive definite matrices having a joint density which is a generalized real type-2 Dirichlet density of the following form :

$$f(X_1, \dots, X_k) =$$

$$\begin{aligned} & c_k |X_1|^{\alpha_1 - \frac{p+1}{2}} |X_k|^{\alpha_k - \frac{p+1}{2}} |I + X_2 + \dots + X_k|^{\beta_1} |I + X_3 + \dots + X_k|^{\beta_2} \\ & \times \dots |I + X_1 + \dots + X_k|^{-(\alpha_1 + \dots + \alpha_{k+1} + \beta_1 + \dots + \beta_k)}. \end{aligned} \quad (9)$$

for $X_j = X'_j > 0$, $j = 1, \dots, k$, $\Re(\alpha_j) > \frac{p-1}{2}$, $\Re(\alpha_{j+1} + \dots + \alpha_{k+1} + \beta_j + \dots + \beta_k) > \frac{p-1}{2}$, $j = 1, \dots, k$ and $f(X_1, \dots, X_k) = 0$ elsewhere, where c_k is the normalizing constant. This normalizing constant can be evaluated by integrating out the matrices one by the starting with X_1 . Collecting the factors containing X_1 we have following. Let the integration over X_1 be denoted by L_1 . Then

$$\begin{aligned} L_1 &= \int_{x_1=x'_1>0} |X_1|^{\alpha_1 - \frac{p+1}{2}} |I + X_1 + \dots + X_k|^{-(\alpha_1 + \dots + \alpha_{k+1} + \beta_1 + \dots + \beta_k)} dX_1 \\ &= |I + X_2 + \dots + X_k|^{-(\alpha_1 + \dots + \alpha_{k+1} + \beta_1 + \dots + \beta_k)} \int_{x_1=x'_1>0} |X_1|^{\alpha_1 - \frac{p+1}{2}} \\ &\quad \times \left| I + (I + X_2 + \dots + X_k)^{-\frac{1}{2}} X_1 (I + X_2 + \dots + X_k)^{-\frac{1}{2}} \right|^{-(\alpha_1 + \dots + \alpha_{k+1} + \beta_1 + \dots + \beta_k)} dX_1 \end{aligned}$$

where $(I + X_1 + \dots + X_k)^{-1/2}$ is the symmetric positive definite square root of $(I + X_1 + \dots + X_k)^{-1}$. Now, applying the Jacobian from (A1) of the Appendix by making the transformation

$$\begin{aligned} Y_1 &= (I + X_2 + \dots + X_k)^{-1/2} X_1 (I + X_2 + \dots + X_k)^{-1/2} \Rightarrow \\ dY_1 &= |I + X_2 + \dots + X_k|^{-\frac{(p+1)}{2}} dX_1 \text{ for fixed } X_2, \dots, X_k. \end{aligned} \quad (10)$$

$$L_1 = |I + X_2 + \dots + X_k|^{-(\alpha_2 + \dots + \alpha_{k+1} + \beta_1 + \dots + \beta_k)}$$

$$\begin{aligned}
& \times \int_{Y_1=Y'_1>0} |Y_1|^{\alpha_1-\frac{p+1}{2}} |I+Y_1|^{-(\alpha_1+\dots+\alpha_{k+1}+\beta_1+\dots+\beta_k)} dY_1 \\
& = |I+X_2+\dots+X_k|^{-(\alpha_2+\dots+\alpha_{k+1}+\beta_1+\dots+\beta_k)} \\
& \times \frac{\Gamma_p(\alpha_1)\Gamma_p(\alpha_2+\dots+\alpha_{k+1}+\beta_1+\dots+\beta_k)}{\Gamma_p(\alpha_1+\alpha_2+\dots+\alpha_{k+1}+\beta_1+\dots+\beta_k)} \quad (11)
\end{aligned}$$

for $\Re(\alpha_1) > \frac{p-1}{2}$, $\Re(\alpha_2 + \dots + \alpha_{k+1} + \dots + \beta_k) > \frac{p-1}{2}$. The integral is evaluated by using a real matrix-variate type-2 beta integral of Appendix (A6). Now, integral over X_2 yields the following, denoting it by L_2 :

$$\begin{aligned}
L_2 &= \int_{x_2=x'_2>0} |X_2|^{\alpha_2-\frac{p+1}{2}} |I+X_2+\dots+X_k|^{-(\alpha_2+\dots+\alpha_{k+1}+\beta_2+\dots+\beta_k)} dX_2 \\
&= |I+X_3+\dots+X_k|^{-(\alpha_3+\dots+\alpha_{k+1}+\beta_2+\dots+\beta_k)} \\
&\times \frac{\Gamma_p(\alpha_2)\Gamma_p(\alpha_3+\dots+\alpha_{k+1}+\beta_2+\dots+\beta_k)}{\Gamma_p(\alpha_2+\dots+\alpha_{k+1}+\beta_2+\dots+\beta_k)} \quad (12)
\end{aligned}$$

for $\Re(\alpha_2) > \frac{p-1}{2}$, $\Re(\alpha_3+\dots+\alpha_{k+1}+\beta_2+\dots+\beta_k) > \frac{p-1}{2}$ $j = 1, \dots, k$. Proceeding like this we have the final result as follows:

$$c_k^{-1} = \left\{ \prod_{j=1}^k \frac{\Gamma_p(\alpha_j)\Gamma_p(\alpha_{j+1}+\dots+\alpha_{k+1}+\beta_j+\dots+\beta_k)}{\Gamma_p(\alpha_j+\dots+\alpha_{k+1}+\beta_j+\dots+\beta_k)} \right\} \quad (13)$$

From the gamma structure in (13) we can have an interesting result.

Theorem 1 For arbitrary t_1, \dots, t_k the joint product moment of the determinants of X_1, \dots, X_k is given by the following :

$$E[|X_1|^{t_1} | X_2|^{t_2} \dots | X_k|^{t_k}]$$

$$= c_k \left\{ \prod_{j=1}^k \frac{\Gamma_p(\alpha_j + t_j) \Gamma_p(\alpha_{j+1} + \dots + \alpha_{k+1} + \beta_j + \dots + \beta_k - t_1 - \dots - t_j)}{\Gamma_p(\alpha_j + \dots + \alpha_{k+1} + \beta_j + \dots + \beta_k - t_1 - \dots - t_{j-1})} \right\} \quad (14)$$

with $t_0 = 0$, for $\Re(t_j) > -\Re(\alpha_j)$, $j=1, \dots, k$, $\Re(t_1 + \dots + t_j) < \Re(\alpha_{j+1} + \dots + \alpha_{k+1} + \beta_j + \dots + \beta_k)$, $j = 1, \dots, k$. Note that (2.6) is available from c_k^{-1} of (14) by changing α_j to $\alpha_j + t_j$, $j = 1, \dots, k$. Some interesting results can be derived from (14). Let $t_1 = 0 = \dots = t_{j-1} = t_{j+1} = \dots = t_k$. Then from (14) we get

$$E[|X_j|^{t_j}]$$

$$= \frac{\Gamma_p(\alpha_j + t_j)}{\Gamma_p(\alpha_j)} \frac{\Gamma_p(\alpha_{j+1} + \dots + \alpha_{k+1} + \beta_j + \dots + \beta_k - t_j)}{\Gamma_p(\alpha_{j+1} + \dots + \alpha_{k+1} + \beta_j + \dots + \beta_k)} \quad (15)$$

$$= \prod_{m=1}^p \frac{\Gamma(\alpha_j + t_j - \frac{m-1}{2}) \Gamma(\alpha_{j+1} + \dots + \alpha_{k+1} + \beta_j + \dots + \beta_k - t_j - \frac{m-1}{2})}{\Gamma(\alpha_j - \frac{m-1}{2}) \Gamma(\alpha_{j+1} + \dots + \alpha_{k+1} + \beta_j + \dots + \beta_k - \frac{m-1}{2})} \quad (16)$$

$$= E(Z_{1j}^{\frac{t_j}{2}}) \cdot E(Z_{pj}^{\frac{t_j}{2}}) \quad (17)$$

where Z_{1j}, \dots, Z_{pj} are independently distributed type-2 beta random variables with the parameters $(\alpha_j - \frac{m-1}{2}, \alpha_{j+1} + \dots + \alpha_{k+1} + \beta_j + \dots + \beta_k - \frac{m-1}{2})$, $m = 1, 2, \dots, p$

Corollary 1 : When X_1, \dots, X_k have the joint density in (9) then for a specific j , $|X_j|$ is structurally a product of p independent real type-2 scalar beta random variables and the t_j^{th} moment of $|X_j|$ is given in (16).

Theorem 2. Let $W_j = W'_j > 0$, $j = 1, \dots, k$ be independently distributed real matrix variate type-2 beta random variables with the parameters $(\alpha_j, \alpha_{j+1} + \dots + \alpha_{k+1} + \beta + \dots + \beta_k)$, $j = 1, \dots, k$. Consider the transformation

$$\begin{aligned} X_1 &= (I + W_k)^{1/2} \cdot (I + W_2)^{1/2} \cdot W_1 (I + W_2)^{1/2} \cdot (I + W_k)^{1/2} \\ X_2 &= (I + W_k)^{1/2} \cdot (I + W_3)^{1/2} \cdot W_2 (I + W_3)^{1/2} \cdot (I + W_k)^{1/2} \\ &\vdots \\ X_{k-1} &= (I + W_k)^{1/2} \cdot W_{k-1} (I + W_k)^{1/2} \\ X_k &= W_k \end{aligned} \tag{18}$$

where $(I + W_j)^{1/2}$ denotes the symmetric positive definite square root of $(I + W_j)$ for $j = 1, \dots, k$. Then X_1, \dots, X_k have the joint density as given in (9).

Proof Since X_2 is free of W_1 , X_3 is free of W_1, W_2 , and so on, the Jacobian matrix in the transformation (18) is of a triangular block matrix format. Hence the Jacobian is available from the product of the determinants of the diagonal blocks. The j^{th} diagonal block behaves like $X_j \leftrightarrow W_j$ with $W_{j+1}, \dots, W_k, j = 1, \dots, k$ fixed. Then for fixed W_{j+1}, \dots, W_k ,

$$dX_j = |I + W_{j+1}|^{\frac{p+1}{2}} \cdot |I + W_k|^{\frac{p+1}{2}} dW_j, \quad j = 1, \dots, k.$$

Hence,

$$\begin{aligned} dX_1 \wedge \dots \wedge dX_k &= |I + W_k|^{\frac{(k-1)(p+1)}{2}} |I + W_{k-1}|^{\frac{(k-2)(p+1)}{2}} \dots \\ &\quad \times |I + W_2|^{\frac{(p+1)}{2}} dW_1 \wedge \dots \wedge dW_k. \end{aligned} \tag{19}$$

Since W_1, \dots, W_k are assumed to be independently distributed the joint density of W_1, \dots, W_k is the product of matrix-variate type-2 beta densities Denoting the joint density of W_1, \dots, W_k by $g(W_1, \dots, W_k)$ we have

$$\begin{aligned} g(W_1, \dots, W_k) dW_1 \wedge \dots \wedge dW_k \\ = \left\{ \prod_{j=1}^k B_p(\alpha_j, \alpha_{j+1} + \dots + \alpha_{k+1} + \beta_j + \dots + \beta_k) \right\} \\ \times \left\{ \prod_{j=1}^k |W_j|^{\alpha_j - \frac{p+1}{2}} |I + W_j|^{-(\alpha_j, \alpha_{j+1} + \dots + \alpha_{k+1} + \beta_j + \dots + \beta_k)} \right\} dW_1 \wedge \dots \wedge dW_k \end{aligned}$$

From the transformation in (18) we have the following

$$I + X_k = I + W_k$$

$$I + X_k + X_{k-1} = (I + W_k)^{1/2} (I + W_{k-1}) (I + W_k)^{1/2}$$

$$I + X_k + \dots + X_1 = (I + W_k)^{1/2} (I + W_{k-1})^{1/2}$$

$$\times \dots (I + W_2)^{1/2} (I + W_1) (I + W_2)^{1/2} \dots (I + W_k)^{1/2}$$

Let us examine,

$$\begin{aligned} & |X_1|^{\alpha_1 - \frac{p+1}{2}} \cdot |X_k|^{\alpha_k - \frac{p+1}{2}} |I + X_2 + \dots + X_k|^{\beta_1} |I + X_k|^{\beta_{k-1}} \\ & \times |I + X_1 + \dots + X_k|^{-(\alpha_1 + \dots + \alpha_{k-1} + \beta_1 + \dots + \beta_{k-1})} dX_1 \wedge \dots \wedge dX_k. \end{aligned}$$

$$\begin{aligned}
&= |W_1|^{\alpha_1 - \frac{p+1}{2}} |W_k|^{\alpha_k - \frac{p+1}{2}} |I + W_1|^{-(\alpha_1 + \dots + \alpha_{k+1} + \beta_1 + \dots + \beta_k)} \\
&\times |1 + W_2|^{-(\alpha_2 + \dots + \alpha_{k+1} + \beta_2 + \dots + \beta_k)} \\
&\times |1 + W_k|^{-(\alpha_k + \alpha_{k+1} + \beta_k)} dW_1 \wedge \dots \wedge dW_k
\end{aligned}$$

The right side multiplied by c_k is the product of the densities of W_1, \dots, W_k . Hence X_1, \dots, X_k have the density as in (9)

The converse also holds

Theorem 3 Let X_1, \dots, X_k have the joint density as in (9). Consider the transformation in (10) for some real symmetric positive definite $p \times p$ matrices W_1, \dots, W_k . Then W_1, \dots, W_k are independently distributed, and further that W_j is a matrix-variate real type-2 beta with the parameters $(a_j, a_{j+1} + \dots + a_{k+1} + \beta_j + \dots + \beta_k)$, $j = 1, \dots, k$

Theorem 3 can also be restated in a different form which looks like fully different but it is essentially the same transformation in a different form.

Theorem 4 Let X_1, \dots, X_k be jointly distributed as in (9). Consider the transformation

$$W_k = X_k$$

$$W_{k-1} = (I + X_k)^{-1/2} X_{k-1} [(I + X_k)^{-1/2}]'$$

$$W_{k-2} = (I + X_k + X_{k-1})^{-1/2} X_{k-2} [(I + X_k + X_{k-1})^{-1/2}]'$$

⋮

(20)

$$W_1 = (I + X_k + \dots + X_2)^{-1/2} X_1 [(I + X_k + \dots + X_2)^{-1/2}]'$$

Then W_1, \dots, W_k are independently distributed where W_j has a real matrix-variate type-2 beta density with the parameters $(a_j, a_{j+1} + \dots + a_{k+1} + \beta_j + \dots + \beta_k)$, $j = 1, \dots, k$.

Proof Here we will use the property that a real symmetric positive definite matrix A can be written as $A = A^{1/2}(A^{1/2})'$ where $A^{1/2}$ need not be symmetric but square and nonsingular. From the transformation in (20) observe the following.

$$X_k = W_k \Rightarrow I + X_k = I + W_k$$

$$X_{k-1} = (I + X_k)^{1/2} W_{k-1} [(I + X_k)^{1/2}]' = (I + W_k)^{1/2} W_{k-1} [(I + W_k)^{1/2}]'$$

$$X_{k-2} = (I + X_k + X_{k-1})^{1/2} W_{k-2} [(I + X_k + X_{k-1})^{1/2}]'$$

But

$$\begin{aligned} I + X_k + X_{k-1} &= I + W_k + (I + W_k)^{1/2} W_{k-1} [(I + W_k)^{1/2}]' \\ &= (I + W_k)^{1/2} ((I + W_{k-1}) [(I + W_k)^{1/2}]') \\ &= (I + W_k)^{1/2} (I + W_{k-1})^{1/2} [(I + W_{k-1})^{1/2}]' [(I + W_k)^{1/2}]' \end{aligned}$$

Therefore we may take

$$= (I + X_k + X_{k-1})^{1/2} = (I + W_k)^{1/2} (I + W_{k-1})^{1/2}$$

and

$$= [(I + X_k + X_{k-1})^{1/2}]' = [(I + W_{k-1})^{1/2}]' [(I + W_k)^{1/2}]'$$

Then

$$X_{k-2} = (I + W_k)^{1/2} (I + W_{k-1})^{1/2} W_{k-2} [(I + W_{k-1})^{1/2}]' [(I + W_k)^{1/2}]'$$

and so on, and finally

$$X_1 = (I + W_k)^{1/2} (I + W_{k-1})^{1/2} \dots (I + W_2)^{1/2} W_1 [(I + W_2)^{1/2}]' \dots [(I + W_k)^{1/2}]'$$

Thus

$$I + X_k + \dots + X_2 + X_1 = (I + W_k)^{1/2} \dots (I + W_2)^{1/2} (I + W_1) [(I + W_2)^{1/2}]' \dots [(I + W_k)^{1/2}]'$$

But this is the same transformation in (19) and hence by Theorem 3 the result follows

Note that if W_j has a real matrix-variate type-2 beta distribution with the parameters $(\alpha_j, \alpha_{j+1} + \dots + \alpha_k + 1 + \beta_j + \dots + \beta_k)$, then W_j^{-1} must have a real matrix-variate type-2 beta distribution with the parameters $(\alpha_{j+1} + \dots + \alpha_k + \beta_j + \dots + \beta_k, \alpha_j)$. But from first principles it is quite difficult to prove this result. We will state this as a theorem.

Theorem 5. Let, (X_1, \dots, X_k) have the joint density as in (9). Consider the following transformation.

$$V_k = X_k^{-1}$$

$$V_{k-1} = (I + X_k)^{-1/2} X_{k-1}^{-1} [(I + X_k)^{-1/2}]'$$

$$V_{k-2} = (I + X_k + X_{k-1})^{-1/2} X_{k-2}^{-1} [(I + X_k + X_{k-1})^{-1/2}]'$$

⋮

(21)

$$V_1 = (I + X_k + \dots + X_2)^{-1/2} X_1^{-1} [(I + X_k + \dots + X_2)^{-1/2}]'$$

Then V_1, \dots, V_k are mutually independently distributed, and further, that V_j is a real matrix-variate type-2 beta with the parameters $(\alpha_{j+1} + \dots + \alpha_k + \beta_j + \dots + \beta_k, \alpha_j)$, $j = 1, \dots, k$.

Proof. We will provide an independent derivation of this result rather than observing that V_j is of the form $V_j = W_j^{-1}$ of Theorem 4. Observe the following : For any real symmetric positive definite matrix A one can find a square nonsingular matrix C such that $A = CC'$, $|C| \neq 0$. In the following steps we will denote this C by $A^{1/2}$ and write $A = (A^{1/2})(A^{1/2})'$. From the transformation in (21) we have the following :

$$X_k = V_k^{-1} \Rightarrow I + X_k = I + V_k^{-1}$$

$$I + V_j = (I + X_k + \dots + X_{j+1})^{1/2} (I + X_j^{-1}) [(I + X_k + \dots + X_{j+1})^{1/2}]'$$

for $j = 1, \dots, k-1$. Also

$$X_{k-1} = (I + X_k)^{1/2} V_{k-1}^{-1} [(I + X_k)^{1/2}]'$$

$$= (I + V_k^{-1})^{1/2} V_{k-1}^{-1} [(1 + V_k^{-1})^{1/2}]'$$

$$X_{k-2} = (I + X_k + X_{k-1})^{-1/2} V_{k-2}^{-1} [(I + X_k + X_{k-1})^{-1/2}]'$$

$$= (I + V_k^{-1})^{1/2} (1 + V_{k-1}^{-1})^{1/2} V_{k-2}^{-1} [(1 + V_{k-1}^{-1})^{1/2}]' (1 + V_k^{-1})^{1/2}]'$$

⋮

$$X_1 = ((I + V_k^{-1})^{1/2} \dots (I + V_2^{-1})^{1/2} V_1^{-1} \dots [(I + V_2^{-1})^{1/2}]' \dots [(I + V_k^{-1})^{1/2}]')$$

Further,

$$I + X_k = I + V_k^{-1}$$

$$I + X_k + X_{k-1} = (I + V_k^{-1})^{1/2} (1 + V_{k-1}^{-1}) [(I + V_k^{-1})^{1/2}]'$$

⋮

$$I + X_k + \dots + X_1 = (I + V_k^{-1})^{1/2} \dots (1 + V_2^{-1})^{1/2} (I + V_1^{-1})$$

$$\times [(1 + V_2^{-1})^{1/2}]' \dots [(1 + V_k^{-1})^{1/2}]'$$

Hence,

$$\begin{aligned}
 |X_1|^{\alpha_1 - \frac{p+1}{2}} &= |V_1|^{-\alpha_1 + \frac{p+1}{2}} \cdot |V_k|^{-\alpha_1 + \frac{p+1}{2}} |I + V_k|^{\alpha_1 - \frac{p+1}{2}} \cdot |I + V_2|^{\alpha_1 - \frac{p+1}{2}} \\
 |X_2|^{\alpha_2 - \frac{p+1}{2}} &= |V_2|^{-\alpha_2 + \frac{p+1}{2}} \cdots |V_k|^{-\alpha_2 + \frac{p+1}{2}} |I + V_k|^{\alpha_2 - \frac{p+1}{2}} \cdot |I + V_3|^{\alpha_2 - \frac{p+1}{2}} \\
 &\vdots \\
 |X_k|^{\alpha_k - \frac{p+1}{2}} &= |V_k|^{-\alpha_k + \frac{p+1}{2}} \\
 |I + X_k|^{\beta_{k-1}} &= |V_k|^{-\beta_{k-1}} |I + V_k|^{\beta_{k-1}} \\
 |I + X_2 + X_{k-1}|^{\beta_{k-2}} &= |V_{k-1}|^{-\beta_{k-2}} |V_k|^{-\beta_{k-2}} |I + V_k|^{\beta_{k-2}} |I + V_{k-1}|^{\beta_{k-2}} \\
 &\vdots \\
 |I + X_k + \dots + X_2|^{\beta_1} &= |V_k|^{-\beta_1} \cdot |V_2|^{-\beta_1} |I + V_k|^{\beta_1} \cdots |I + V_2|^{\beta_1} \\
 |I + X_k + \dots + X_1|^{-(\alpha_1 + \alpha_{k+1} + \beta_1 + \dots + \beta_k)} &= |V_k|^{\alpha_1 + \alpha_{k+1} + \beta_1 + \dots + \beta_k} \cdots \\
 &\times |V_1|^{\alpha_1 + \alpha_{k+1} + \beta_1 + \dots + \beta_k} \\
 &\times |I + V_1|^{-(\alpha_1 + \alpha_{k+1} + \beta_1 + \dots + \beta_k)} \cdots \\
 &\times |I + V_k|^{-(\alpha_1 + \alpha_{k+1} + \beta_1 + \dots + \beta_k)}
 \end{aligned}$$

The Jacobian matrix is of a triangular format and the Jacobian is the product of the determinants of the diagonal block matrices. It can be seen to be the following :

$$dX_1 \wedge \dots \wedge dX_k = |V_k|^{-(k-1)\frac{p+1}{2} - (p+1)} |V_{k-1}|^{-(k-2)\frac{p+1}{2} - (p+1)} \dots |V_1|^{-(p+1)} \\ \times |I + V_k|^{(k-1)\frac{p+1}{2}} \dots |I + V_2|^{\frac{p+1}{2}} dV_1 \wedge \dots \wedge dV_k.$$

Now, substituting all these we obtain the following

$$c_k |X_1|^{\alpha_1 - \frac{(p+1)}{2}} \dots |X_k|^{\alpha_k - \frac{p+1}{2}} |I + X_2 + \dots + X_k|^{\beta_1} |I + X_3 + \dots + X_k|^{\beta_2} \dots \\ \times |I + X_k|^{\beta_{k-1}} |I + X_k + \dots + X_1|^{-(\alpha_1 + \dots + \alpha_{k-1} + \beta_1 + \dots + \beta_k)} dX_1 \wedge \dots \wedge dX_k \\ = \left\{ \prod_{j=1}^k c_j |V_j|^{\alpha_{j+1} + \dots + \alpha_{k+1} + \beta_{j+1} + \dots + \beta_k - \frac{p+1}{2}} |I + V_j|^{-(\alpha_j + \dots + \alpha_{k+1} + \beta_{j+1} + \dots + \beta_k)} \right\} \quad (22)$$

where

$$c_j = \frac{\Gamma_p(\alpha_j + \dots + \alpha_{k+1} + \beta_j + \dots + \beta_k)}{\Gamma_p(\alpha_j) \Gamma_p(\alpha_{j+1} + \dots + \alpha_{k+1} + \beta_j + \dots + \beta_k)} \quad (23)$$

for $\Re(\alpha_j) > \frac{p-1}{2}$, $j = 1, \dots, k$, $\Re(\alpha_{j+1} + \dots + \alpha_{k+1} + \beta_j + \dots + \beta_k) > \frac{p-1}{2}$, $j = 1, \dots, k$. This completes the proof that V_j 's are independently distributed and that each V_j is a real matrix-variate type-2 beta matrix random variable with the parameters $(\alpha_{j+1} + \dots + \alpha_{k+1} + \beta_j + \dots + \beta_k, \alpha_j)$, $j = 1, \dots, k$.

Appendix

Some of the Jacobians of matrix transformation, integrals over scalar functions of matrix argument and type-1, type-2 beta integral will be listed here. For details on these as well as for related results see Mathai¹.

$$Y = AXA', \quad X = X', \quad |A| \neq 0 \Rightarrow dY = |A|^{p+1} dX \quad (\text{A1})$$

where the nonsingular matrix A is free of the elements in the real symmetric matrix $X = X'$

Let $T = (t_{ij})$, $t_{jj} > 0$, $j = 1, \dots, p$, $t_{ij} = 0$ for $i < j$ be a lower triangular matrix with positive diagonal elements. Consider a $p \times p$ real symmetric positive definite matrix $X = X' > 0$ such that $X = TT'$. Then

$$X = TT' \Rightarrow dX = 2^p \left\{ \prod_{j=1}^p t_{jj}^{p+1-j} \right\} dT. \quad (\text{A2})$$

With the help of (A2) one can evaluate the matrix-variate gamma integral in (7) and obtain the result in (6). Let X be a $p \times p$ nonsingular matrix of functionally independent real variables. Let $X = X'$. Then

$$Y = X^{-1}, \quad X = X', \quad |X| \neq 0 \Rightarrow dY = |X|^{-(p+1)} dX \quad (\text{A3})$$

With the help of (A1), (A3), (7), (6) we can evaluate the real matrix-variate beta integral and obtain the following results.

$$B_p(\alpha, \beta) = \frac{\Gamma_p(\alpha)\Gamma_p(\beta)}{\Gamma_p(\alpha + \beta)} \quad (\text{A4})$$

$$= \int_{0 < x = x' < I} |X|^{\alpha - \frac{p+1}{2}} |I - X|^{\beta - \frac{p+1}{2}} dX$$

$$= \int_{0 < x = x' < I} |X|^{\beta - \frac{p+1}{2}} |I - X|^{\alpha - \frac{p+1}{2}} dX \quad (\text{A5})$$

$$= \int_{x = x' > 0} |X|^{\alpha - \frac{p+1}{2}} |I - X|^{-(\alpha + \beta)} dX$$

$$= \int_{x=x'>0} |X|^{\beta-\frac{p+1}{2}} |I-X|^{-(\alpha+\beta)} dX \quad (\text{A6})$$

where (A5) and (A6) are called real matrix-variate type-1 and type-2 beta integrals respectively

References

- 1 Mathai, A M (1997) *Jacobians of Matrix Transformations and Functions of Matrix Argument*, World Scientific Publishing, New York
- 2 Conradie, W.J. & Troskie, C G. (1984) *South African Statistical Journal* 18 123
- 3 Gupta R D & Richards, D St P (1987) *Journal of Multivariate Analysis* 23 233

Equilibrium of self gravitating polytropes

N.K SOOD and KULDIP SINGH

Department of Physics, Guru Nanak Dev University, Amritsar - 143005, India.

Received October 17, 2003, Accepted March 13, 2004

Abstract

The equilibrium of a self gravitating cylindrical polytrope with a general magnetic field and rotation has been discussed

(Keywords polytropes/ self-gravitating)

Introduction

There has been interest in the study of self-gravitating systems in different geometrical configurations¹⁻⁶. Recently, study of perfectly conducting, self gravitating infinite cylinders(and jets),of compressible as well as incompressible fluids, has gained renewed interest, for example by Radwan⁶ as it has relevance in describing and finding condensations within astronomical bodies especially the spiral arms of the galaxies. Most of the workers have assumed a homogeneous density for fluid cylinder. In order to generalize this for variable density cylinders we have chosen a polytropic equation of state. Even though the effect of geometry can be visualised, explicit results are not available except for spherical geometry. A spherical self- gravitating polytrope has been discussed in detail by Chandrashekhar¹, who has observed that the equilibrium size of the sphere approaches infinity for $n=5$; n being the polytropic index. In the present work, we intend to find such limits when the configuration is a cylindrical one and determine the effect of a general magnetic field (with toroidal and poloidal components) and rotation on it. Incidentally it has been found that the cylinders do not become boundless even for values far beyond $n=5$.

Basic Equations

Here we consider an ideally conducting polytropic fluid cylinder pervaded by a general magnetic field of the form $\mathbf{H} = (0, H_z(\bar{\omega}), H_\phi(\bar{\omega}))$ where H_ϕ and H_z are the toroidal and the axial magnetic field components respectively and $\bar{\omega}$ denotes the

radial coordinate. The configuration is assumed to be rotating with a uniform angular velocity \mathbf{V} about the z -axis.

The equations determining the equilibrium (Sood³) are

$$-\nabla P + \rho \nabla \Phi - \rho \mathbf{V} \times (\mathbf{V} \times \bar{\omega}) + \frac{1}{4\pi} (\nabla \times \mathbf{H}) \times \mathbf{H} = 0 \quad (1)$$

$$\nabla^2 \Phi = -4\pi G \rho \quad (2)$$

and

$$\nabla \cdot \mathbf{H} = 0 \quad (3)$$

where $\mathbf{V} = V \hat{I}_z$, \hat{I}_z is the unit vector along z -axis and Φ, p and ρ are the gravitational potential, kinetic pressure and density respectively

It is convenient to express \mathbf{H} as

$$\mathbf{H} = \bar{\omega} T \hat{I}_\phi + \frac{1}{\bar{\omega}} \frac{d}{d\bar{\omega}} (\bar{\omega} P) \hat{I}_z \quad (4)$$

where T and P are toroidal and poloidal scalars

The Lorentz force (except for a constant multiplier) thus becomes

$$\frac{1}{4\pi} (\nabla \times \mathbf{H}) \times \mathbf{H} = \frac{1}{4\pi} \hat{I}_{\bar{\omega}} \left[-\bar{\omega} \frac{d}{d\bar{\omega}} (\bar{\omega}^2 P) + \frac{1}{\bar{\omega}} \frac{d}{d\bar{\omega}} (\bar{\omega}^2 P) - \bar{\omega} T \frac{d}{d\bar{\omega}} (\bar{\omega}^2 T) \right] \quad (5)$$

Choosing the equation of state in the form $p = K \rho^{1+1/n}$, p is the pressure and ρ is the density of the fluid and K is a constant, we obtain [after taking divergence of equation (1)]

$$\frac{1}{\bar{\omega}} \frac{d}{d\bar{\omega}} \left[\bar{\omega} \frac{d}{d\bar{\omega}} \left\{ K(n+1) \rho^{1/n} \right\} \right] + 4\pi G \rho - 2V^2 - \frac{1}{4\pi} \nabla \cdot [\nabla \times \mathbf{H}] = 0 \quad (6)$$

If we choose the magnetic field to be purely toroidal and also take

$$\frac{T}{\rho} \frac{d}{d\bar{\omega}} (\bar{\omega}^2 T) = K_1 \bar{\omega}$$

we obtain

$$\nabla \left[\frac{1}{4\pi\rho} (\nabla \times \mathbf{H}) \times \mathbf{H} \right] = \frac{1}{2\pi} K_1$$

For a purely axial magnetic field we choose

$$\frac{1}{2\rho} \frac{d}{d\bar{\omega}} (H_z^2) = \frac{1}{2\pi} K_2$$

Now assuming that the magnetic field has both the axial and the toroidal components, the eqn 6) takes the simple form

$$\frac{1}{\bar{\omega}} \frac{d}{d\bar{\omega}} \bar{\omega} \frac{d}{d\bar{\omega}} (K(n+1)\rho^{1/n}) + 4\pi G \rho - 2V^2 + \frac{1}{2\pi} (K_1 + K_2) = 0$$

With $\rho = \lambda \Theta^n$, this equation further reduces to the following form

$$\frac{1}{\xi} \frac{d}{d\xi} \left(\xi \frac{d}{d\xi} \Theta \right) + \Theta^n - \epsilon = 0 \quad (8)$$

where ξ is a dimensionless variable defined by $\bar{\omega} = \alpha \xi$ with

$\alpha = \left[\frac{K}{4\pi G} (n+1) \lambda^{1/(n+1)} \right]$ and $\epsilon = \frac{1}{4\pi G} [2V^2 - (K_1 + K_2)/2\pi]$. The eqn. (8) for the special case $\epsilon = 0$ is

$$\frac{1}{\xi} \frac{d}{d\xi} \left(\xi \frac{d}{d\xi} \Theta \right) + \Theta^n = 0 \quad (9)$$

which is similar to the Lane-Emden equation for spherical polytropes and is to be solved under the initial condition $\Theta = 1$ and $d/d\xi \Theta = 0$ at $\xi = 0$. The first condition defines λ as the density along the axis of the cylinder while the second condition follows directly from eqn (9)

Existence of Solutions

The eqn (9) is analytically soluble for $n=1$ yielding the solution $\Theta(\xi)=J_0(\xi)$ with its first zero at $\xi_1 = 2.4048$. For other values of n , the equation has to be solved numerically. It is obvious that the value of ϵ plays an important role in the solution of the equation

- (i) For $\epsilon=0$, where the magnetic energy balances the rotational energy, we find that the value of n hardly exceeds 30.
- (ii) For positive values of ϵ that is when rotational energy dominates the solution is found only in a limited region as depicted in Fig 1
- (iii) The solution is found to exist for all negative values of ϵ as expected. Here magnetic energy is the dominant factor

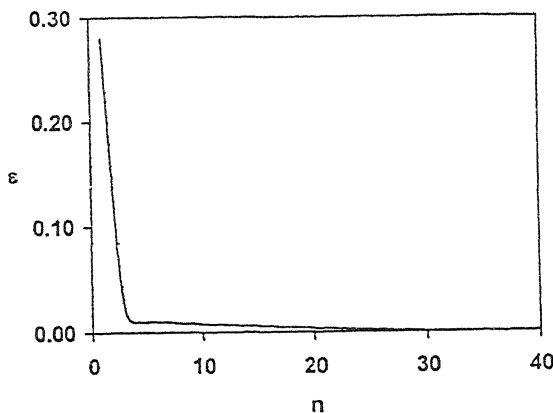


Fig 1—Existence of solution

However, it is found that the radius of the cylinder hardly undergoes any change with increasing polytropic index when $\epsilon \leq -0.5$. Since the equation becomes non-linear for $n \geq 1$, the above results are based on numerical computations even though the results for $n = 1$ can be obtained analytically.

Physical Characteristics

The radius of the cylinder is given by

$$\bar{\omega}_1 = \alpha \xi_1 = [K(n+1) \frac{1}{4\pi G}]^{1/2} \lambda^{(1-n)} 2n \xi_1$$

where ξ_1 is the first zero of $\Theta(\xi)$

The mass per unit length is

$$M = 2\pi \rho \bar{\omega} d\bar{\omega} = -\xi_1 [K(n+1) \lambda^{1/n} \frac{1}{2G}] \left(\frac{d}{d\xi} \Theta \right)_{\xi=\xi_1}$$

and the mean density is given by $\rho = M/(\pi \alpha r^2 \xi_1^2)$ so that $\rho/\lambda = \frac{2}{\xi} \left(\frac{d}{d\xi} \Theta \right)_{\xi=\xi_1}$

Results and Conclusions

- (i) The variation of the radius of the cylinder (denoted by ξ_1) is shown in Fig. 2 for $\epsilon = 0$. We can conclude that for $n > 25$, ξ_1 almost approaches infinity. In fact the variation of the size of the cylinder with n can be described by a quartic function of the form

$$\xi_1 = 2.414 - 0.3176 (n-1) + 0.3973 (n-1)^2 - 0.04351 (n-1)^3 + 0.00245 (n-1)^4$$

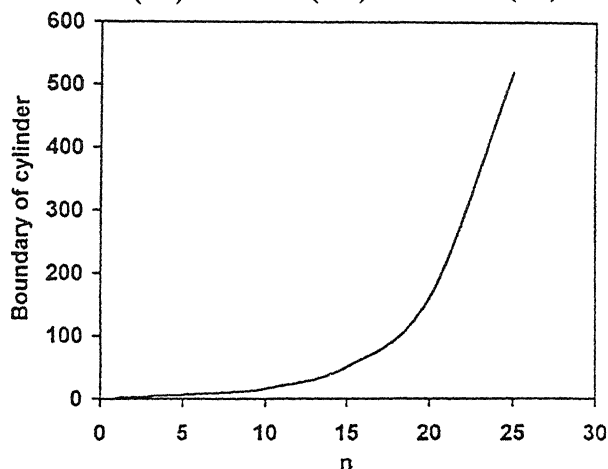


Fig. 2—Size of cylinder vs. n

(ii) From the polytropic equation of state, a large value of n implies a near isothermal behaviour. An analytical solution exists only for $n = 1$ in this geometry as well as in spherical geometry. For $n = 5$ the boundary in the spherical case approaches infinity whereas the boundary is finite for the cylindrical case and may be regarded infinite for much larger values of n as mentioned above. This difference may be assigned to the different topologies. The effects of magnetic field and rotation are depicted explicitly by the parameters $\epsilon < 0$ and $\epsilon > 0$ respectively (Fig. 3)

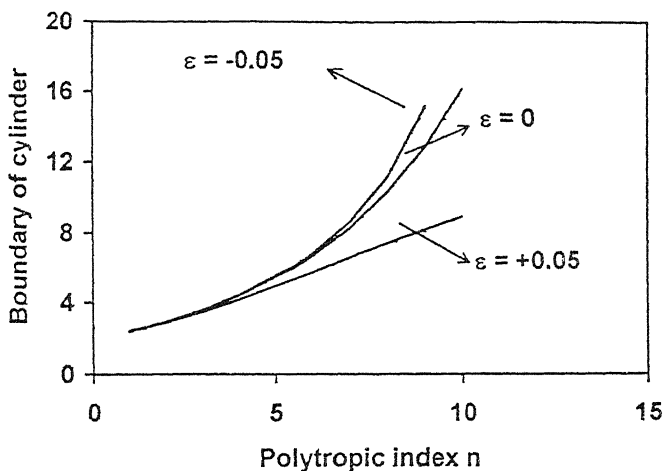


Fig. 3—Magnetic field and rotation

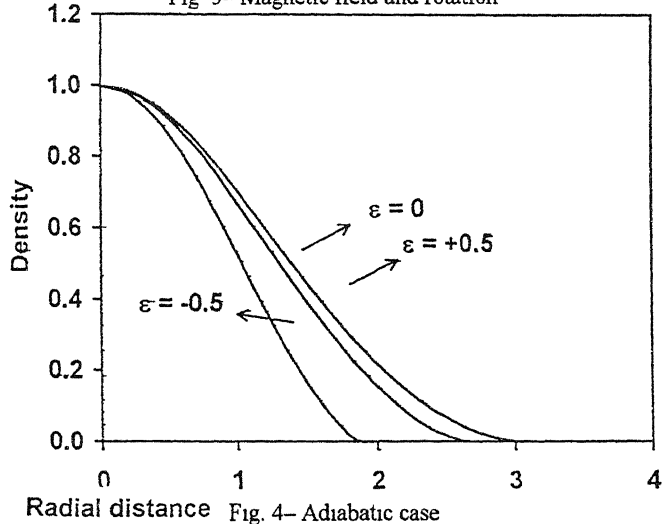


Fig. 4—Adiabatic case

(iii) Variation of ρ with the radial distance ξ for different ϵ has been depicted in Fig 4 where it is observed that the equilibrium size of the cylinder decreases as ϵ decreases i.e. the magnetic field confines the boundary. In Fig 5 effect of n on density has been shown graphically for $\epsilon=0$. It is interesting to note that for large values of n nearly the complete mass of the cylinder shrinks close to axis even though the boundary of the cylinder is still large (Fig 1) bearing a semblance to possible black holes in this geometry. Changes in the value of ϵ give results on the expected lines as is evident from Fig 5.

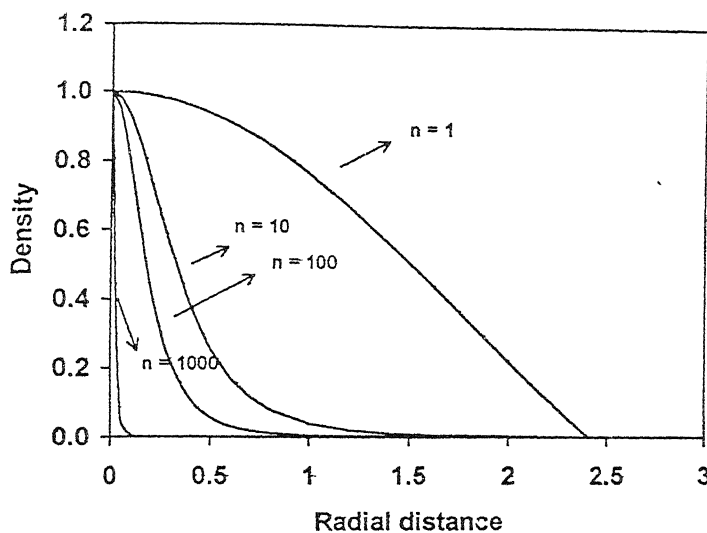


Fig 5—Effect of n on density

Acknowledgements

The authors express their gratitude to Prof S K Trehan for his continuous encouragement during the completion of this work.

References

1. Chandrasekhar, S (1961) *Hydrodynamic and Hydromagnetic Stability*, Dover Publication, New York, p 516, Ch XII
2. Karnik, A & Talwar, S P (1978) *Astophys. Space Sci.* **57** 141

- 3 Sood, N K (1980) *Astrophys Space Sci* **73** 213
- 4 Kendall, J M (1986) *Phys Fluids* **29** 2086
- 5 Friedmann, J L (1996) *J Astrophys Astron.* **17** 199
- 6 Radwan, A E (1998) *Ind J Pure Appl Math.* **29** 855
- 7 Sood, N K (1983) *Astrophys Space Sci* **97** 379

Relationship between cosmic rays and geomagnetic activity during Forbush decrease events of February and August, 1999

PANKAJ K SHRIVASTAVA and PRASANTI SHRIVASTAVA

Department of Physics, Government New Science College Rewa-486001, India

Email pankaj_in_2001@rediffmail.com

Received July 10, 2001, Revised February 20, 2002, Re-Revised September 3, 2002,
Re-Re-Revised July 19, 2003, Accepted March 26, 2004

Abstract

Transient decrease in cosmic ray intensity followed by a slow recovery is called a Forbush decrease event in cosmic ray studies. Such two Forbush decrease events were noted first in August 19 to 29, 1999 another in February 15 to 23, 1999, which occurred during high solar activity period of solar cycle 23. It is noteworthy that both the events were accompanied with several intense solar flares and geomagnetic storms. In this work we have done a systematic study to derive relationship between cosmic ray decrease and increase in geomagnetic activity. We have found a significant relationship between cosmic ray intensity and decreasing profile of Dst values. Results of analysis indicate a strong relationship between geomagnetic activity and cosmic ray intensity on short-term basis.

(Keywords forbush decrease/solar flares/geomagnetic activity)

Introduction

A number of cosmic ray researchers established that Forbush decrease events in cosmic rays are produced by perturbation in interplanetary conditions and that these perturbations originate either from solar flares or from magnetic field structures associated with interplanetary solar wind streams^{1,2}. The perturbations could be produced from shock waves, coronal mass ejections and flare generated high speed solar wind streams^{3, 4}. In 1975 Barouch and Burlaga⁵ have reported that the high magnetic field regions in interplanetary space are associated with Forbush decreases. Further it has been demonstrated that these cosmic ray decreases are not related to turbulent or random motions in the field, while the regions of high field strength in interplanetary space are found to be responsible for causing Forbush decreases. These regions consist of magnetic blobs and magnetic clouds ejected from active solar regions. Interplanetary shocks have comparatively ordered field structure. The turbulent field in the environment of shocks and high-speed streams are simply tangential discontinuities⁵.

The idea of spiral cone like region, which extends along the interplanetary magnetic field, is also investigated. In this study we have studied the characteristics of Forbush decrease events of August 19 to 29, 1999 and February 15 to 23, 1999 in relation with geomagnetic field variations. Recently, it has been investigated that the transient disturbances in interplanetary medium such as magnetic clouds and bi-directional events are also producing cosmic ray decreases on short-term basis⁶.

Data and Method of Analysis

Forbush decrease events of August and February 1999 were identified from the hourly plots of the cosmic rays intensity. We have used the daily values of the two neutron monitors Kiel (2.23 GV) and Climax (2.97 GV). Solar flares, *Dst* indexes, *Ap* index, Solar sunspot number were taken from the Prompt reports of Solar Geophysical Data books. Data related with geomagnetic activity/solar activity for the event periods were also taken from the Solar Geophysical Data book.

Results and Discussion

Fig. 1 shows the Forbush decrease event of August 1999. Onset time of this event is in early hours of August 19, 1999 and it remains low during four to five days. This figure shows cosmic ray intensity plots for seven neutron monitors- Calgary, GooseBay, Moscow, Climax, Kiel, Beijing and Haleakala covering a wide range of cut off rigidities. Several intense solar flares were observed during the event period, solar flares of August 17 which occurred in Noaa region of 86658 seem to be more powerful in producing decreases in cosmic ray intensity. Further solar flare events of August 19, 20, and 21 in the Noaa region are also support to enhance the decrease in cosmic ray intensity. Major solar flare events of August 20 and 21 are responsible to produce maximum decrease in August 23. A series of geomagnetic events of August 16, 17, 18 and 22 provide the possible solar terrestrial relationship during the period of Forbush decreases.

Similarly Fig 2 shows the plot of Forbush decrease event of same neutron monitor stations for the period February 15 to 23, 1999. Onset time of this event is on February 17 and it remains low during two days. A recovery period of this event is four days. We noticed two major solar flares on February 15 and 16 on Noaa region of 8462 which may have affected to produce the large decrease in cosmic ray intensity. We have also noted geomagnetic storms on February 17 and 18 which coincide with maximum decrease of cosmic ray intensity.

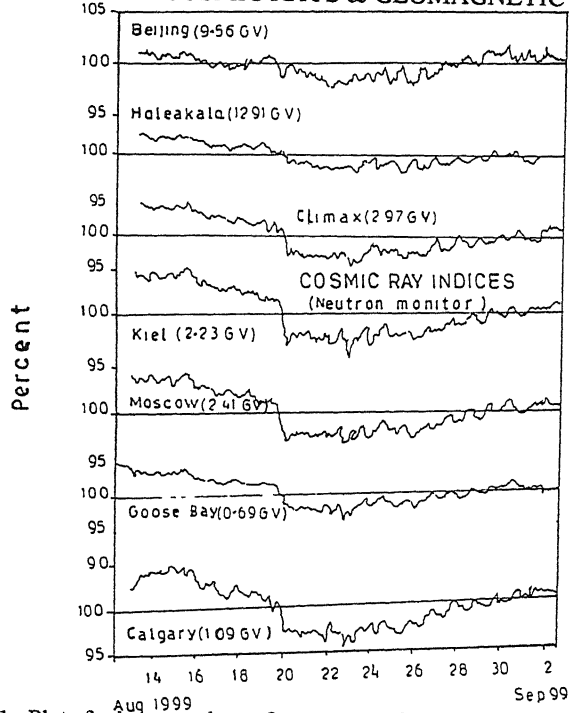


Fig 1—Plots for hourly values of cosmic rays for several neutron monitors for August 1999 Forbush decrease events

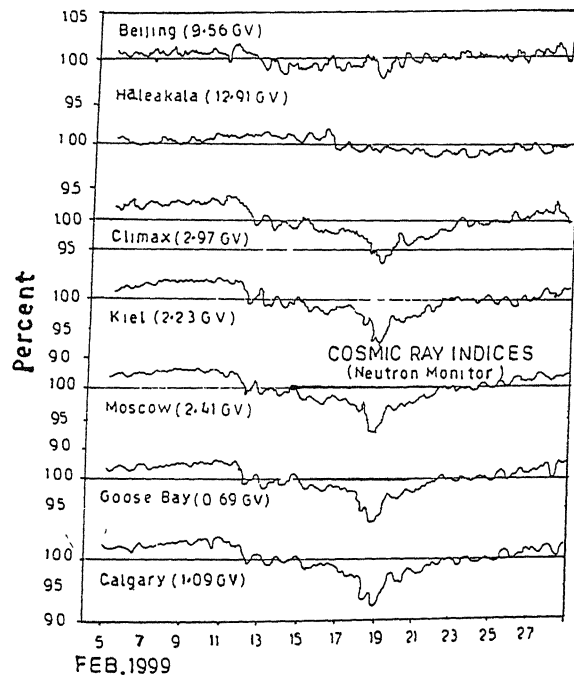


Fig 2—Plots for hourly values of cosmic rays for several neutron monitors for February 1999 event

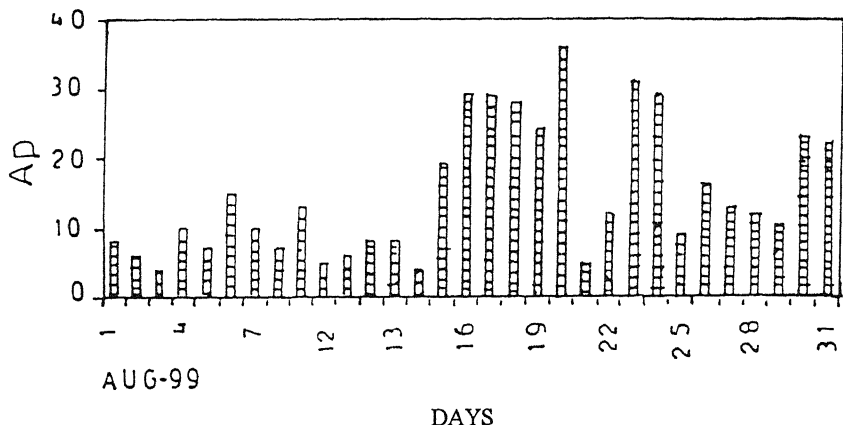


Fig. 3—Daily values of Sun Spot numbers (R_z) and geomagnetic activity (A_p) for August 1999

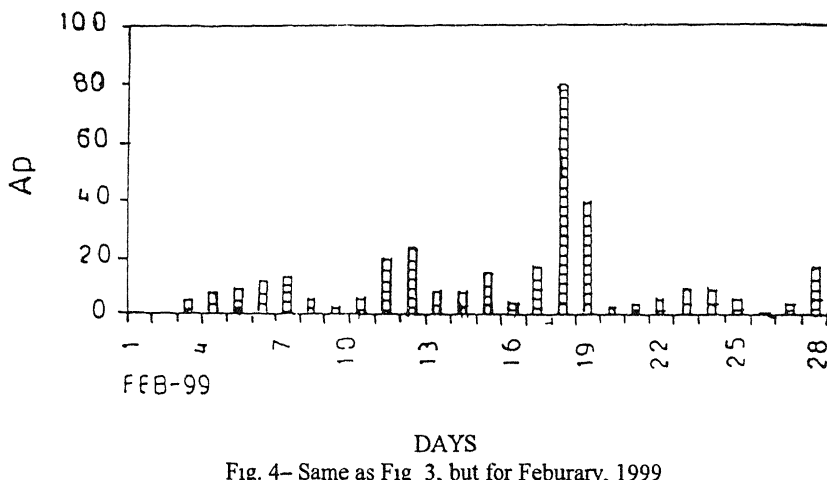


Fig. 4—Same as Fig. 3, but for February, 1999

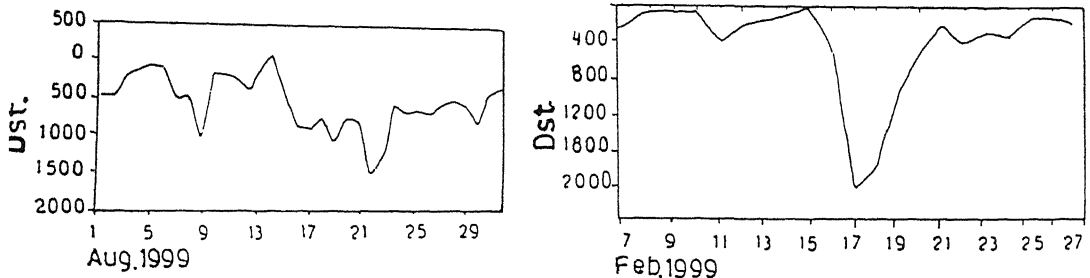


Fig. 5—Variation of Dst values during the event periods of August 1999(left) and February 1999(right)

Further we have plotted the daily values of Ap index for both the events as shown in Fig (3 & 4) respectively Daily values of Ap for the event of August 1999 are plotted on Fig 3 and similarly these geomagnetic indices are plotted in Fig 4 for another Forbush decrease of February 1999. High Ap values are seen for both the event periods

Conditions of interplanetary medium play an important role in energy transmission from solar wind to magnetosphere that significantly modulate cosmic ray particles Forbush decrease events as we observed during August and February 1999 are examples of such events to draw a possible relationship between cosmic ray intensity and interplanetary features.

We observed high solar wind speed and interplanetary magnetic field B (nT) to event periods Occurrence of several intense solar flares along with flare generated solar wind streams are expected as causes of Forbush decrease event of August 1999. High values of B (nT) coincide with the event period and low solar magnetic fields are also observed for event period of February 1999 Solar wind speed data are not available during event period to draw any meaningful conclusions Hence we can infer the same interplanetary conditions for both the events periods. However, variations in cosmic ray intensity of event periods depend on the larger/smaller disturbances in interplanetary conditions. High-speed solar wind streams particularly solar flares generated are found more responsible factor in producing transient decrease in cosmic rays This result is consistent with previous results reported in 1996 by Shrivastava and Shukla⁴ by taking two different types of high-speed solar wind streams.

To show the relationship between geomagnetic activity and cosmic ray intensity we have plotted the daily values of geomagnetic Dst index for both the Forbush decrease event periods. Daily values of Dst index are plotted in Fig 5 for the events of August 1999 and similarly the values of Dst index for the event period of February 1999 are also plotted in right panel of the figure. A significant variation in Dst values is seen for both of events periods. Variational profiles of Dst index for these two events periods vary according to variational profiles of Forbush decrease events. A large decrease in Dst index for the February 15 to 23 coincides with main phase of Forbush decrease event of February 1999. Similarly we also observed a significant decrease in Dst index which coincides with decrease of cosmic ray intensity for entire period of Forbush decrease event of August 1999. In both the events, we observed significant decrease in cosmic ray intensity as well as geomagnetic Dst index during the main phase of storm.

The relationship between the solar flare and cosmic ray intensity decrease observed during these two periods are similar to that in previous investigations^{7,8}

One sudden storm commencement (SSC) was observed on February 17, 1999 in association with the Forbush decrease event of February 1999. As we know SSC is a signature of arrival of shock waves. Therefore it can be inferred that shock waves also play an important role in producing large cosmic ray decreases.

Significant decreases were seen in geomagnetic *Dst* index during both the periods of Forbush decreases. The values of *Dst* index show significant transient decrease in similar pattern as that of Forbush decrease. The geomagnetic disturbance index *Dst* at low latitude comes from the outward blowing zonal current system called the ring current. It is assumed that the massive compression of the magnetosphere and enormous intensification of the large-scale magnetospheric current system reflected in *Dst* leads to a significant effect on cosmic ray measurement near the earth.

Coronal mass ejections (CMEs) are known as one of the causes of interplanetary disturbance because they involve a large amount of mass and energy ejected into interplanetary medium. In a number of recent studies, CMEs are found as a responsible factor in cosmic ray modulation and geomagnetic disturbances⁹. We have observed a series of CMEs events during the period of both the Forbush decrease events. We observed two CMEs events on August 17 & 22, 1999. Similarly a series of CMEs events were observed on February 12, 13, 14, 20 & 21. Now, it can be inferred that the CMEs were also one of the factors in producing decrease in cosmic rays and increase in geomagnetic activity.

Conclusions

It has been concluded from the analysis that-

1. Both of forbush decrease events are found in association with increase in geomagnetic activity.
2. The main phase of cosmic ray decrease coincides with maximum *Dst* values.
3. Solar flares and coronal mass ejections are found to be responsible factors in producing decrease in cosmic ray intensity and increase in geomagnetic activity.
4. One can distinctly see these on the basis of sudden storm commencement (SSCs). Occurrence of SSCs event of February 17, 1999 clearly exhibits the

effect of interplanetary shock waves on cosmic ray intensity which shows a step like decrease with fast recovery in shorter time span.

Acknowledgement

The authors thank the World Data Center A-(USA) for providing the cosmic rays and solar data. One of them (PS) is grateful to Prof. S.P. Agrawal for providing the research facility at Physics Department, A.P.S University, Rewa (M.P.).

References

- 1 Parker, E N (1963) *Interplanetary Dynamical Processes*, Inter Science, John Wiley and Sons, New York
- 2 Kadokura, A & Nishida, A (1986) *J Geophys Res* **91** 13
- 3 Cane H V & Richardson, I G (1995) *J. Geophys Res. (USA)* **100** 1755
- 4 Shrivastava, P K & Shukla, R P (1994) *Solar Physics (Netherlands)* **154** 177
- 5 Barouch, E & Burlaga, L F (1975) *J Geophys Res. (USA)* **80** 449
- 6 Kaushik, S C & Shrivastava, P K. (2000) *Proc. Nat Acad. Sci. India* **70 A(I)** 99
- 7 Shushong, X & Zhonghei, Y (1990) *Proc 21st Int. Cosmic Rays*, Adelaide (Australia) **6** 241.
- 8 Kaushik, S C & Shrivastava, P.K (2001) *Indian J. of Radio & Space Physics (India)* **29** 47.
- 9 Shrivastava, P K (2001) *Proc. 27th Int Conf Cosmic Rays*, Hamburg (Germany) **9** 3481

Stability of superposed viscoelastic (Walters' B')-Newtonian fluids in porous medium	<i>R.C. Sharma, Sunil and P.K. Bharti</i>	... 311
Optimal implementation of parallel divide and conquer algorithm on de Bruijn networks	<i>P.K. Mishra and C.K. Sharma</i>	... 323
Ramanujan number	<i>Baikunth Prasad Ambasht and Jamuṇa Prasad Ambasht</i>	... 329
A matrix-variate extension of inverted Dirichlet integral	<i>K.M. Kurian, Benny Kurian and A.M. Mathai</i>	... 337
Physics		
Equilibrium of self gravitating polytropes	<i>N.K. Sood and Kuldip Singh</i>	... 353
Relationship between cosmic rays and geomagnetic activity during Forbush decrease events of February and August, 1999	<i>Pankaj K. Shrivastava and Prasanti Shrivastava</i>	... 361

EDITORIAL BOARD

Chief Editor

Prof Suresh Chandra, Emeritus Scientist, Department of Physics,
Banaras Hindu University, Varanasi – 221 005,
Fax 91-542-2317040, E-mail schandra@banaras.ernet.in

1 Prof R P Agarwal Former Vice-Chancellor, Rajasthan & Lucknow Universities, B1/201, Nirala Nagar, Lucknow ~ 226 020 (Mathematics)	2 Prof Sushanta Dattagupta Hon Professor JNCASR and Director, S N Bose National Centre for Basic Sciences, JD Block, Sector III, Salt Lake, Kolkata – 700 098 Fax 91-33-23353477 E-Mail sdgupta@bose.res.in (Physics)
3 Dr Anil Kumar Scientist, Physical Chemistry Division, National Chemical Laboratory, Pune – 411 008 Fax 91-20-5893355, 5893761, 5893619, 5893212 E-mail prs@ems.ncl.res.in , rkh@ems.ncl.res.in (Chemistry)	4 Prof B L Khandelwal Emeritus Scientist (CSIR), Defence Materials and Stores Research and Development Establishment, DMSRDE Post Office, G T Road, Kanpur – 208 013 Fax 91-512-2450404 (Chemistry)
5 Dr G S Lakhina Director, Indian Institute of Geomagnetism, Dr Nanabhai Moos Marg, R C Church, Colaba, Mumbai – 400 005 Fax 91-22-22189568 E-mail lakhina@iig.iigm.res.in (Geomagnetism/Atmospheric Sciences)	6 Prof U C Mohanty Professor & Head, Centre for Atmospheric Science, Indian Institute of Technology, Hauz Khas, New Delhi – 110 016 Fax 91-11-26591386, 26862037 E-mail mohanty@cas.iitd.ernet.in (Climate Modeling)
7 Prof K S Valdiya Bhatnagar Research Professor, Jawaharlal Nehru Centre for Advanced Scientific Research, Jakkur P O , Bangalore – 560 064 Fax 91-80-8462766 E-mail nehrucen@jncasr.ac.in (Environmental Geology/Neotectonics)	

Managing Editor

Prof. S.L. Srivastava

Coordinator, K Banerjee Centre of Atmospheric and Ocean Studies, Meghnad Saha
Centre for Space, University of Allahabad, Former Professor & Head, Department
of Physics, University of Allahabad, The National Academy of Sciences, India,
5, Lajpatrai Road, Allahabad – 211 002
Fax 91-532-2641183
E-mail . nasi@sancharnet.in

EDITORIAL ADVISORY BOARD

1 Prof Edwin D Becker
 Chief, Nuclear Magnetic Resonance Section,
 Building 5, Room 124,
 National Institute of Health,
 Bethesda,
 Maryland 20892-0520, U S A
 (**Spectroscopy/NMR**)

2 Prof Sir Herman Bondi
 Professor,
 Churchill College,
 Cambridge, CB3 ODS, U K.
 Fax : 01223-336180
 (**Mathematical Astronomy**)

3 Prof S K. Joshi
 Hon Vikram Sarabhai Professor,
 National Physical Laboratory,
 Dr K S Krishnan Marg,
 New Delhi – 110 012
 Fax 91-11-25726938, 25726952
 E-mail skjoshi@csnpl.ernet.in
 (**Solid State Physics**)

4 Prof. M.G K Menon
 Chairman, Board of Governors of
 IIT (Delhi) and IIIT (Allahabad),
 K-5 (Rear), Hauz Khas,
 New Delhi – 110 016
 Fax 091-11-26510825
 E-mail mgkmenon@ren02.ernet.in
 (**Physics**)

5 Prof A P Mitra
 Honorary Scientist of Eminence,
 Former Director-General, CSIR and
 Secretary to the Govt of India,
 National Physical Laboratory,
 Dr K S Krishnan Marg,
 New Delhi – 110 016
 Fax 91-11-25752678, 25764189
 E-mail apmitra@doe.ernet.in,
apmitra@ndf.vsnl.net.in
 (**Ionospheric Physics/Radio Communication/Space Physics/Space Science**)

6 Prof Jai Pal Mittal
 Director, Chemistry & Isotope Group,
 Bhabha Atomic Research Centre,
 Trombay, Mumbai – 400 085,
 Mumbai – 400 085,
 and Honorary Professor, JNCASR,
 Bangalore,
 Fax : 91-22-25505151, 25505331
 E-mail jmittalp@magnum.barc.ernet.in
 (**Radiation and Photochemistry/Chemical Dynamics/Laser Chemistry**)

7 Prof C K N Patel
 Chairman & CEO,
 Pranalytica, Inc.,
 1101 Colorado Avenue,
 Santa Monica, CA 90401-3009, U S.A.,
 Fax 310-450171
 E-mail patel@pranalytica.com
 (**Physics**)

8 Dr. B L S Prakasa Rao
 Distinguished Scientist,
 Indian Statistical Institute,
 7, S J S Sansanwal Marg,
 New Delhi – 110 016
 Fax : 91-11-26856779
 E-mail blsp@isid.ac.in
 (**Mathematical Statistics**)

9 Prof T V Ramakrishnan
 DAE Homi Bhabha Chair,
 Department of Physics,
 Banaras Hindu University,
 Varanasi – 221 005
 (**Theoretical Condensed Matter Physics/Statistical Mechanics**)

10 Dr P Rama Rao
 ISRO Dr Brahm Prakash Distinguished Professor, International Advanced Research Centre for Powder Metallurgy and New Materials (ARCI),
 Balapur P.O.
 Hyderabad – 500 005
 Fax : 91-40-24441468, 24443168
 E-mail : pallerama_rao@yahoo.co.in
 (**Physical & Mechanical Metallurgy/Alloy Development**)

11 Prof. M.M. Sharma
 Kothari Research Professor (Hon.),
 JNCASR, Bangalore,
 Formerly Professor of Chemical Engineering & Director, University Deptt of Chemical Technology, Matunga, Mumbai – 400 019
 E-mail : mmsharma@bom3.vsnl.net.in
 (**Mass Transfer with Chemical Reaction/Catalysis with Ion Exchange Resins**)

12 Prof. Govind Swarup
 INSA Honorary Scientist,
 Ex. Director, NCRA/GMRT,
 National Centre for Radio Astrophysics, Tata Institute of Fundamental Research NCRA, Post Bag 3, Ganeshkhind, Pune – 411 007
 Fax : 91-20-5692149/7257
 E-mail : gswarup@ncra.tifr.res.in
 (**Radio Astronomy/Cosmology**)

13. Prof Suresh Chandra
 (Chief Editor)
 Emeritus Scientist,
 Department of Physics,
 Banaras Hindu University,
 Varanasi – 221 005,
 Fax : 91-522-2317040,
 E-mail : schandra@banaras.ernet.in
 (**Physics**)

CONTENTS

Chemistry

Ternary complexes of bivalent metals with kojic acid or maltol and selected amino acids

Mohd Zakee and Deva Das Manwal

Intramolecular hydrophobic ligand-ligand interaction in mixed ligand complexes containing kojic acid or maltol and aliphatic amino acids

Mohd Zakee and Deva Das Manwal

Synthesis and characterization of Mn(II), Cr(III) and Fe(III) complexes with 4,4'-diaminostilbene-2,2'-disulphonate Schiff bases

K. Siddappa and S. D. Angadi

Speciation studies of calcium(II) and magnesium (II) complexes of L-glutamine and succinic acid in acetonitrile-water mixture

G Nageswara Rao and S.B. Ronald

Charge transfer interactions of L-aminoacids with chloranil : Conductometric studies

H S. Randhawa, P. Patyar and B S Sekhon

New sensitive methods for the spectrophotometric determination of some catecholamine derivatives

R A Vasantha, P. Nagaraja and H S Yathirajan

Spectrophotometric determination of nickel with di(o-ethylphenyl) carbazole using the synergistic effect with 1,10-phenanthroline

T. Suresh

Titrimetric and spectrophotometric methods for the assay of albendazole in non-aqueous medium

K. Basavaiah, P. Nagegowda and V. Ramakrishna

Mathematics and Statistics

Weak-waves in reacting gases

K. Pandey and R. Chaturvedi

Turbulent free jet with suspended particulate matter (SPM)

T C. Panda, S K. Mishra and A.K. Das

..... Contd.